Pergamon

0301-9322(95)00016-X

Int. J. Multiphase Flow Vol. 21, Suppl. pp. 1–97, 1995

0301-9322/95 $29.00 + 0.00

PWR STEAM GENERATORS

S. J. GREEN[1] and G. HETSRONI[2]

[1]Steam Generator Project Office, Electric Power Research Institute, Palo Alto, CA 94303, U.S.A. and
[2]Danciger Professor of Engineering, Technion—Israel Institute of Technology, Haifa 32000, Israel

(Received 20 February 1995)

1. INTRODUCTION

Steam generators (SG) in power plants based on pressurized water reactors (PWRs) transfer heat from a primary coolant system (pressurized water) to a secondary coolant system. Primary coolant water is heated in the core and passes through the steam generator, where it transfers heat to the secondary coolant water to make steam. The steam then drives a turbine that turns an electric generator. Steam is condensed and returns to the steam generator as feedwater.

A general schematic view of a PWR plant is shown in figure 1. Notice that the steam from the steam generator (SG) flows out of the containment structure and it must, therefore, be pure and not contain any radioactive materials. Since the primary fluid does contain radioactive material, one must preserve the complete separation between these two fluids, i.e. the integrity of the tubes which carry the primary fluid through the SG must be maintained. This is the primary concern in the design, construction, operation and maintenance of PWR SG.

Two types of PWR steam generators are in use: recirculating steam generators (RSGs) and once-through steam generators (OTSGs). Most of the units are vertical and this review will be limited to vertical units. Some of these steam generators have operated with a minimum of problems while other designs have experienced a variety of corrosion and mechanically induced problems. The discussion will focus more on the designs that have experienced problems and the effort expended to correct them. Corrosion problems include denting, wastage, intergranular attack, stress corrosion cracking, corrosion fatigue, pitting on the outside surfaces of the tubes and stress corrosion cracking on the inner surfaces of the tubes. Mechanical concerns have included water hammer, thermal stratification in feedwater pipes, fretting and wear of the tubes caused by excessive tube vibration and erosion–corrosion. These problems have caused unscheduled outages and expensive repairs. Where most extensively affected, steam generators have been replaced after 8–12 years of operation, far short of the expected plant operating period of 40 years. Table 1 shows the number of plants reporting SG problems worldwide.

The worldwide cost of unplanned steam generator outages is summarized in table 2, as reported by the International Atomic Energy Agency (IAEA). IAEA tracks unplanned reactor outages. The IAEA reports that over the last 10 years unplanned steam generator outages have resulted in over 87 billion kilowatt hours of lost generation. The economic consequences of these unplanned outages are shown in table 2. Using an estimated price of four cents per kilowatt hour and replacement power costs of one cent per kilowatt hour, unplanned steam generator outages over the last 10 years have accounted for over three billion dollars in lost revenue and 870 million dollars in replacement power costs. The totals are approximately five or six times this amount when both planned and unplanned outages are included. The incentive to utilities for improved steam generator performance is certainly significant.

Over the last 10 years, steam generator problems in the United States rank second, behind refuelling outages, as the most significant contributor to lost generation, EPRI report says.

During the last 10 years, the capacity factor loss for U.S. PWRs due to steam generator problems has averaged 3.0%. In 1992 the capacity factor loss was 3.3%. From 1980 to 1984 the average U.S. PWR capacity factor was 57.2%. During this time steam generator problems resulted in a reduction in the average U.S. PWR capacity factor of 5.7%. Of this amount, 1.5% was due to steam generator replacement and 4.2% due to steam generator tube problems.

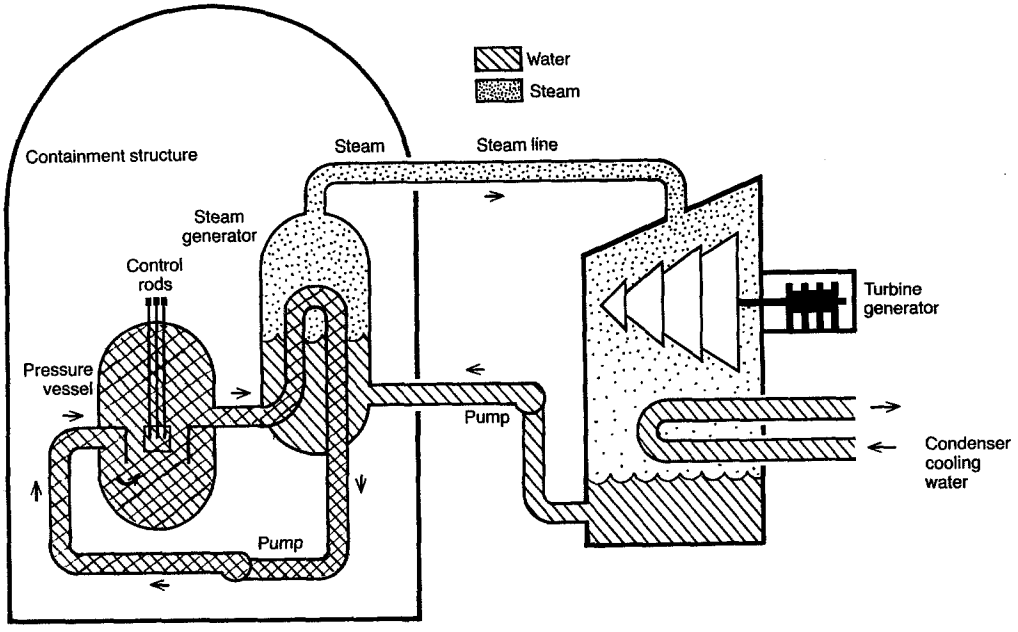

Figure 1. General view of a PWR power plant.

These problems, and some of the solutions which were derived recently to alleviate these problems, are discussed in this review. This review will cover the following topics:

- Steam generator description
- Steam generator problems

Table 1. Units reporting steam generator problems worldwide

	1977	1982	1992
	No. of units		
	52	99	205
Reported problems			
Denting			
Tube support corrosion	15	30	34
Tubesheet corrosion	6	12	50
Tubing corrosion			
Wastage	19	28	39
Pitting	0	3	14
ID cracking	1	22	90
OD SCC/IGA	6	22	74
Mechanical damage			
Fretting	9	15	117
Fatigue cracking	3	4	10
Impingement	0	2	9
No problems	26	32	33
No. of units reporting no problems after five years operation/total number of units with more than 5 years operation	1/14	4/57	13/168
Names of units reporting no problems after five years operation	Trino	Kewaunee; Mihama 3; Neckarwestheim; Davis Besse	Brokdorf; Chinon B3; Cruas 3; Cruas 4; Genkai 2; Grohnde; Loviisa 1; Loviisa 2; Obrigheim (replacement SGs); Philippsburg 2; Robinson 2 (replacement SGs); Unterweser

Table 2. Worldwide cost for unplanned steam generator outages

Year	Number of unplanned SG outages	Lost generation (10^9 kWh)	Replacement power costs (Million $)	Lost revenue (Million $)
1975	44	6.3	63	252
1976	56	9.1	91	365
1977	62	13.4	134	535
1978	72	2.8	28	111
1979	78	6.2	62	248
1980	87	5.1	51	204
1981	94	9.5	95	379
1982	113	14.8	148	592
1983	137	11.4	114	458
1984	136	9.0	90	361
1985	153	8.5	85	340
1986	196	4.9	49	196
1987	238	18.6	186	744
1988	253	15.9	159	636
Total	1695	135.3	1353	5415

- Thermal and hydraulic analysis
- Thermal and hydraulic correlations
- Thermal–hydraulic transients and safety considerations
- Steam separators
- Sludge deposition
- Local concentration processes
- Concentration in sludge piles
- Concentration in tube/tubesheet crevices (closed end)
- Concentration in tube/tubesheet support crevices (double-ended)
- Effect of concentrated solutions
- Tube fretting and wear.

2. STEAM GENERATOR DESCRIPTION

A general description is given of the two common types of steam generators, i.e. the once-through steam generator (OTSG) and the U-tube steam generator (UTSG).

2.1. The Once-through Steam Generator (OTSG)

The OTSG is typically associated with an NSSS which has the following general characteristics:

	Oconee 1	Max unit†
Rated power (MWe)	860	1300
Rated heat output (MWth)	2568	3760
System pressure (bar)	149	153
Primary coolant flow rate (10^6 kg/h)	29.5	35.6
Primary coolant temperature (°C)	317.8	329.7
Number of loops	2	2
Number of pumps	4	4
Number of steam generators	2	2
Shell side design pressure (bar)	71.4	84.0
Steam flow at full load (10^6 kg/h)	5.0	7.4
Steam temperature at full load (°C)	299	308
Steam superheat at full load (°C)	19.4	19.4
Feedwater temperature (°C)	235	241
Number of tubes	15,530	16,000
Diameter of tubes (mm)	15.9	15.9

A general view of the system is depicted in figure 2, and the general arrangement of the OTSG is given in figure 3.

Reactor coolant water enters the steam generator at the top, flows downward through the tubes and out at the bottom. The high pressure parts of the unit are the hemisphere heads, the tubesheets

†Conforming to the current Nuclear Regulatory Commission (NRC) size limitation of 1380 MWth.

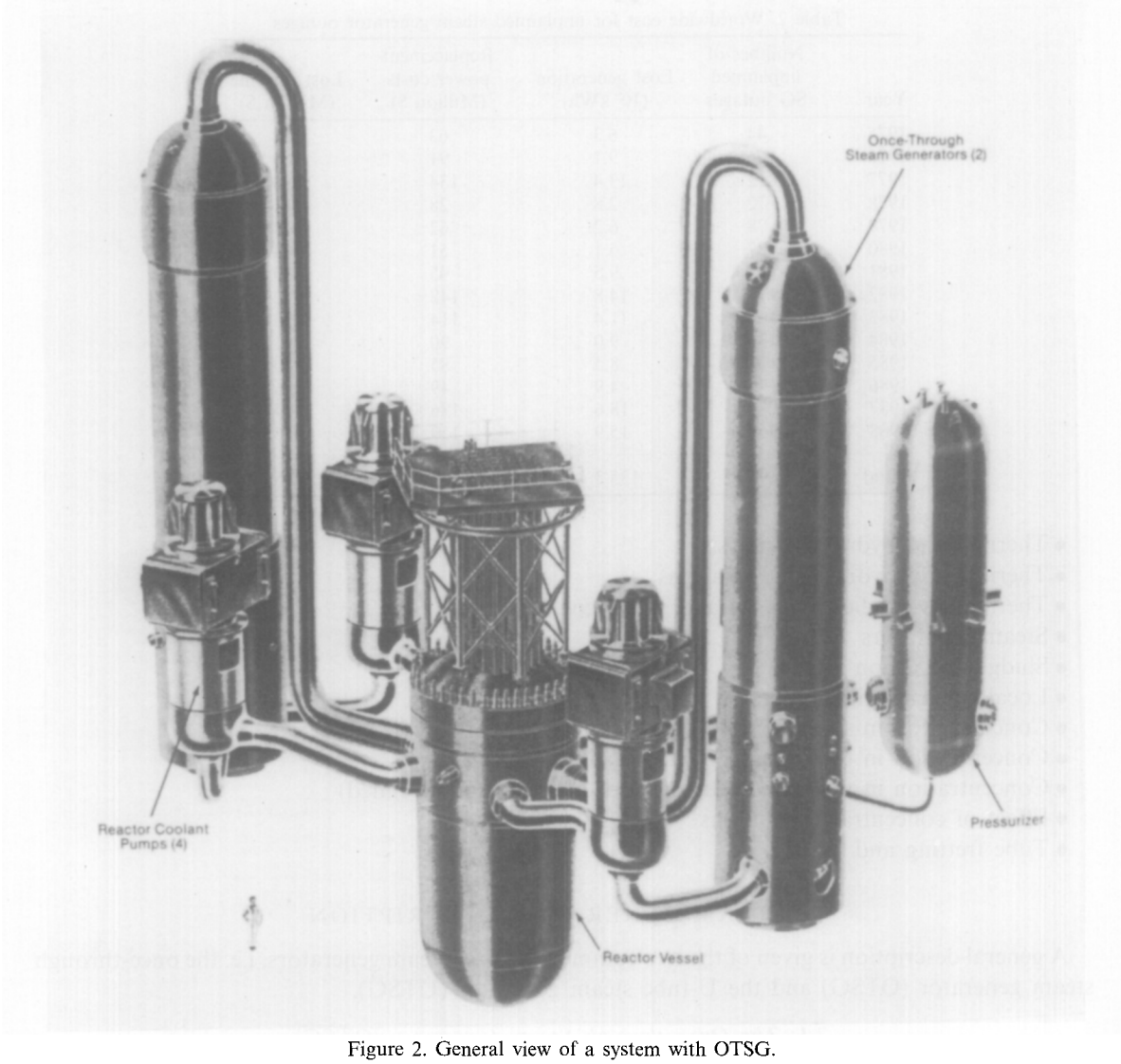

Figure 2. General view of a system with OTSG.

and the straight tubes between the tubesheets. The tube material is Inconel Alloy 600. Tube support plates, with trefoil holes, hold the tubes in a uniform pattern along their length. The unit is supported by a skirt attached to the bottom tubesheet.

Figure 3 indicates the flow paths on the steam side of the unit. Feedwater enters the side of the shell. It flows down through an annulus just inside the shell where it is brought to saturation temperature by mixing with steam. The saturated water enters the heating surface at the bottom, is converted to steam and is superheated as it passes upward through the generator.

The shell, outside of the tubes, and the tubesheets form the boundaries of the steam-producing section of the vessel. Within the shell, the tube bundle is surrounded by a shroud, which is in two sections. The upper part of the annulus between the shell and the baffle is the superheater outlet, while the lower part is the feedwater inlet heating zone. Vents, drains, instrumentation nozzles and inspection openings are provided on the shell side of the units.

Superheated steam is produced at a constant pressure over the power range. At full power, the steam temperature of 300°C provides about 22–33°C of superheat at 6.3 MPa. As the load is reduced, steam temperature approaches the reactor outlet temperature, thus increasing the superheat slightly. Below 15% load, steam temperature decreases to saturation. The primary coolant flow is from top to bottom. It enters at about 316–327°C and leaves at about 291–293°C. The temperature differences between the primary and secondary sides at the bottom of the steam generator is similar to that on the cold leg of a recirculating steam generator.

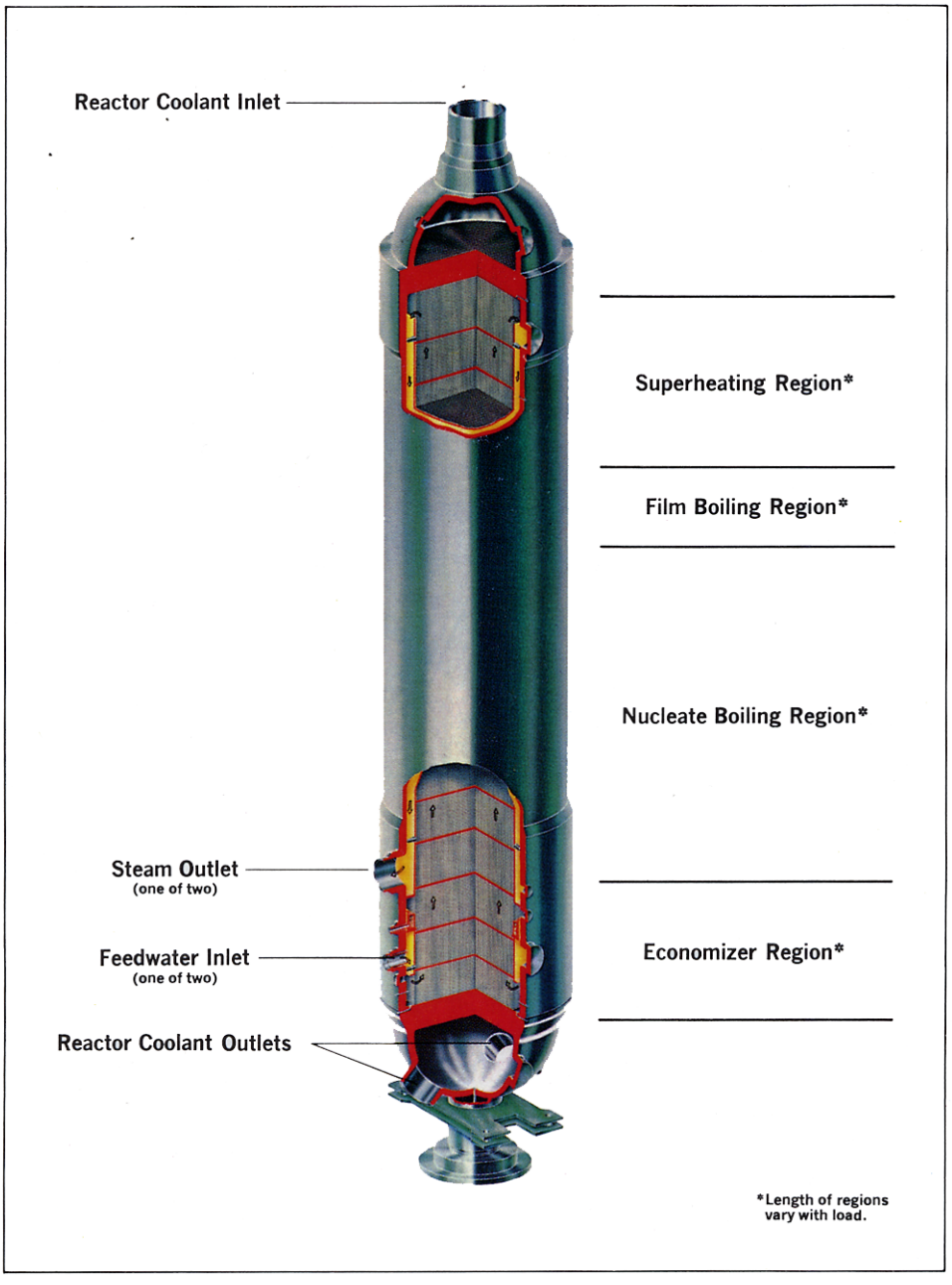

Figure 3. Once-through steam generator (OTSG, B & W).

The ability to maintain a constant (secondary) steam pressure is achieved by varying the boiling length with the load, i.e. the mass flow rate of the feedwater is controlled (above 15% load) by the pressure. When the outlet steam pressure decreases, the mass flow of the feedwater increases, thus increasing the boiling length and the steam flow rate. This can best be illustrated as follows: the total heat transferred in the steam generator Q is proportional to the overall heat transfer coefficient U, to the total transfer area A and to the temperature difference between the primary and secondary fluids ΔT, i.e.

$$Q = UA\Delta T$$

This equation can be written in an equivalent form

$$W \propto UL_{\mathrm{B}}(T_{\mathrm{p}} - T_{\mathrm{sat}})$$

Table 3(a). OTSG feedwater specifications. Normal power operation (≥15% reactor power)

Parameter	Normal value
Total suspended solids (ppb)	>10
Cation conductivity (μs/cm)	≤0.2
Dissolved oxygen as O_2 (ppb)	≤5
Hydrazine (ppb)	≤20
Silica as SiO_2 (ppb)	≤20
Total iron as Fe (ppb)	≤10
Total copper as Cu (ppb)	≤2
pH @ 25°C (Ferrous system)	≥9.3
pH @ 25°C (Ferrous/copper system)	8.8–9.2

Table 3(b). Recirculating steam generator power operation (>5% reactor power). Blowdown sample

Parameter	Normal value
pH (ferrous system)	≥9.0
pH (ferrous, copper system)	8.5–9.2
Cation conductivity	≤0.8
Sodium (ppb)	≤20
Chloride (ppb)	≤20
Sulfate (ppb)	≤20

where W is the steam flow rate, U is the heat transfer coefficient (mainly controlled by the boiling region since the amount of heat transferred in the superheated steam region is relatively small), L_B is the boiling length, T_p is the primary temperature and T_{sat} is the saturation temperature.

Note that the above equations represent averaged quantities—a temporal averaging and averaging over the cross section of the generator. Actually, heat transfer coefficients and local temperatures are complex functions of space and time and depend on local flow rates, quality, etc. In order to make more precise evaluation of the heat transferred in the steam generators, one needs two-phase, three-dimensional, thermal–hydraulic computer codes which are now becoming available in the industry.

Another feature of the OTSG is its smaller size (compared with UTSG of comparable capacity)—mainly because it does not have moisture separators. The smaller size of the OTSG results, of course, in low secondary water inventory, which is about a sixth of the water inventory of a UTSG.

Since it was always expected that corrosion may be a problem in OTSG because the secondary water is completely evaporated, water chemistry was emphasized. All plants have almost full flow condensate polishing (powdered resin or deep bed system), and an all volatile chemical treatment of the feedwater. This treatment involves the addition of ammonia for pH control, and hydrazine for oxygen control. The specification for OTSG feedwater and UTSG blowdown during normal operation is given in table 3(a) and (b), respectively (Blomgren *et al.* 1980).

2.2. The U-tube Steam Generator (UTSG)

The U-tube steam generator is installed in a wide variety of commercial NSSS, from the early 1957 90-MWe Shippingport 4 loop system, to new 1300-MWe plants. Two typical systems are characterized in the following table:

	Surry	Westinghouse Model 414
Rated power (MWe)	822	1300
Rated heat output (MWth)	2441	3819
System pressure (bar)	153	153
Primary coolant flow rate (10^6 kg/h)	45.3	67.9
Primary coolant temperature (°C)	318.7	332.0
Number of loops	3	4
Number of pumps	3	4
Steam generators		
Number	3	4
Shell side design pressure (bar)	53.4	77.0
Steam flow at full load (10^6 kg/h)	4.8	7.9
Steam temperature (°C)	268.9	294.1
Feedwater temperature (°C)	225.4	239.4
Number of tubes	3388	6970
Diameter of tubes (mm)	22.2	17.4
Heat transfer area (m^2)	4784	7665

The general arrangement of the UTSG is given in figure 4.

Reactor coolant enters the steam generator at the inlet nozzle (on the bottom left-hand side of figure 4) and enters the tube bundle in the hot leg, completing the U-bend through the cold leg to the primary outlet.

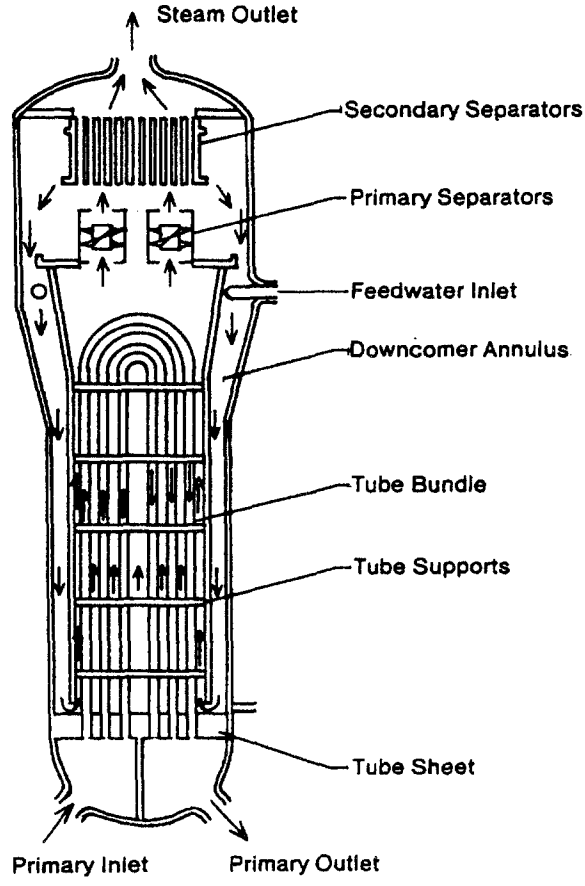

Figure 4. Recirculating steam generator.

Feedwater enters the side of the shell. It flows down through an annulus just inside the shell (downcomer), where it mixes with water coming from the separator deck. The water enters the heating surface (tube bundle) at the bottom and increases in quality as it rises through the steam generator. The steam–water mixture enters the steam–water separators (where steam is passed through to the driers and then to the steam nozzle) and the water is recirculated, through the downcomer, to the bottom of the heating surface.

The shell, outside of the tubes and the tubesheet form the steam production boundaries. Within the shell, the tube bundle is surrounded by a wrapper (or shroud). The first steam generators were made with stainless steel tubes (18 Cr, 10 Ni, 2 Mo). For better heat transfer performance, the tubes have been primarily made of Ni–Cr–Fe alloy 600. In Kraftwerk Union (KWU) and later B&W/AECL designs (Babcock & Wilcox/Atomic Energy of Canada Limited), the tubes have been made of alloy 800. The mill-annealing conditions vary among the manufacturers, while B&W/AECL have used stress-relieved (680°C/8 h) tubing for their alloy 600 tubed steam generators. Some of the more recent designs using alloy 600 tubing have thermally treated tubing (704°C/15 h) to improve resistance to stress corrosion cracking. Later designs and recent replacement units use Inconel 690 almost exclusively.

The tube support structures for most of the early units were made of carbon steel, while later units have switched to type 405, 409 and 410 stainless steels for additional corrosion resistance. Type 347 stainless steel has always been used for KWU steam generator tube support structures.

Early units used tube support plates with drilled holes [figure 5(a) and (b)], plates with broached holes [figure 5(c)] and lattice bars or egg crates [figure 5(e)]. When the drilled hole support plates were found to promote accumulation of corrodents, they were changed to a quatrefoil design hole with lands [figure 5(d)] or to a lattice support structure [figure 5(e)]. The U-tube region of the tube is additionally supported by antivibration bars. Vents, drains, instrumentation nozzles and inspection openings are provided on the shell side of the units.

The UTSGs are characterized by a widening of the shell by about 2/3 of the height of the steam generator. This is done in order to increase the area available for the separators at the separator deck.

In the UTSG there is always a water level in the downcomer in order to balance the pressure losses of steam–water mixture as it flows through the tube bundle. The pressure drop in the tube bundle is due to friction along the tubes, pressure drop at the tube support plates and separators, acceleration of the flow and hydrostatic head. Quality in the downcomer, e.g. steam bubbles, reduces the density and thus the available head substantially. This can be a result of imperfect separation of steam and water at the separators and is termed carryunder.

The ratio of flow rate of the steam–water mixture which flows through the steam generator tube bundle to the flow rate of steam out of the steam nozzle is called the circulation ratio. It is desirable to maintain a high circulation ratio (maybe over 5) to reduce concentration of chemicals, debris, etc., in various places in the steam generator. Current steam generators frequently have circulation ratios of around 3 at full load—which is probably one of the causes of the difficulties with these units. The thermodynamic quality of the water–steam mixture at the top of the bundle is about 17–33% when it enters the steam separators, which corresponds to a circulation ratio in the range of 6:1 to 3:1. As the load decreases, the circulation ratio increases. The pressure on the secondary side is about 7.5 MPa. The primary coolant flows through U-tubes at a pressure of about 15.0 MPa. It enters the steam generator at about 310–327°C and leaves at about 257–288°C. At the primary inlet, the temperature difference across the tube wall is about 36–50°C corresponding to a heat flux of 315–442 kW/m^2. At the primary outlet or cold side, the temperature difference between the primary and secondary sides is about 11–14°C corresponding to a heat flux of about 94 kW/m^2. The Westinghouse, Combustion Engineering, Kraftwerk Union, Framatome and Mitsubishi designs have comparable operating parameters, while the Babcock & Wilcox/Atomic Energy of Canada Limited (B&W/AECL) design operates at lower temperatures and pressures.

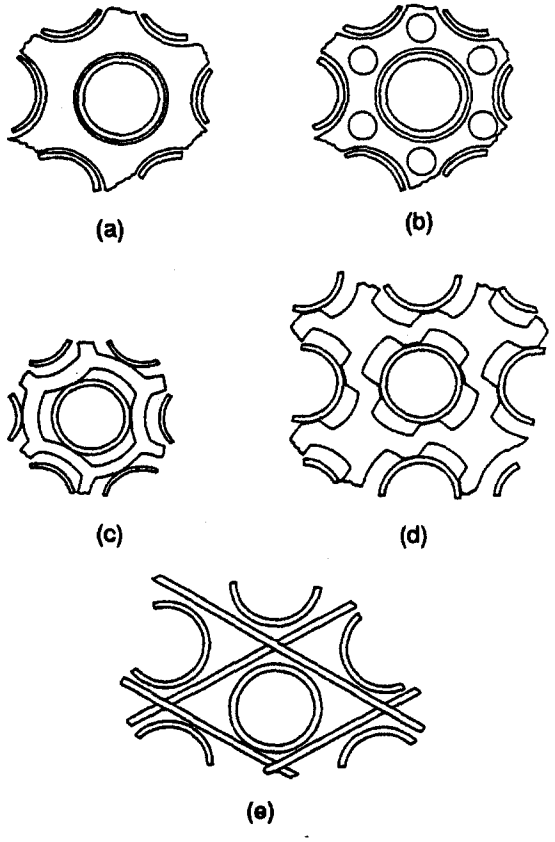

Figure 5. Sketches of some support plate hole designs. (a) Drilled, without flow holes; (b) drilled, without flow holes; (c) broached-trefoil; (d) broached-quatrefoil; (e) egg crate.

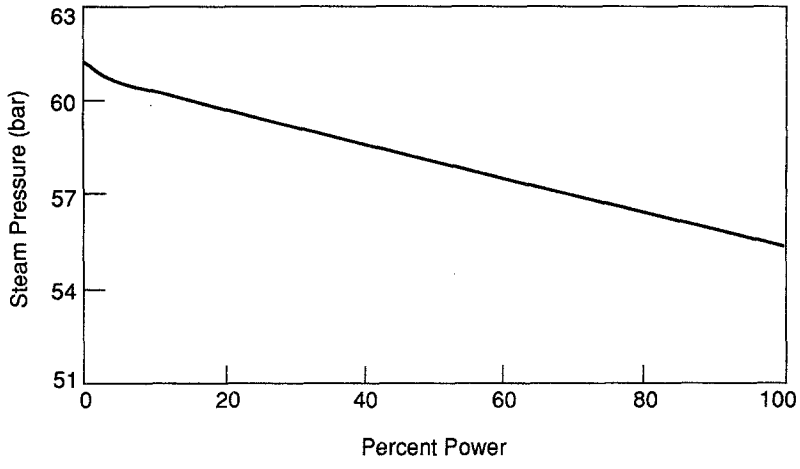

Figure 6. Steam pressure variation with power generation for a U-tube steam generator.

The steam pressure variation with power generated is depicted in figure 6.

3. DESIGN OF STEAM GENERATORS

3.1. General

The design of steam generators is a complicated procedure which involves many steps, iterations and interaction with other components of the system.

The NSSS, as part of the power station, is designed to minimize the power cost. This consideration is subject to many constraints—the primary one being safety. Other constraints are imposed by availability of major equipment (e.g. primary coolant pumps), manufacturing capabilities (e.g. can vessel be fabricated), shipping consideration, etc.

Thus, the design of the steam generators is subject to many outside constraints and requirements. For example, the primary fluid conditions (i.e. temperatures, allowable pressure drop in the steam generator) is determined mostly by the reactor design and availability of pumps. The performance requirements, i.e. steam pressure, temperature and flow rates, are determined mostly by the turbine design and as part of the system performance. It follows, therefore, that the tube bundle size (namely, the required heat transfer area as well as allowable pressure drop of the primary fluid) is determined by system considerations. Typically, steam generator vendors will get these specifications (termed functional design description) from the group dealing with the design of the system and with optimization of the power cost.

The first step in a design of a steam generator would generally be the preparation of layout drawings which include the basic configuration and sizing of the steam generator. These drawings are prepared after preliminary structural, mechanical and thermal–hydraulic designs.

The preliminary structural design is performed in the U.S., for example, in accordance with the ASME Boiler and Pressure Vessel Code, Section III. Also, steam generators, as with all power plant components, are required to be designed to withstand various accident situations. For steam generators, these consist of the following conditions:

- Small steam-line break, loss of feedwater, turbine trip, etc.
- LOCA (loss of coolant accident)
- MSLB (main steam-line break)
- SSE (safe shutdown earthquake).

The preliminary design may be concluded by a design review where it must be shown that the proposed (preliminary) design satisfies the functional design description and is in compliance with plant control and safety criteria.

Detailed design includes detailed structural and thermal–hydraulic analyses and studies, and is later used to prove to the customer and regulatory agencies that the steam generator design is in compliance with the ASME code, NRC regulations or the regulatory bodies of the country, etc.

Some of the more detailed design objectives may be as follows:

- Provide for reduced residual stresses in the U-tubes
- Provide for reduced tube sheet deflection due to operation-pressure differences
- Provide for reduced residual stresses in the tubes at the end of the tube expansion (at tube sheet)
- Eliminate tube-to-tubesheet crevice
- Qualify all materials for continuous steady-state operation reactor coolant temperature of 343°C
- Use tube material which minimizes the potential for stress corrosion crackiang (SCC) in primary reactor coolant and which minimizes wastage, pitting, SCC and other forms of corrosion on the secondary side
- Provide for sludge collecting regions which are outside the tube bundle region and preferably not on a hot surface
- Minimize flow stagnation regions throughout the tube bundle in order to minimize concentration of chemicals
- Limit flow induced vibrations and fretting to an acceptable level
- Provide for moisture content in the steam at the SG outlet, less than 0.1–0.25 wt%, at full load and at 20 bars below the nominal full load
- Prevent water hammer
- Select tube material and dimensions so that tubing leak-before-burst is assured under the maximum fault pressure differential, with an allowance for wall thinning
- Select tube support material so as to eliminate or reduce growth of oxide which might cause tube denting

3.2. Thermal–Hydraulic Design of Steam Generators

3.2.1. General

Boiling heat transfer and two-phase flow are complex subjects even for idealized conditions (see Hetsroni 1982). For conditions such as encountered in steam generators, modeling is very difficult. As a result, empirical correlations are used and mostly only averaged quantities are calculated. A typical design procedure for an OTSG is given in an ORNL (Oak Ridge National Laboratory) design guide (1975).

The U-tube steam generator has four main regions. The first includes the U-tube zone, where heat is added to the secondary fluid and boiling occurs. The second is the riser (see figure 4), the zone between the tube bundle and the separator deck. The riser increases the natural circulation driving force. Above the riser is the moisture separation region where saturated water is removed from the steam and returned to the top of the downcomer where it mixes with cold feedwater. The subcooled fluid then flows to the bottom of the downcomer to complete the circuit. The natural circulation driving force is provided by the difference between the density of the water in the downcomer and that of the steam–water mixture in the heating zone and riser.

There is a corresponding circuit in the OTSG, less the separators.

The driving force for the natural circulation flow is resisted by the pressure losses. There are pressure losses in all regions described above. Of these, the single-phase pressure drop is fairly straightforward to calculate using well known correlations.

The pressure drop in the tube support plates and U-tube region depends largely on the geometry and is, therefore, specific to any particular design. Mostly, the calculations are based on loss coefficients which are determined by the various vendors experimentally. The same is true for the steam separators.

3.2.2. Computer codes

Computer codes are used for thermal and flow analysis of steam generators. The overall analysis encompasses the bulk properties and the local properties. Bulk properties include the primary side flow and temperature distribution, distribution of flow exiting the tube bundle, circulation ratio and feedwater distribution. Local properties include secondary side distributions of pressure, velocity, temperature, quality and void fraction. Thermal and hydraulic conditions within crevices (support plates and tubesheets) and the peripheral gap between the edge of a support plate and the shroud may also be considered local properties.

The overall performance of the steam generator, namely the ability to transfer the required amount of heat from primary to secondary coolant, has never been an issue. The individual components of the overall heat transfer coefficient—the inside tube convection coefficient, heat conduction through the walls and the outside tube convection coefficient—are well known. The primary water on the inside of the tube is very clean (no fouling) and the sludge (usually magnetite with some copper) that sometimes forms on the outside of the tube does not significantly affect the boiling coefficient. In the case of the OTSG, the upper portion of the bundle operates through

the nucleate boiling into the superheated region, but again these coefficients are generally well known.

However, it is desired to be able to calculate the local conditions as accurately as possible since many of the problems discussed above are related to the thermal and hydraulic conditions. Tube vibration resulting in fretting, settling of solids in low-velocity regions of the tubesheets of most plants, flow stagnation that could lead to flow starvation and corrosion, overloaded primary separators and economizer water hammer might be avoided if accurate three-dimensional flow calculations were performed and used. Thermal–hydraulic computer codes provide the analysis tool necessary to help resolve steam generator problems. Code analyses may also be used to optimize new designs.

In 1977, at the inception of the Steam Generator Owners Group I (SGOG) at EPRI, thermal–hydraulic codes for steam generator analysis were relatively limited. Most of these codes were new and not yet verified against experimental data. The three-dimensional codes that existed or were under development were revised and further developmental effort was expanded. Most of the codes were eventually superceded by ATHOS and PORTHOS, which were developed for EPRI. A brief description of the codes is given below.

The CALIPSOS (Fanselau *et al.* 1980, 1981; Thakkar *et al.* 1981) code is a steady-state, three-dimensional, homogeneous two-phase flow computer code that was developed for Combustion Engineering Incorporated. It is based on the distributed resistance concept. That is, it treats the secondary side as a porous medium in which the transport equations apply. The tubes, baffles and other objects in the steam generator are described in terms of porosity β. These solid objects provide flow resistance, which may vary with position and direction. For a homogeneous secondary two-phase fluid, three momentum equations, one continuity equation and one energy equation are solved by the code.

The THIRST code (Carlucci 1980; Inch 1981; Carver 1982), which has the same features as the CALIPSOS code, was originally developed for Atomic Energy of Canada Limited. The code calculates the flow in the downcomer as well as the flow in the tube region, the expansion region and the separator region.

The computer code THEDA-1 (Oberjohn *et al.* 1982) was developed for Babcock & Wilcox to calculate thermal–hydraulic conditions within the B&W once-through steam generator. THEDA-1 is based on a quasi-continuum model of the three-dimensional, two-phase flow of the secondary or shell-side fluid of the OTSG. The tube bundle and tube support plates are represented as porous media with distributed resistance to flow and heat transfer. With this approach, it is possible to model a 15,000-tube OTSG, including local features such as tube support plates and untubed inspection lanes. The equations for THEDA-1 are the same as those used for the later version, THEDA-2.

Extensive reformulation of the THEDA-1 code led to the THEDA-2 code. THEDA-2 is capable of analyzing both recirculating steam generators and once-through steam generators. In addition, the flexible structure of THEDA-2 allows the code to be used to analyze other steam generator designs, such as a helical tube bundle design, with a minimum of computer code modifications.

THEDA-2 solves a finite-difference approximation to the three-dimensional conservation equations for mass, momentum and energy. These equations are formulated in a cylindrical co-ordinate system. The structure of the code and the numerical solution algorithm employed in the code allow very large and detailed models of a steam generator to be constructed and solved efficiently. The code has been successfully verified against experimental data. The verification focused on the effect of blocking the tube-free inspection lane. This open lane creates a path of low resistance to flow. The path is believed to permit liquid droplets with highly concentrated impurities to be carried to the upper tubesheet by the steam. It is postulated that these droplets have dried out at the upper tubesheet; that the impurities cause corrosion; and that this corrosion has contributed to the tube cracking that has occurred at that location. To divert the flow back into the tube bundle to cause complete evaporation of water droplets prior to further concentrating the impurities, lane blockers have been considered.

Proper placement of the lane blockers and assessment of their success depend on predictions of the THEDA computer code. To gain confidence in the code's predictions, model tests were used to verify the code. These tests included isothermal air (Carter *et al.* 1982), heated air (Carter &

Promey 1982) and a 30-tube model with prototypical steam–water conditions (Carter *et al.* 1983). The steam–water model consisted of 30 tubes and 15 tube support plates, each having 37 trefoil-type broached holes. The extra seven holes formed the untubed zone across the center of the cross section to produce the desired open lane. The tube bundle was enclosed by a hexagonal shroud within 20 cm schedule 160 pipe that extended from the lower tubesheet to the upper tubesheet. The ranges of tested variables were as follows:

- Simulated power level, 65–100%
- Secondary side pressure, 6.2 MPa
- Feedwater flow rate, 1–2.2 kg/s
- Feedwater temperature, 264–274°C
- Primary side pressure, 14.5–15.0 MPa
- Primary inlet temperature, 312–317°C
- Lane conditions, blocked and unblocked.

Data from these studies led to minor modifications in the way an OTSG is modeled with the THEDA-2 code. Figure 7 illustrates the good agreement between THEDA code predictions and laboratory measurements following minor adjustments to the code. Shown are the predicted and measured profiles of primary side water temperature and secondary side fluid temperature in the tubes adjacent to the lane. Primary and secondary fluid temperature was generally predicted within 2–3°C throughout the 30-tube model steam generator.

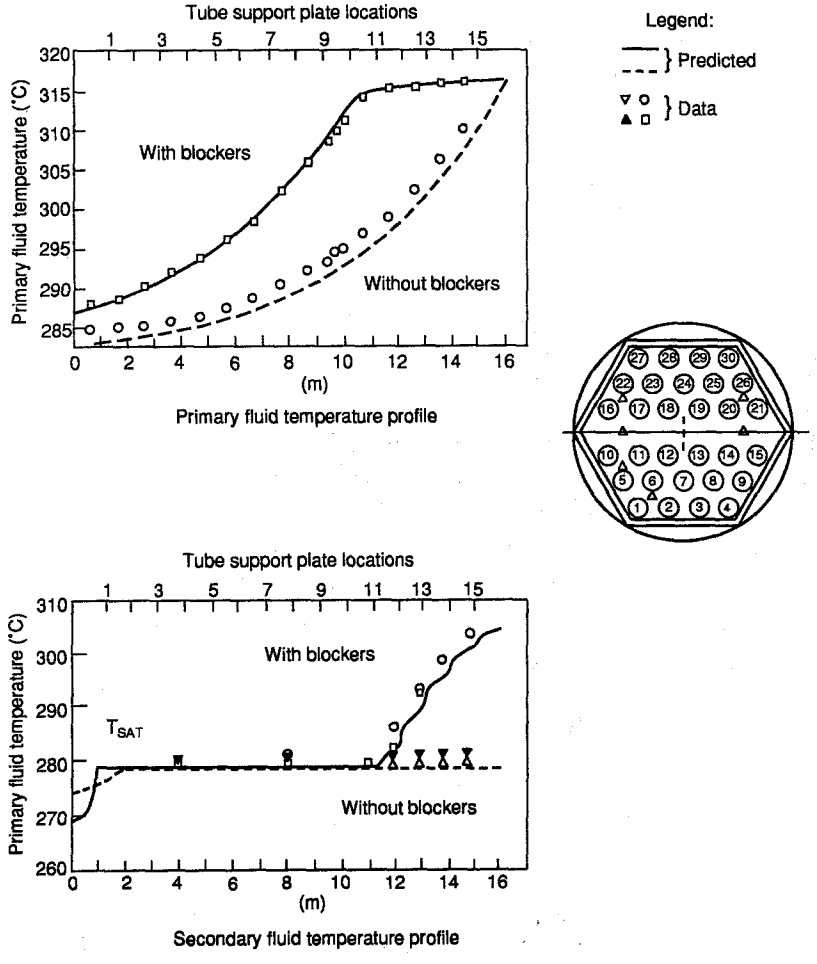

Figure 7. THEDA predictions of lane blocker effect at tube 14 at 100% load.

The computer program ATHOS (Analysis of the Thermal Hydraulics of Steam Generators, Singhal *et al.* 1984 and Singhal & Srikantiah 1991) is capable of simulating the geometry and internal structure, including tube bundle, tube support plates and baffles. An earlier (non-released, three-dimensional, steady state and transient) version of the ATHOS code was named URSULA during code development.

The important features and assumption of the ATHOS code are as follows:

(1) Options for polar and Cartesian co-ordinates with one-, two- and three-dimensional analyses are available.
(2) Options for two-fluid models, in which steam and water phases can be assigned different temperatures and velocities are available.
(3) Mass, momentum and energy equations for the mixture of liquid and vapor plus an algebraic equation for the relative velocity are used for flow description.
(4) Diffusion and turbulence effects are considered negligible in comparison with the effect of distributed resistances.
(5) Saturated properties of liquid and vapor are calculated as functions of a single reference pressure, the dome pressure.
(6) The primary side flow is treated as single phase and incompressible.
(7) The downcomer is represented by two point models, one for each half (hot and cold sides).
(8) The steam dome is also treated by a point model.
(9) For U-tube steam generators, either the heat load or the primary fluid inlet temperature can be specified as a boundary condition.

The computation domain normally includes the whole SG, from the tube sheet to the separator deck. Normally, the separators are not included in this computation. Actually, due to geometrical symmetry of the SG, one can simulate only half of the SG, as in figure 8. The domain is then divided into typically, a few thousand control cells. Each control cell may include a number of tubes and/or other solid objects, such as TSP etc.

For computations of steady state operation, the following boundary conditions are imposed (Singhal & Srikantiah 1991):

(1) Mass flow rate of primary fluid, $\dot{m}_p$.
(2) Mass flow rate of feedwater added into the downcomer, $\dot{m}_{fd}$.
(3) Mass flow rate of feedwater added (directly) into the economizer, $\dot{m}_{fe}$.
(4) Feedwater inlet temperature, T_{fd}.
(5) Carry-over fraction, or mass quality of steam leaving the dome, x_s.
(6) Carry-under fraction, or mass fraction of steam entrained in the recirculating water flowing from the dome to the downcomer, x_w.
(7) Pressure in steam dome, p_d.
(8) Height of the water level in the downcomer, h_{WL}.
(9) Fraction of the downcomer feedwater added to the hotside, f_{dh} [this implies that the fraction $(1-f_{dh})$ is added on the cold side].

The results of the three-dimensional thermal–hydraulic analysis also should include, in addition to local conditions, the following global parameters (Singhal & Srikantiah 1991):

(1) Circulation ratio, defined as the ratio of the total mass flow rate and steam flow rate approaching the separator deck.
(2) Liquid (mass) inventory in the tube bundle and riser section. Sometimes quantities such as liquid collapse level or liquid hold-up volume fraction are used as the indicators of liquid inventory.
(3) Liquid inventory in the downcomer.
(4) Temperature of the downcomer water at the entry to the tube bundle region.
(5) The inlet temperature of primary fluid, which is to be calculated when the total heat load is prescribed.
(6) In transient calculations, the primary inlet temperature is generally prescribed as a function of time, and the primary outlet temperature and heat load are calculated as a function of time.

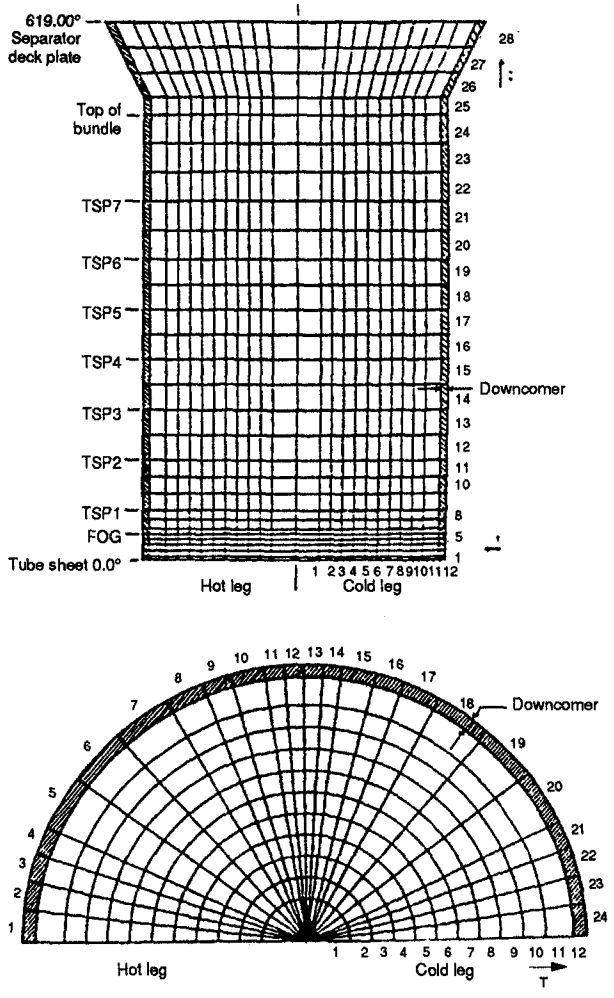

Figure 8. A sample computational grid for a UTSG.

The local thermal–hydraulic parameters of interest for UTSGs include the three-dimensional distributions of:

(1) Three velocity components of the steam and water phases.
(2) Mass quality and void fraction of the secondary side fluid.

Table 4. Three-dimensional thermal–hydraulics codes for steam generators

	Codes					
Features	ATHOS3	PORTHOS Mod-01	THEDA2	THIRST	FAUST	CAFCA-e
Developer	EPRI/CFD Res.	EPRI/JAYCOR	EPRI/B&W	AECL	KAIST	EDF
Status (existing or development)	E	D	E	E	D	D
Applicability	UTSG and OTSG	UTSG and OTSG	OTSG	UTSG	UTSG	UTSG
Co-ordinates	θ,r,z and x,y,z	θ,r,z and x,y,z	θ,r,z	θ,r,z	θ,r,z	θ,r,z and x,y,z
Transient	Yes	Yes	Yes	Yes	Yes	No
Turbulence	Yes	Yes	Yes	Yes	No	No
(Homogeneous, Algebraic slip, Two-fluid)	H.A	H.A.T.	H	H.A	T	H.A
Variable properties	Yes	Yes	?	?	?	Yes
Grid in downcomer	Yes	Yes	No	Yes	Yes	?
Dome model	Yes	Yes	No	No	Yes	No

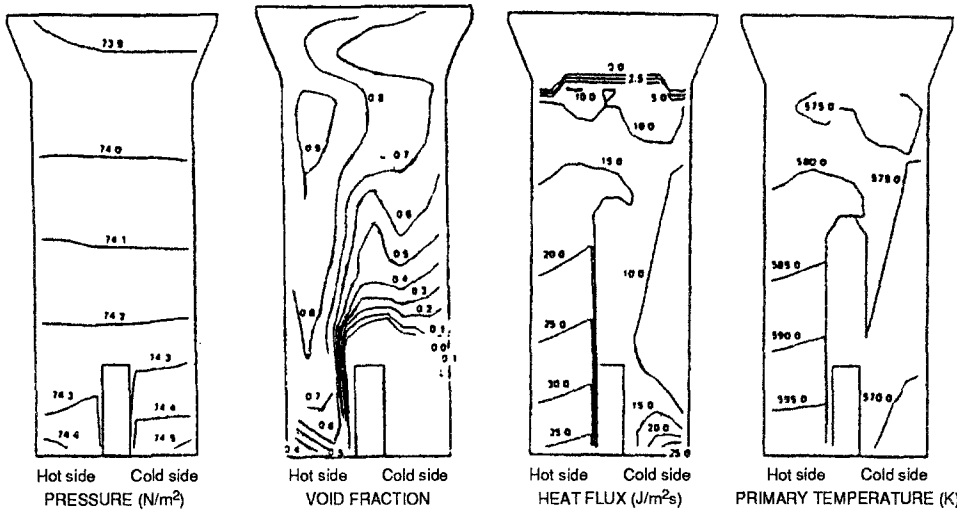

Figure 9. Distributions of some variables in a vertical plan $\theta = 45$–$225°$ of a UTSG.

(3) Enthalpy and temperature of the secondary side fluid.
(4) Heat flux to the secondary side fluid.
(5) Secondary side pressure.
(6) Primary fluid temperature.
(7) Tube-metal and mid-wall and/or outside surface temperature.
(8) Maximum tube-gap velocities normal to tubes (for flow induced vibration analysis).

The appropriate equations, continuity, momentum and energy, together with the closure laws and jump conditions, are solved numerically by standard computer codes, which were developed for various vendors or for EPRI. Some of these codes are listed in table 4. While most of these codes are proprietary, they are basically similar, i.e. they treat the SG as a porous medium. The major difference between the codes is in the form of the two-phase flow model used and in the solution scheme (implicit, semi-implicit or explicit). The ATHOS 3 code is probably the most widely used by the industry for thermal–hydraulic analysis of SG. It is well documented and probably the best validated code, since EPRI invested a considerable amount of money and efforts to do so. A description of the code, its features and validation can be found in Singhal & Srikantiah (1991).

Typical output of the code is depicted in figure 9, where distributions of pressure, void fraction, heat flux and primary temperature are plotted for a vertical plane $\theta = 45$–$225°$.

As discussed in Srikantiah & Kalra (1983), ATHOS code predictions compare reasonably well with measurements from the Frigg small test, the MB-2 medium test and the Electricité de France (EDF) full-size tests.

The Frigg facility (Hiestand & Thakkar 1984) consisted of a 36-rod electrically heated tube bundle, through which water flowed, and a gamma-ray densitometer system to measure void fraction. Each rod was 13.7 mm in diameter, had a heated length of 4.3 m and simulated full-scale boiling heavy-water reactor fuel elements. The rods were arranged around three concentric circles and enclosed in a 160 mm i.d. housing.

The ranges of variables covered by the comparison of ATHOS predictions to Frigg measurements were as follows:

- Pressure, 3.0–6.8 MPa
- Mass flux rate, 500–2000 kg/m^{2}s
- Average heat flux, 425–765 kw/m^2
- Inlet subcooling, 2–27°C
- Exit quality, 0.07–0.47.

Figure 10 shows a typical comparison of ATHOS predictions to Frigg measurements for void fraction. These and similar comparisons show good agreement between ATHOS and the experimental data.

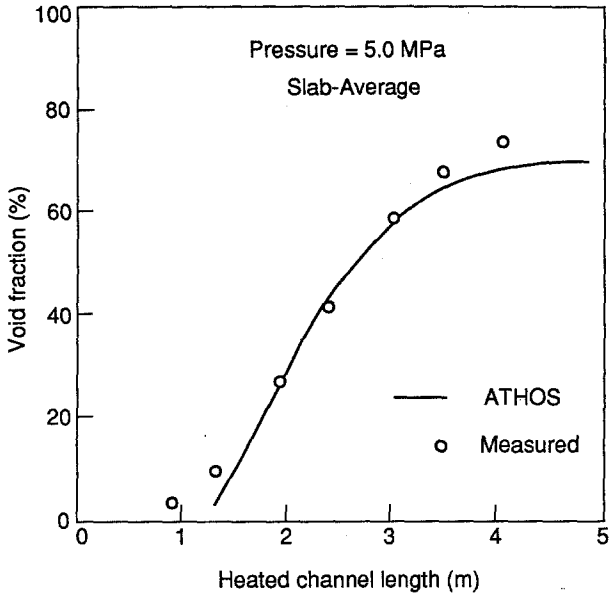

Figure 10. Verification of ATHOS with Frigg data.

The MB-2 test was a 1% (10 MW) power-scaled model of the Westinghouse Model F steam generator. The tube bundle is composed of 52 tubes arranged in a rectangular array having 13 tube rows and 4 tube columns. All tubes were fabricated from alloy 600 with the same outside diameter (17.5 mm) and wall thickness (1 mm) as the tubes in the Model F and are configured in the same 25 mm square-pitch array. The straight length of the tube bundle is 6.7 m, which is about 0.5 m shorter than in the Model F. The heat transfer area for the MB-2 is 39.8 m^2. As shown in figure 11, the MB-2 test section was instrumented for pressure drop, downcomer flow rate and fluid temperature (secondary and primary).

The ranges of variables covered by the comparison of ATHOS predictions to MB-2 measurements were as follows:

- Power level, 25–100%
- Pressure, 6.8–7.5 MPa
- Feedwater flow rate, 0.8–3.8 kg/s
- Feedwater inlet temperature, 154–227°C
- Exit quality, 0.076–0.35.

A comparison of the MB-2 secondary fluid temperatures with the ATHOS prediction is shown in figure 12. Both homogeneous and algebraic slip model options were used with a combination of different friction and heat transfer correlations available in the code. The agreement between the data and the ATHOS-2 predictions (for the algebraic slip model) is good.

An operational transient of a 30–100% load ramp at 5% per minute was also used for comparison with ATHOS. The results of the comparisons made with the homogeneous and algebraic slip models indicated that the ATHOS predictions compare reasonably well with the MB-2 measurements for both steady-state and transient tests.

For plant data comparisons with ATHOS predictions, steam generators of Westinghouse Model 51 design have been instrumented by EdF at the nuclear power plants Bugey 4 and Tricastin 1 (Procaccia *et al.* 1982). In addition to operational data, the following measurements have been made:

(1) Secondary fluid temperature and water sampling at eight positions along a diameter perpendicular to the tube lane, at a height of approximately 2.5 cm above the top surface of the tubesheet.

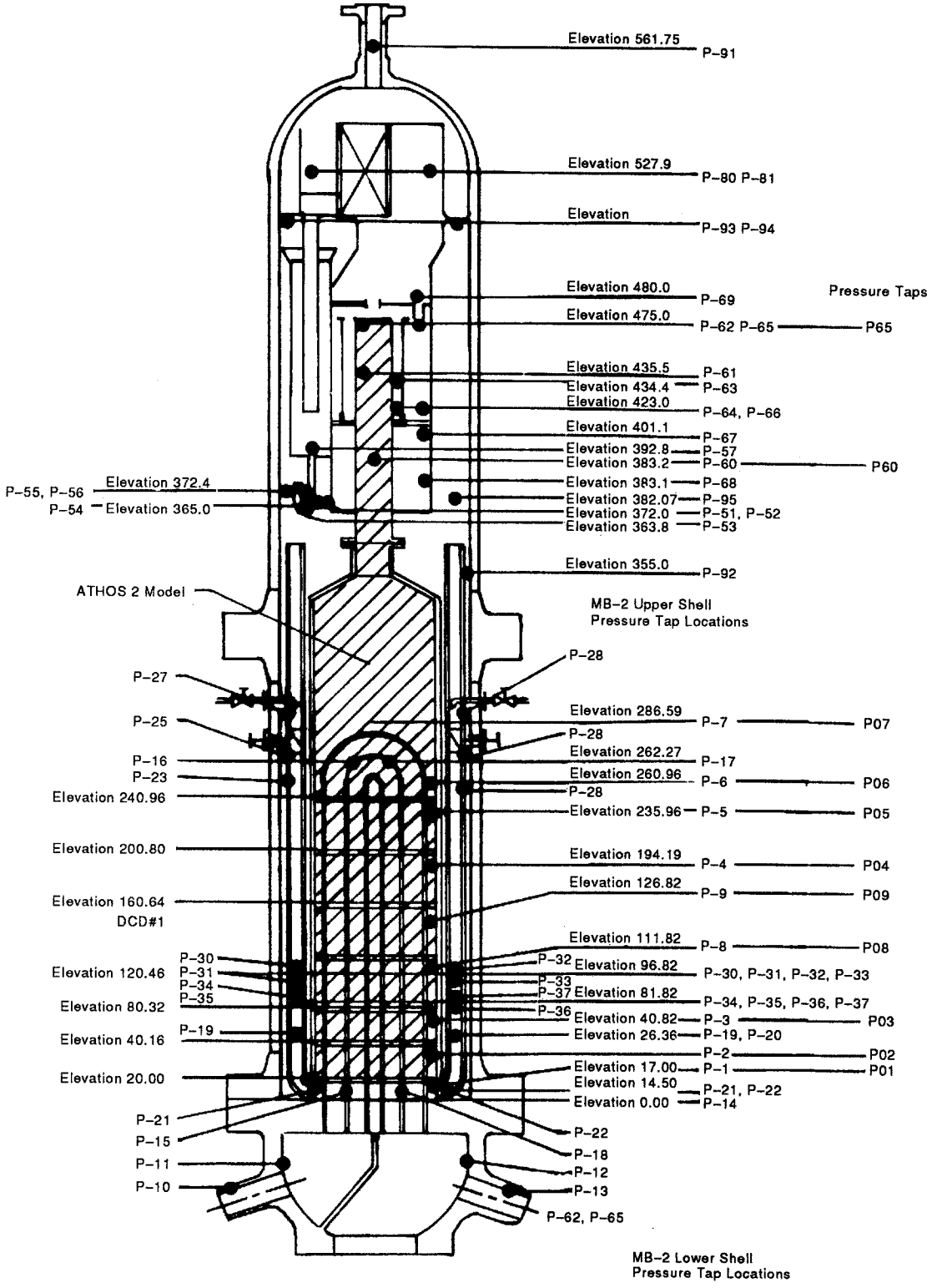

Figure 11. MB-2 and ATHOS-2 model, elevation view.

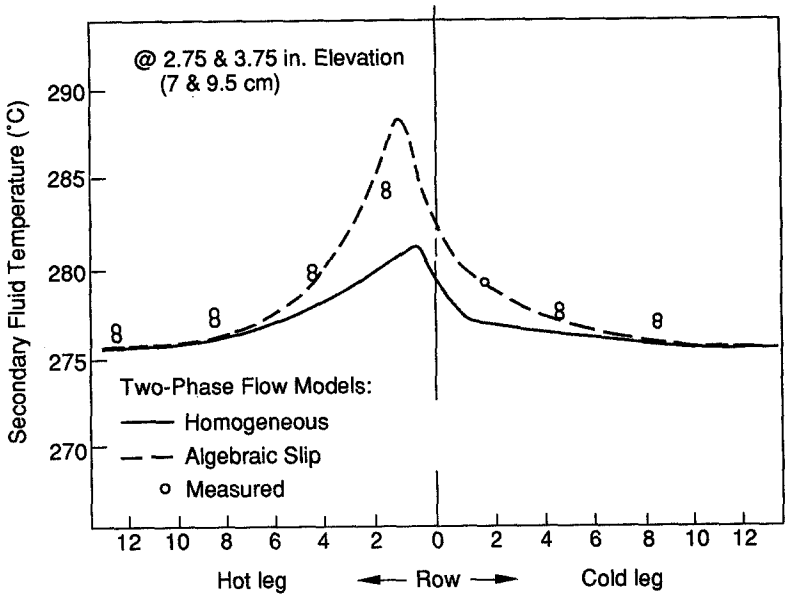

Figure 12. Comparison of ATHOS predictions and MB-2 measured secondary fluid temperatures at 50% power.

(2) Total and static pressure (Pitot measurements) and liquid temperature at eight circumferential locations within the downcomer at a height of 5.60 cm above the tubesheet.
(3) Metal temperatures on the steam generator outer shell at the same circumferential locations as in item (2) above, at heights of 5.60 and 891.4 cm above the tubesheet.
(4) Stress measurements on two legs of the U-tube bundle.

The measurements that are central to this comparison are the eight secondary fluid temperatures above the tubesheet and the circulation ratio, which EdF has evaluated from Pitot measurements made inside the downcomer.

The range of variables covered in these tests is as follows:

- Power load, 11–100%
- Secondary side pressure, 5.8–6.8 MPa
- Feedwater flow rate, 50–510 kg/s
- Feedwater inlet temperature, 162–221°C.

ATHOS predictions (Singhal *et al.* 1982) and measured (Procaccia *et al.* 1984; Wazzan *et al.* 1984) profiles for secondary temperature above the tubesheet for the Bugey 4 test are shown in figure 13. The degree of uncertainty in the secondary fluid temperature measurement, ± 0.5°C, is

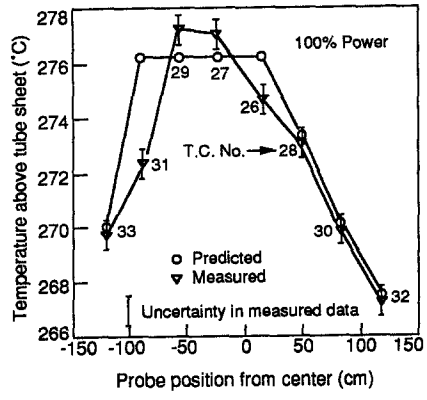

Figure 13. ATHOS prediction and Bugey 4 measurements.

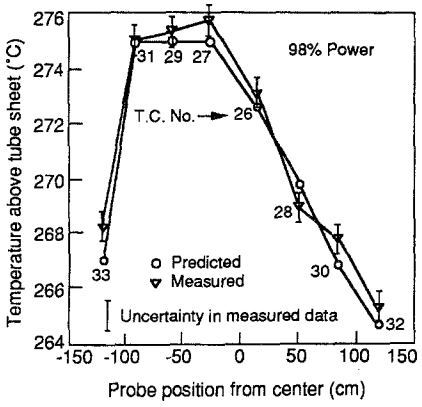

Figure 14. ATHOS predictions and Tricastin 1 measurements.

indicated by means of error bars. According to the figure, agreement with measured data is very good; at four of the eight probe locations, predicted data lie within the range of uncertainty of the measurements. Good agreement is also seen in the comparison of predicted and measured data for the Tricastin 1 unit in figure 14.

The plant operation transients of load rejection from 100% power were also analyzed. Again, the prediction of the transient response shows good agreement with the plant data.

Summaries of the good comparison of ATHOS-3 predictions and small-scale and large-scale data are presented in Singhal *et al.* (1984) and Keeton *et al.* (1988). Using ATHOS-3, the effects of tube plugging on local and global parameters are analyzed for a full-scale once-through steam generator (Keeton *et al.* 1986). The calculations indicate that, although the plugged tubes do not have any major effect on the overall thermal–hydraulic parameters, they do induce severe non-uniformities in the flow field. For example, over a small circumferential section, wet steam is predicted to be exiting radially to the steam outlet. (The unit is designed to produce 33°C superheated steam at the outlet.)

Two examples of how Kraftwerk Union of West Germany uses the ATHOS code in the area of steam generator thermal–hydraulics are given in Schwartz & Bouecke (1985). The first is the simulation of the Grafenrheinfeld steam generators. For this purpose, the ATHOS code has been adapted to the Grafenrheinfeld split-flow economizer design. Operational data recorded during commissioning of the plant are used as an input for the calculations. Moreover, locally measured pressure differentials and temperatures are applied to a parameter adjustment study with the intention of reaching optimal reproduction of experimental data.

The second ATHOS application presented is an analysis of the flow characteristics above the steam generator tubesheet. An axial flow tube lane blocking device and a flow distribution plate design are compared to the non-plate design. The design alternatives investigated are judged by their impact on the vaporization and low-flow-velocity zone above the tubesheet.

CAFCA is a three-dimensional code developed by EDF (Boivin *et al.* 1987). Similar to previous codes, this also considers the bundle as a porous medium, in which the equations are averaged. The control volume is made of liquid and solids, and is characterized by its porosity

$$\phi = \frac{\text{volume of fluid}}{\text{total volume}}$$

The equations are written in the normal fashion for the velocity v and pressure p with ρ the density, h the enthalpy, α_t turbulent diffusivity and E heat per unit volume, F interaction force per unit volume and ν_t turbulent kinematic viscosity:

—mass equation

$$\frac{\partial \phi \rho}{\partial t} + \frac{\partial}{\partial x_i}(\phi \rho v_i) = 0 \qquad [1]$$

—momentum equation (jth component)

$$\frac{\partial v_j}{\partial t} + v_i \frac{\partial v_j}{\partial x_i} = -\frac{1}{\rho}\frac{\partial p}{\partial x_j} + g_j + \frac{\partial}{\partial x_i}\left(v_t \frac{\partial v_j}{\partial x_i}\right) + \frac{F_j}{\phi\rho} \quad [2]$$

—energy equation

$$\frac{\partial h}{\partial t} + \frac{1}{\rho\phi}\frac{\partial}{\partial x_i}(\phi\rho h v_i) + \frac{h}{\phi\rho}\frac{\partial \phi\rho}{\partial t} = \frac{1}{\phi\rho}\frac{\partial}{\partial x_i}\left(\phi\rho\alpha_t \frac{\partial h}{\partial x_i}\right) + \frac{E}{\phi\rho} \quad [3]$$

In the above equations

—The mechanical energy term has been neglected for the energy equation.
—In lieu of the usual boundary conditions, the homogenization of the liquid and solids led to unknown source terms such as E, F and v_t, which need to be estimated by some means.

In the two-phase fluid the following assumptions were made:

—the pressures of the two-phases are equal
—the turbulence within each phase is negligible
—the accumulation of momentum and energy at the interface is negligible.

A system of six equations—three conservation equations for each phase—is obtained. If the two-phase mixture is in thermodynamic equilibrium, we get only four differential equations:

—mass conservation for the mixture
—momentum conservation for the mixture
—relative velocity equation $\mathbf{v}_r = \mathbf{v}_G - \mathbf{v}_L$
—energy conservation for the mixture.

The mixture properties are defined by the following relations:

- density: $\rho_m = \epsilon\rho_G + (1-\epsilon)\rho_L$, ϵ being the void fraction
- velocity: $\mathbf{v}_m = \frac{\epsilon\rho_G}{\rho_m}\mathbf{v}_G + \frac{(1-\epsilon)\rho_L}{\rho_m}\mathbf{v}_L$
- enthalpy: $h_m = \frac{\epsilon\rho_G}{\rho_m}h_G + \frac{(1-\epsilon)\rho_L}{\rho_m}h_L$
- vapor weight fraction (quality): $x_m = \frac{\epsilon\rho_G}{\rho_m} = \frac{h_m - h_L}{h_G - h_L}$.

Such a system—called the "two-velocity model"—contains several unknown terms which can hardly be modeled (interface velocity, interface friction, voluminal force exerted by solids on gas only or on liquid only). The computation is further simplified by replacing the relative velocity by an empirical correlation for the velocity ratio s from which the dynamic quality x is computed (x is the vapor flowrate to the total flowrate through some cross section)

$$X = \frac{sx_m}{1 + x_m(s-1)}$$

The average dynamic enthalpy of the mixture is now defined

$$h = Xh_G + (1-X)h_L$$

$$h = h_m + X_m(1-X_m)(h_G - h_L)\frac{s-1}{1 + x_m(s-1)}$$

with these definitions, the conservation equations are solved for a pseudo-homogeneous single-phase fluid. In addition, in the code are given the closure relations for the forces exerted by the solids on the fluid F, and the volumetric power dissipation by the solids E and the two diffusion coefficients α_t and v_t. Since the closure relations are based on empirical correlations, code verification was performed by comparing the computations to experimental studies. EDF performed these experimental studies on two loops—Medoc and Frida.

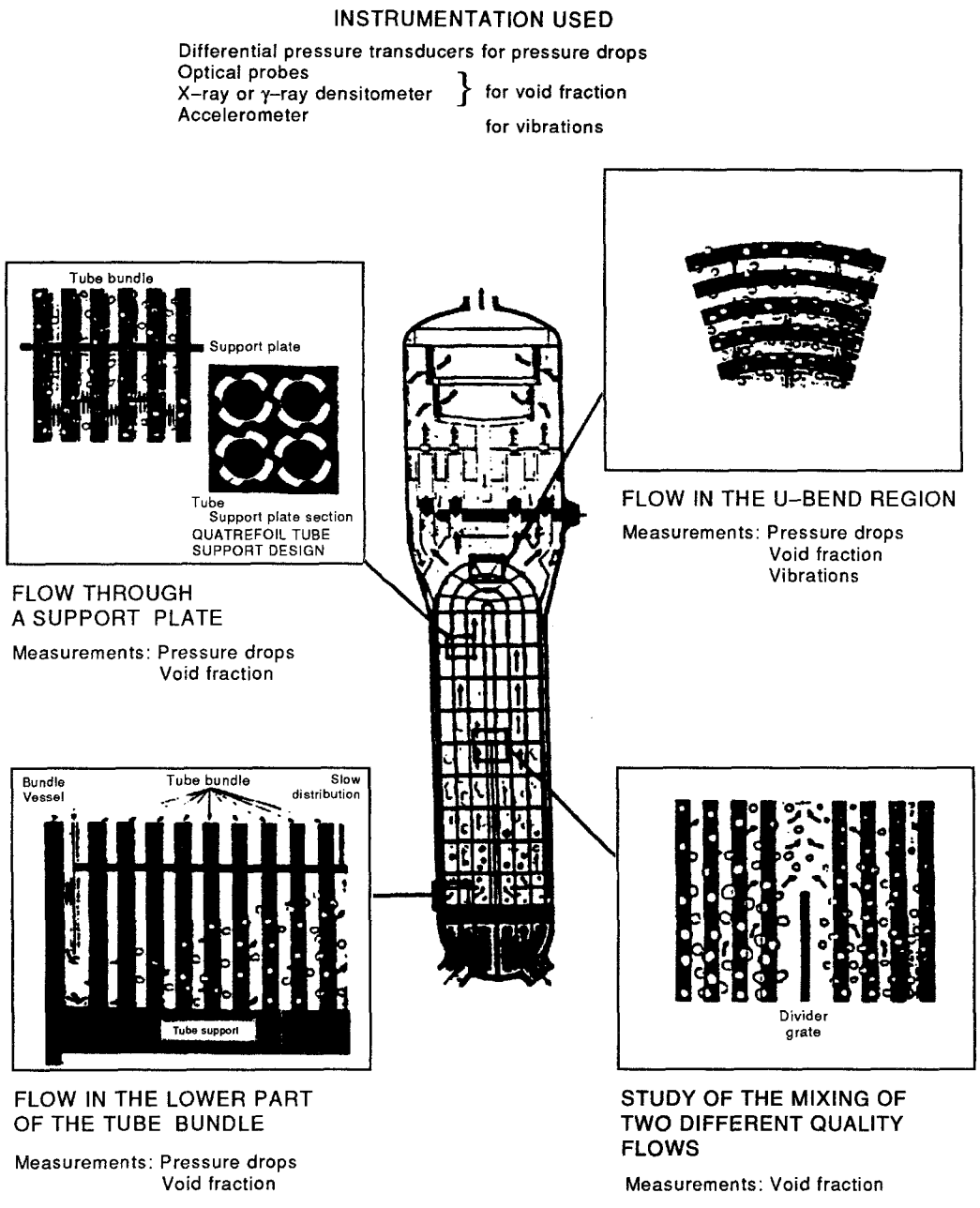

Figure 15. Measurements required for validating multidimensional codes on the Medoc loop.

In the Medoc loop pressure and void fraction were measured when flow was about orthogonal to the tube bundle (triangular and square pitch). A mixture of R-13 vapor and liquid was used in the loop at 0.75 MPa (which has a density ratio $\rho_L/\rho_G = 20$, the same as water at 7.0 MPa). Some of the measurements are described in figure 15 and results for the pressure drop multiplier are shown in figure 16.

In the Frida loop velocity ratio and pressure drop were measured in boiling fluid flowing orthogonally to a tube bundle. The fluid used in this loop was R114, which allows for boiling simulation at much lower power input than water (the loop has a 500 kW input). An example of the results obtained from this loop is depicted in figure 17, where the pressure drop multiplier is plotted versus the quality, and where the data are compared to various models.

The CAFCA code was further verified by comparing the computations to thermal–hydraulic measurements which were performed on one of the Paluel steam generators (Tincq *et al.* 1988). The mesh used in the computations was 8 radial × 20 circ. × 33 axial and was limited only to the

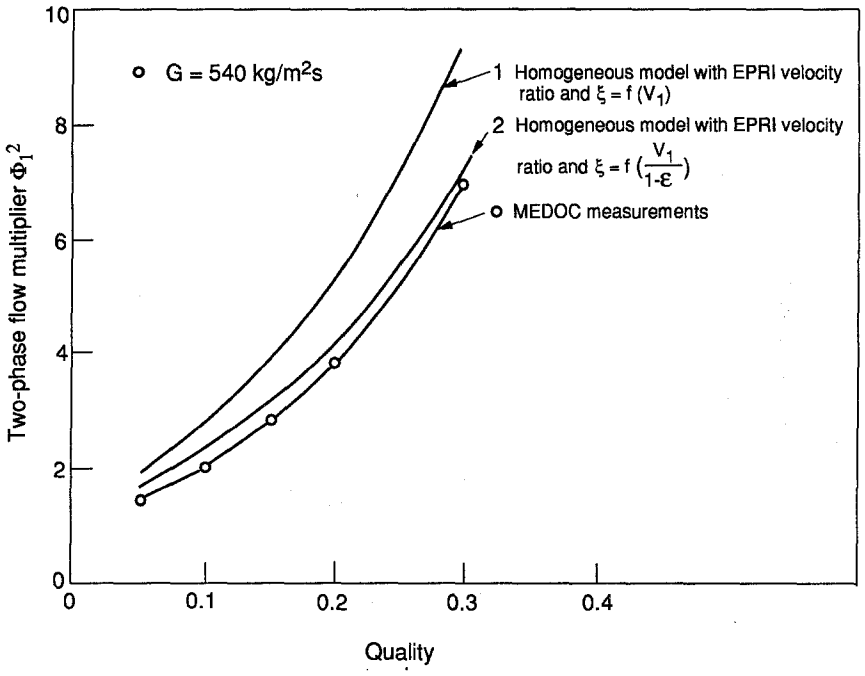

Figure 16. Two-phase flow pressure drop multiplier vs quality. Comparison between Medoc measurements and calculations.

Table 5. Paluel data used for CAFCA computations

Tube bundle area (porosity)	0.6212
Peripheral area (porosity)	0.7631
Tube lane area (porosity)	0.7295
Form of loss coefficients	
Support plates	
Tube bundle area	3.0
Peripheral area	3.0
Tube lane area	10.0
Distribution plate	
Tube bundle area (inner)	13.8
Tube bundle area (outer)	46.0
Peripheral area	46.0
Tube lane area	1000

tube bundle below the U-bend region. The inlet velocities and enthalpies from the downcomer were used as boundary conditions, together with stipulating a uniform pressure at the exit. The porosities which were used in the computations are listed in table 5. The results of computation and measurements showed satisfactory agreement (Olive 1982).

The form of loss coefficients in table 5 are given in terms of the number of dynamic head lost with the flow flowing through the component.

The calculations were performed for three power levels, as shown in the table below:

Primary conditions	100.9%	62.5%	32.6%	
Pressure	158.2	158.0	158.1	bar
Flow rate	4709	4719	4702	kg/s
Inlet temperature	327.3	315.8	306.3	°C
Secondary conditions				
Outer pressure	72.3	75.5	77.2	bar
Average inlet enthalpy	1208.3	1233.3	1255.0	kJ/kg
Downcomer flow rate	2278	2253	1841	kg/s

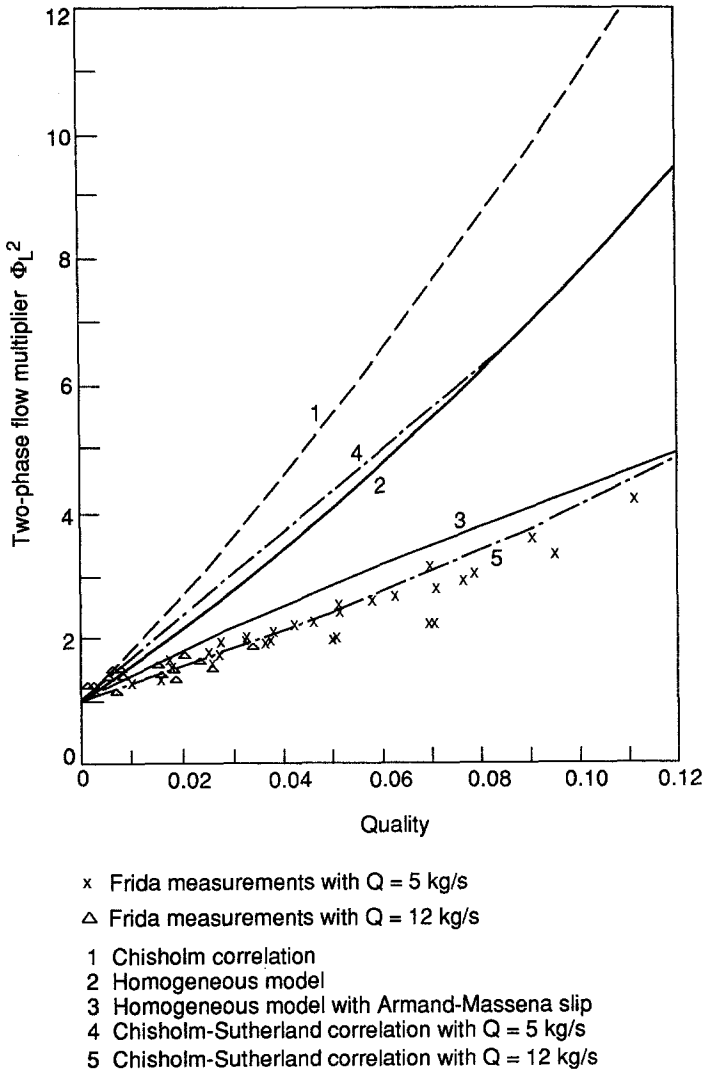

Figure 17. Two-phase flow multiplier vs quality: comparison between Frida measurements and calculations.

The temperatures on the tube sheet and on the flow distribution plate were computed and measured and comparison between the two can be seen in figure 18(a–c).

It seems that agreement between computations and measurements is good in the periphery of the SG, but less satisfactory closer to the center of the hot leg side—where more boiling occurs. It is also possible that the tube lane is not modeled well (it is quite difficult to model it in cylindrical co-ordinates). The discrepancy is attributed by the authors to not having modeled the void fraction in the subcooled boiling region.

The French CEA has developed a new three-dimensional code to model the thermal–hydraulic behavior of steam generators. The salient features of that code are the following:

- *three or four equation model* with separate equations for gas and liquid momentum,
- the use of an *object oriented language* which allows to combine, without limit, any kind of physical modeling, number of equations, type of algorithms, internal device representation and computational mesh; the code is divided in a hundred or so independent functionalities (named operators) which can be run independently by the user if desired,
- the *finite element method* for space discretization which allows a generality of shape representation with cartesian co-ordinates,
- *geometric meshes of internal structures* such as tube bundle, distribution baffle, tube support plates, anti-vibrating bars and separator deck,

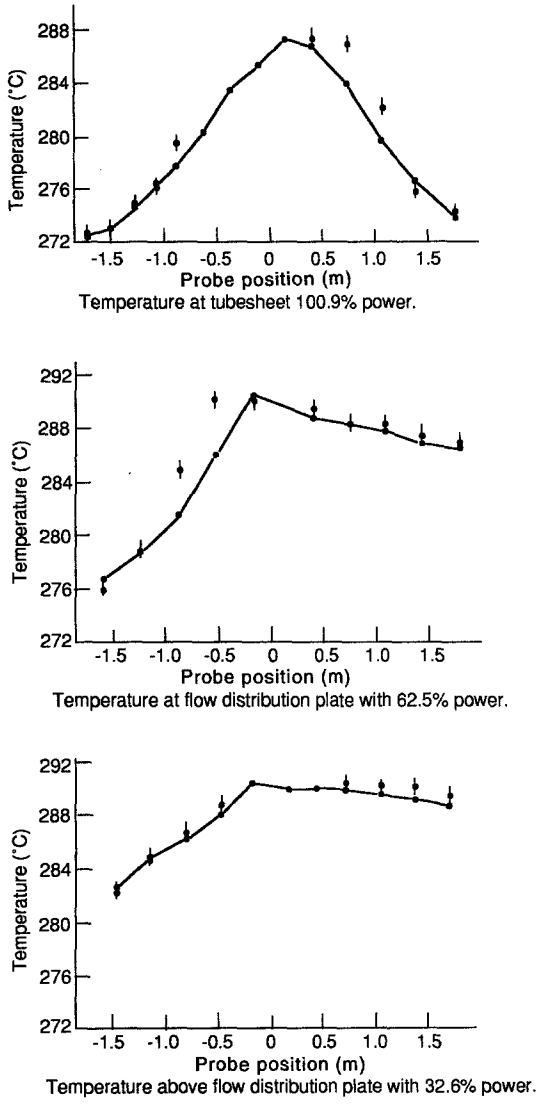

Figure 18. (top) Paluel—100.9%–Z-Probes–CAFCA 4.2, (middle) Paluel—62.5%–X Probes–CAFCA 4.2, (bottom) Paluel—32.6%–X Probes–CAFCA 4.2.

- an *automatic geometric intersection* between these devices and the computational mesh which is performed to determine porosity fields, local tube or plate orientations, cell transparency; in these conditions the modifications in steam generator design or mesh refinement are easily done with minimum engineering work, which is very interesting for designers,
- an *easy coupling with a tube vibration analysis* developed in parallel by CEA (GERBOISE code),
- local conservation equations for two-phase flow are volume averaged and lead to three-dimensional governing equations (mass, momentum in each direction and enthalpy balances for a two-phase mixture) which are solved on an equivalent solid–fluid medium defined by its volume porosity. An additional equation is solved for primary liquid temperature which provides the heat transfer term in the secondary fluid enthalpy equation,
- finite element analogues of governing equations are derived: mass flux components, enthalpy are calculated at the nodes of the mesh whereas pressure and primary temperature are calculated at the center of each element; three-dimensional eight-node elements are employed.

The qualification work is underway using as major data bases:

—CLOTAIRE
—MEGEVE
—Frida/Medoc (EdF)
—Field data.

ATHOS-3 is recommended for thermal–hydraulic analysis of PWR steam generators at this time. However, a new code, PORTHOS, has been developed (Chan *et al.* 1986) and is now being evaluated.

PORTHOS is a computer code for calculating three-dimensional steady-state or time-dependent two-phase flow in porous or non-porous media. It employs a finite-difference technique to solve the complete set of two-fluid equations, i.e. the "six-equation" model, which includes two mass conservation equations, two momentum equations, two energy equations, as well as constitutive equations to effect closure of the system and empirically represent the interaction between phases. The use of volume porosity and surface permeability allows the treatment of complex geometry. The six-equation model can be modified to include other familiar models as subsets, such as the homogeneous equilibrium model (HEM) and the drift flux model. The only part of the code requiring change is the coefficient matrix which represents the entire equation set. This flexibility and ease of changing the equations makes it a very useful tool for testing various two-phase flow models in a single algorithm. Other features of PORTHOS include three different configurations of recirculating U-tube steam generators, built-in options for heat transfer correlations, choice of polar cylindrical or cartesian co-ordinates, detailed flow pattern in the downcomer and general equations of state for each phase. Chan *et al.* (1986) present the results of comparisons with two sources of experimental data: the 8-MW FRIGG loop experiment and the Bugey 4 steam generator test. Calculations of the FRIGG experiment by PORTHOS, in terms of void fraction distribution, are in good agreement with measurements. Verification against the EdF data is also quite satisfactory (figure 19).

The THERMIT-UTSG computer code has been evaluated with respect to steady-state and transient test results obtained from Bugey 4 and Tricastin 1 steam generators. THERMIT-UTSG, originally developed at the Massachusetts Institute of Technology, is a two-fluid, three-dimensional, transient thermal–hydraulic analysis code for recirculating-type steam generators (Wang & Chang 1986). The calculated circulation ratios over the power range investigated show agreement with Bugey 4 experimental data. Slight underprediction of the experimental results is observed for the Tricastin test. The calculated primary temperature drops and feedwater flow rates are also in

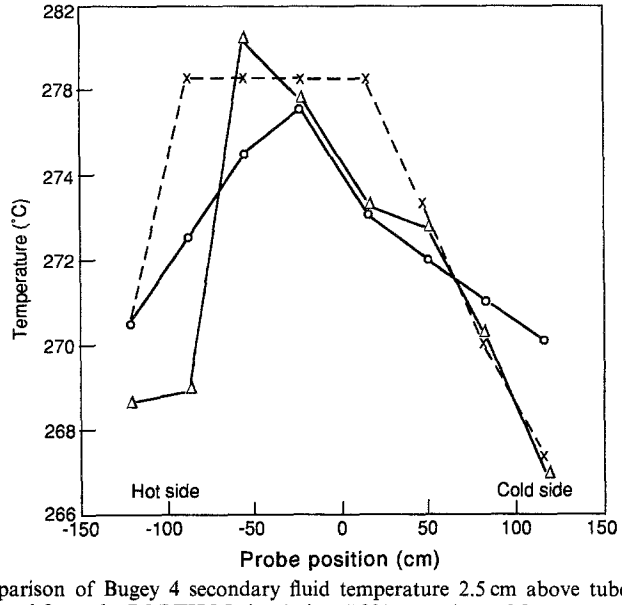

Figure 19. Comparison of Bugey 4 secondary fluid temperature 2.5 cm above tubesheet with mixture temperature inferred from the PORTHOS simulation (72% power). △, Measurements at Bugey 4 steam generator; ×, ATHOS-2 prediction; ○, PORTHOS-2 prediction.

agreement with experimental data. Most of the predicted values agree with measured data within experimental uncertainty. For the loss-of-feedwater test, conducted at Tricastin 1, the calculated transient responses of the SG water level, steam flow rate and primary outlet temperatures agree reasonably well with measured data until the reactor is scrammed. After that, larger discrepancies between calculated and measured values are observed because of lack of adequate input data.

A computer code, FAUST (flow analysis of U-tube steam generators), for U-tube steam generator design analysis has been developed based on the PWR core transient analysis code THERMIT (Lee & No 1986). The original (x, y, z) co-ordinates used in THERMIT are transformed into cylindrical (r, θ, z), co-ordinates for FAUST, which are better fitted to the geometry of steam generators. To couple the primary side with the secondary side, a one-dimensional simple tube heat transfer model is developed with a geometric mapping between the primary and secondary side. The special unitary group SU(2) is used to treat the complex geometry of the U-bend region for frictional wall force. A form-loss model for tube support plates in two-phase flow is implemented in the code. The steam dome model developed enables the consideration of different amounts of feedwater distributed into the hot and cold sides of the downcomer.

Measured data from the steam generator at the Bugey 4 nuclear power plants have been used for the assessment of FAUST. Predicted results for the measured parameters are in good agreement with the measured data: circulation ratio within 8% error and total power within 2% error. Considerable liquid recirculation is found in the U-bend region.

Two major experimental tests to evaluate thermal and hydraulic performance in steam generators are performed. The first, called CLOTAIRE (Bouchter *et al.* 1986), is a Freon test facility. Of particular interest are the local measurements of void fraction and steam velocity within the bundle. Freon 114, 78°C and 0.89 MPa are used to scale the steam–water density ratio at nominal prototype conditions. The CLOTAIRE program has produced some useful results which are available to the sponsors. The data are now being compared to several thermal and hydraulic codes.

The second facility, a 25 MW loop called MEGEVE (Campan & Castello 1986), is intended to validate the design of Framatome's new steam generator that will be installed in an N4 plant (a plant with an axial economizer). The experimental program will also allow the validation and qualification of specific thermal–hydraulic codes for steam generators with a preheater zone. Vibratory behavior of the bundle will also be studied.

In all the codes described above, there are various formulations of the mass, momentum and energy equations. It must be emphasized that the accuracy of the calculation is based on the correlations, formulations, equations, etc. used for heat transfer, friction, void fraction, two-phase density, form losses, interfacial shear, etc. Many of the codes have the capability to use different correlations. Often, certain correlations are "adjusted" to match the experimental data.

For example, the boiling (outside diameter) heat transfer correlation is often adjusted ("fine-tuned") to match the overall heat transfer between the primary and secondary fluids. The internal natural circulation flow within the steam generator is driven primarily by the difference in density between the single-phase cooler liquid (well known) in the downcomer and the two-phase density (uncertain value) within the riser of the heated bundle. Therefore, the correlation for the two-phase density is often adjusted to match the overall recirculation ratio. In many cases, the particular correlation used by a steam generator manufacturer is proprietary. However, each of the thermal and hydraulic code reports usually describes the various corrections that are available for use within that code.

3.2.3. Transients and safety considerations

Steam generators are subject to transients as a result of operational changes and to off-normal accidents. Operational changes such as a power increase or decrease were covered previously. Off-normal accidental transients include loss of feed, primary line break and steam line break events.

The steam generator provides a dynamic link between the reactor core and the turbine generator in PWR plants and therefore plays an important role in the safe and reliable operation of these plants. A thorough knowledge of the dynamic behavior of PWR plants is therefore required for both safety assessment and control system design. Next to the reactor, the steam generators are the most important components with respect to transient phenomena.

The physical processes that determine the thermal performance and operational behavior of the steam generator under steady-state and transient conditions include two-phase flow, natural circulation and heat transfer phenomena. A good understanding of, and capability of predicting, the normal and off-normal behavior of a steam generator are essential for evaluating the load-following mechanism and the operating and accident transients of PWRs. It is therefore necessary to model the steady-state and transient two-phase flow and the void distribution in the steam generator to accurately predict PWR plant response.

The mathematical models, which are currently used to describe steam generators, though simple, are not very accurate. Usually, design calculations are performed by using conservative assumptions to produce bounding values—but this approach suffers from three drawbacks (Liao *et al.* 1986):

(1) For a specific bounding calculation it is very difficult, or even impossible, to quantify the degree of conservatism associated with the calculation. Sometimes it is also difficult to tell which direction is conservative.
(2) A bounding calculation causes distortion in our perception of the overall system behavior and precludes the understanding of actual system response.
(3) Due to the distortion in the sequence of events, there are very complex effects resulting from the interaction of the distorted system operations. As a result, conservative assumptions do not necessarily lead to conservative calculations. Therefore, the trend is now to switch from the bounding calculations to the best estimate calculations.

The most important transients which are usually analyzed are those associated with steam line break or feed line break, e.g.

- Pressurized thermal shock (PTS), which is a result of a transient
- Steam tube rupture (though this may occur also without steam line break or feed line break)
- Reactivity insertion in a primary system.

Since the phenomena are usually very complex, it is common to decouple the secondary side of the SG from the rest of the system in order to make the calculations more tractable.

One of the key parameters in the secondary side is the heat transfer on the secondary side. This is important because it predicts the degree and duration of the overcooling on the secondary system, which drives the transient such as pressurized thermal shock (PTS) induced by SG blowdown.

The principal factors that affect the heat transfer on the secondary side of the affected steam generator include (Liao *et al.* 1986):

(1) The local heat transfer coefficient and the corresponding heat transfer area. As long as the tubes are wet on the secondary side, the heat transfer is excellent. On the other hand, whenever the tubes are dry the heat transfer is negligible. Therefore, the fraction of wetted area is particularly important. Carryover, fallback and mixture level propagation are the key parameters for determining the amount of wetted area.
(2) The temperature of the steam generator secondary side. The temperature on the steam generator secondary side is mainly determined by the depressurization rate.
(3) The time span for the heat transfer on the pressure vessel wall. Thermal stress peaks 10–20 min into the transient. It is the heat transfer up to that time that is most important.

3.2.4. Scenario of some transients

Pressurized thermal shock. Because of neutron irradiation of the reactor vessel wall, the fracture toughness of the wall decreases. In case of a sudden cooling of the wall and high pressure in the reactor, there is concern over the pressure vessel integrity. If a small crack is present on the vessel inner surface, such as subcritical flaw in service, that crack may grow to a size that threatens vessel integrity. One of the initiating events leading to a possible pressurized thermal shock in a pressurized water reactor is a steamline or a feedline break. When the break occurs, the pressure in the steam generator secondary side drops and the heat transfer rate from the primary side to the secondary side of the affected steam generator increases. The excess amount of heat transfer results in an overcooled primary system. Moreover, the reactor trip following a steam generator

blowdown will enhance the effect of overcooling. As a result of this overcooling in the primary system, the emergency core cooling (ECC) may come on and lead to repressurization, thereby threatening pressurized thermal shock. Clearly, the sequence of events depends on the heat generation and removal rate in the primary system. The heat in the primary system can be removed by both the normal and affected steam generators. Therefore, there are three mutually interacting systems—the primary system, the secondary side of the intact steam generator and the secondary side of the broken steam generator.

Steam generator tube rupture. The normal operating pressure in a PWR is 15 MPa in the primary system and about 7.0 MPa in the secondary system. After a steam line break, the fast depressurization in the secondary system creates an increased pressure difference across the steam generator tubes. If this pressure is greater than the steam generator tube burst pressure, tube ruptures may occur and radioactive primary coolant will mix with the secondary coolant and cause a forced shutdown. When primary coolant enters the secondary system, the reduced pressure there causes it to flash—which further complicates the modeling of this transient.

Reactivity insertion in the primary system. In a reactor with a negative moderator temperature coefficient, such as a standard PWR, a decrease in primary coolant temperature leads to a reactivity insertion. Such a temperature decrease in the primary coolant can result from a sudden increase in the heat removal rate from the primary system which in turn could be due to the blowdown of the secondary system.

The potential for a recriticality and the resulting core power burst has always been a safety concern. Following a streamline break, the reactivity insertion due to overcooled primary coolant decreases the shutdown margin provided by the control rods. If the negative reactivity from the Doppler effect and the high boron concentration ECC do not become effective within a short period, the positive moderator reactivity may exceed the negative control rod reactivity and lead to a recriticality. The duration of the recriticality then determines the possibility of fuel rod damage. Obviously, a better estimate of heat transfer from the primary side to the secondary side is required for a better modeling of reactivity insertion accident.

3.2.5. *Analytical models*

A one-dimensional model was proposed by Liao *et al.* (1986) to calculate the SG transient during a blowdown of the secondary system. The SG is divided into control volumes, and the conservation equations are integrated in these volumes.

Their formulation consists of one mixture mass equation and one mixture energy equation. Since the pressure is assumed to be uniform in the SG secondary side, no momentum equation is needed. The transient two-phase flow is assumed to be in thermal equilibrium but not homogeneous. The difference between liquid phase velocity and vapor phase velocity is taken into account by the drift flux model. This model is the simplest one that can adequately describe the important two-phase flow phenomena, in particular, the water level

—mixture mass equation

$$\frac{\partial}{\partial t}(\epsilon\rho_G + (1-\epsilon)\rho_L) + \nabla\cdot(\epsilon\rho_G \bar{V}_G + (1-\epsilon)\rho_L \bar{V}_L) = 0$$

where ϵ is the void fraction, ρ are the densities and $\bar{V}$ are the velocities

—mixture energy equation

$$\frac{\partial}{\partial t}(\epsilon\rho_G e_G + (1-\epsilon)\rho_L e_L) + \nabla\cdot(\epsilon\rho_G e_G \bar{V}_G + (1-\epsilon)\rho_L e_L \bar{V}_L) = -p\nabla\cdot(\epsilon\bar{V}_G + (1-\epsilon)\bar{V}_L) + \dot{q}_{wG} + \dot{q}_{wL}$$

where $\dot{q}_w$ is the heat transfer rate from the wall to the vapor G and liquid L, and e are the internal energies.

The criteria for flow regimes were as follows:

bubbly flow

$$j_L > 2.34 - 1.07S \text{ and } \epsilon < 0.1$$

churn–turbulent flow

$$|j_G| < \left(\frac{\Delta\rho g D}{\rho_G}\right)^{0.5} \cdot \left(\frac{1}{C_0} - 0.1\right) \text{ and } \epsilon < 0.8$$

annular flow

$$|j_G| > \left(\frac{\Delta\rho g D}{\rho_G}\right)^{0.5} \cdot \left(\frac{1}{C_0} - 0.1\right) \text{ and } \epsilon > 0.8$$

where the dimensional group $S \equiv g\Delta\rho\sigma/\rho_L^{1/2}$, where j are the superficial velocities, σ the surface tension, g acceleration due to gravity, D the diameter of the tubes and C_0 is the drift flux model constant discussed below and $\Delta\rho = \rho_L - \rho_G$.

The velocities of the phases are related by the drift flux model

$$\langle j_G \rangle = \langle \epsilon \rangle (C_0 \langle j \rangle + V_{Gj})$$

where $\langle j_G \rangle$ is the superficial vapor velocity averaged over a cross section, ϵ is the void fraction, $j = j_G + j_L$, V_{Gj} is the weighted mean drift velocity $= \langle \epsilon(V_G - j) \rangle / \langle \epsilon \rangle$, V_G is the vapor velocity and the distribution parameter C_0 reflects the effect of void fraction in a cross section and is given by:

$$C_0 = \frac{\langle \epsilon j \rangle}{\langle \epsilon \rangle \langle j \rangle}$$

Roughly, $C_0 > 1$ indicates more void in the center of the cross section than at the periphery—which is common in two-phase flow. $C_0 < 1$ indicates more vapor flows in the periphery of the cross section than in the center—which may happen in subcooled boiling. The weighted mean drift velocity V_{Gj} reflects the effect of the difference in superficial velocities between vapor j_G and the total j.

For bubbly flow Wallis (1969) suggested

$$\bar{V}_{Gj} = 1.53(1 - \epsilon)^2 S^{0.25}$$

and

$$C_0 = 1.0$$

For churn–turbulent flow Ishii (1977) suggested

$$C_0 = \left[1.20 - 0.2\left(\frac{\rho_G}{\rho_L}\right)^{0.5}\right](1 - e^{-18\epsilon})$$

and

$$\bar{V}_{Gj} = 1.53 S^{0.25}$$

For annular flow Ishii (1977) suggested

$$\bar{V}_{Gj} = (C_0 - 1)\left(\frac{\Delta\rho g D(1 - \epsilon)}{0.015\rho_L}\right)^{0.5}$$

and

$$C_0 = 1 + \frac{(1 - \epsilon)}{\epsilon + 4\sqrt{\frac{\rho_G}{\rho_L}}}$$

Liao *et al.* (1986) incorporated the various models into a computer program and added more terms to correctly account for the effect of pressure. In the program, they also smoothed the transition between flow regimes, since abrupt changes may lead to instability of the calculations.

The flow from the broken line is critical (i.e. choked), as long as the pressure inside the SG is larger than 0.18 MPa, that is, during most of the transient. There are a number of two-phase critical flow models available. These can be broadly classified into three categories:

(1) Homogeneous equilibrium model (HEM)
(2) Slip equilibrium model (e.g. Henry–Fauske model, Moody model)
(3) Two-fluid model.

Of these, the Henry–Fauske model was found to be adequate since it is simple and correctly accounts for the effect of the length to diameter ratio.

Another very important parameter is the mixture water level, which affects the heat transfer and, therefore, the whole transient behavior. The level can be computed from basic conservation equations, and the models used are usually quite adequate to calculate level change, such as pool swelling, under intermediate transients.

The MIT code was compared to a number of experimental data sets:

Battelle–Frankfurt blowdown test

Test description: the SWR-2R test conducted at the Battelle Institute in Frankfurt is designated as the OECD-CSNI Standard Problem No. 6, and has been simulated by TRAC-PD2 and other codes. Valuable information about the experimental data as well as the results from the code prediction are provided and compared by Saha *et al.* (1982).

The test apparatus is a vertically oriented steel vessel of 0.776 m in inside diameter and 11.18 m in height. The vessel is fitted with a rod bundle heater located between 2.69 and 5.19 m from the bottom of the vessel. A horizontal discharge pipe of 0.143 m in inside diameter and 0.47 m in length is connected to the vessel at an elevation of 9.94 m from the bottom of the vessel. A square-edged orifice plate of 0.064 m in inside diameter is mounted at the end of the discharge pipe. Blowdown is initiated by destroying a rupture disk installed downstream of the orifice.

To perform the test, the vessel was filled with subcooled water up to a certain level and then heated up to a pressure of 7.06 MPa and an average water temperature of 558 K. After this condition is attained, the heater is turned off and the blowdown is initiated.

Several pressure taps were placed at different vessel levels as well as in the discharge pipe to monitor the pressure during the transient. The errors in the pressure measurements were approximately 1%. The fluid density at the discharge nozzle was measured by a two-beam gamma densitometer. The accuracy of this measurement was approximately 12%. There were also two drag bodies to measure the fluid momentum at the discharge nozzle. The break mass flow rate was determined from the fluid density and the drag body measurements. The error in the measured discharge flow rate was estimated to be between 10 and 15%. The time history of the mixture water level was measured by a stack equipped with electrical contacts at many axial locations. The accuracy of the mixture level measurement is ± 0.02 m.

Input model description: for this particular calculation, the test vessel was represented by 23 nodes, the same as that calculated by the TRAC-PD2 drift flux model. The geometric effects of the rod bundle heater were taken into account by decreasing the flow area by 22% and hydraulic diameter by a factor of 10 compared to those for the vessel without a heater. To make a simple one-dimensional model, the vapor space above the break location was neglected. Two separate calculations were performed with two different drift flux model constants in churn–turbulent

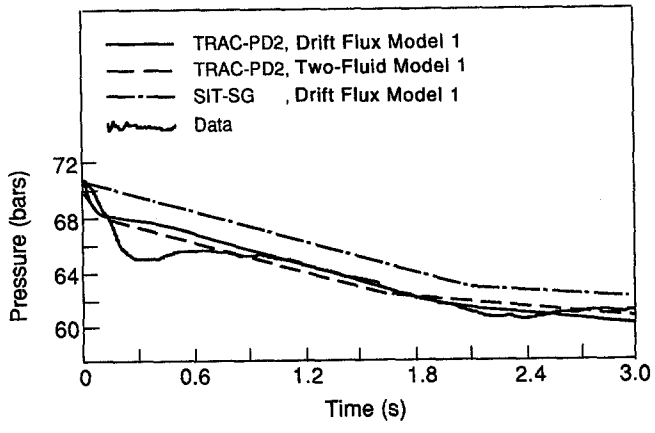

Figure 20. Comparison between the measured and predicted pressure for Battelle–Frankfurt blowdown test SWR-2R (Liao *et al.* 1986).

flow regime. The first drift flux constant was given by the Wilson model and the second was given by

$$\bar{V}_{Gj} = 0.33S^{0.25}.$$

Code prediction and comparison with data: it was found that there is almost no difference between the results performed with the two different drift flux constants. Therefore, no distinction can be made between these two results. Figure 20 shows the comparison of the pressure predictions by the code (SIT-SG, Liao *et al.* 1986), by TRAC-PD2 and the measured data. The slope of the prediction is about the same as that of TRAC prediction and the data. The initial under-shoot of the data, which is present because of the delay in the onset of flashing, is missed by all the code predictions. There is a sudden slope change at about 0.1 s in both TRAC predictions. It is not clear why the slope changes in the TRAC calculations. There is no slope change in SIT-SG prediction during the initial blowdown period and as a result, the pressure prediction in SIT-SG is overestimated. Figure 21 shows the mass flow rate through the break. During the early part of the transient ($t < 2$ s), only steam flows through the discharge pipe. As the transient progresses, the two-phase mixture in the vessel swells. When the mixture level arrives at the discharge pipe, the break mass flow rate increases sharply because of a sudden increase in the fluid density. This happens at approximately 2.3 s in the test. A very close prediction of this time has been made by the SIT-SG code. The slightly early arrival of the mixture level at the discharge pipe and the slight overprediction of the break mass flow rate were observed for all code predictions. This can be attributed to the fact that no discharge coefficient is used in any of the calculations while the reduction of the break flow area at the orifice plate was to be expected in the experiment.

Figure 22 shows the measured and the predicted mixture level. Except the first 0.3 s, when the mixture water level does not rise due to the delay in flashing, all the models predict a fairly good water level swelling speed.

Other comparisons, with various data sets, were also performed with normally the same degree of accuracy.

4. MOISTURE SEPARATORS

4.1. General

Separation of liquid water from the steam–water mixture is done in the upper part of steam generators, and usually consists of three phases:

- primary separation—normally done by means of centrifugal separators
- gravity separation—achieved in the space between the primary separators and the driers (or secondary separators)
- secondary separation—done by means of chevron-type, or corrugated shape, separators.

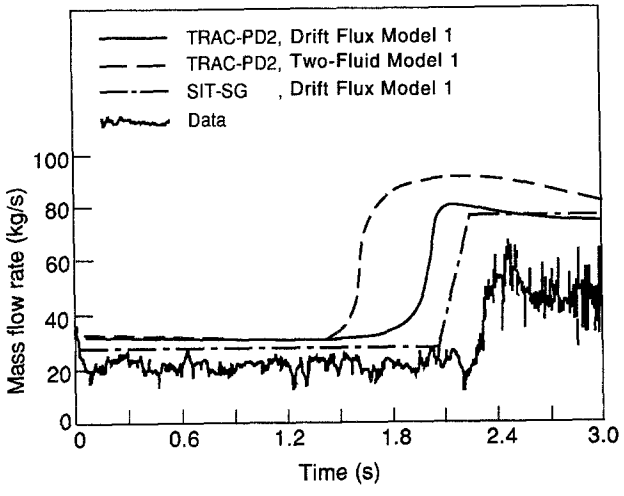

Figure 21. Comparison between the measured and predicted break mass flow rate for Battell–Frankfurt test SWR-2R (Liao *et al.* 1986).

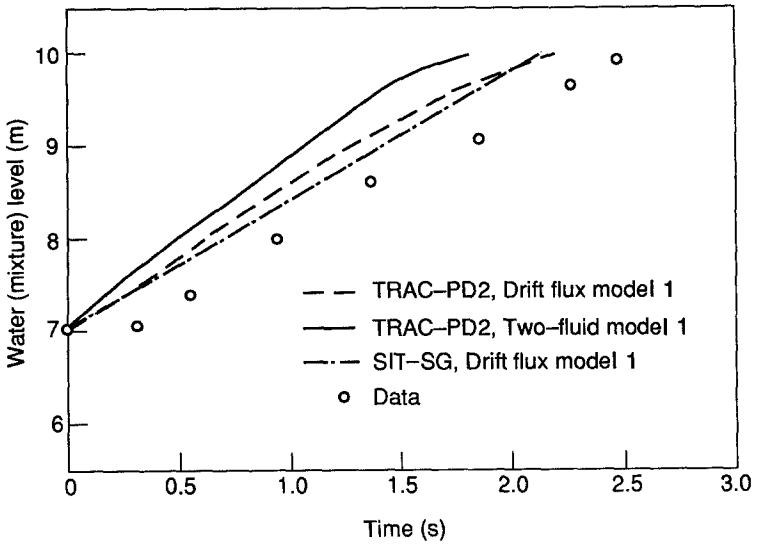

Figure 22. Comparison between the measured and predicted mixture level for Battelle–Frankfurt test SWR-2R (Liao *et al.* 1986).

The efficiency of the separation package is normally measured in terms of carryover, which is the mass flow rate of water droplets in the steam, normally expressed in percent. It is generally accepted that this should be quite low, and an industry accepted standard was frequently quoted as "not to exceed 0.25%". However, it is not at all clear that this limit is low enough to minimize damage to turbines, and a standard of "less than 0.1%" is now frequently quoted.

Furthermore, in a number of cases the plants did not meet the specified dryness of the steam (in a particular case 1.5% moisture in the steam was measured—causing many difficulties to plant operation and resulting in reduced plant efficiency).

Another aspect of the separation performance is the carryunder, which is the amount of steam in the separated water. The carryunder is a factor in determining the circulation ratio of the steam generator. However, since carryunder was not a serious issue in the past, it will not be discussed here.

The other most important feature of separators, besides their separation efficiency, is their pressure drop. Low separator pressure drop will result in higher circulation ratio. Furthermore, since the separators are located at the downstream end of the flow in the steam generator, a zone which has two-phase mixture flowing through it, large pressure drop can cause instability in the circulating flow. It is not an easy task to calculate stability of two-phase flows (Hetsroni 1982), but there have been indications from operating plants that the circulating flow was unstable, resulting in unstable operation of the plant and eventual forced shut-down for repair. Vendors, who are aware of this problem, sometimes add flow-resistance devices in the single-phase region, e.g. in the downcomer, to stabilize the flow. This solution is, of course, counterproductive since it reduces the circulation ratio, which may result in other problems prevalent in steam generators today, such as corrosion.

The performance of most separators deteriorates significantly as the mass flow rate is increased. The deterioration is expressed as a very rapid increase of carryover. Since the flow distribution upstream of the separators is not uniform, some separators are more loaded than others. For this reason, as well as for future expansion, the separators should have a wide margin to mass flow rate.

Thus, in developing a separator, one should aim at a mechanically sturdy device, with low pressure drop and high separation efficiency over a wide range. Those were the goals of the development program described herein, a program which resulted in a very successful product.

Unfortunately, many primary separators have been developed by trial and error and with little experimental verification. The Electric Power Research Institute (EPRI) reviewed the separators then available on the market (Carson & Williams 1980) and identified three designs with potential

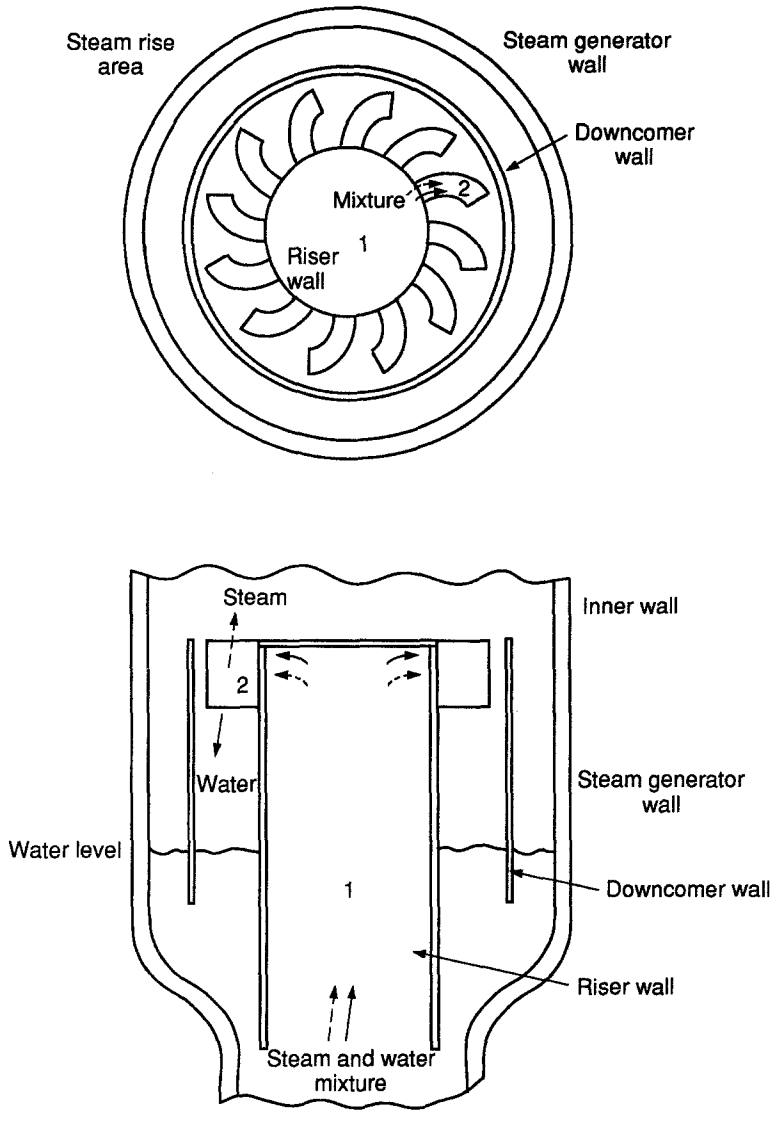

Figure 23. (Part 1). Curtis–Wright steam separator (Carson & Williams 1980).

for acceptable performance (figure 23). But efforts by EPRI to put the design of primary separators on a firm analytical foundation were not entirely successful, and one must still rely on experiments, and on trial and error methods (Vander Vorst & Steininger 1982). Also, analytical or numerical calculations are not used today as the only design tool, though much progress has been achieved in these areas (Prints 1974; Wisman 1979; van der Welle 1983; Wong 1985).

The predictive technique usually follows the same general approach as that used to calculate the flow field within a steam generator, i.e. conservation equations describing the flow field are solved numerically. In the separator application, solution of the equations representing two-phase homogeneous flow, as is usually performed for the steam generator, would produce inaccurate results. A complete equation set is required to represent the two-phase flow field within the separator in a manner similar to that incorporated in the PORTHOS code discussed earlier. The assumption of homogeneous flow is not used to reduce the complexity of the flow equations.

The flow through the separator is described by the momentum equations for both the vapor and the liquid including drag (six equations), the continuity equation and the void transport equation. Partial differential equations for transient, two-phase axisymmetric, three-dimensional incompressible swirling flow are developed.

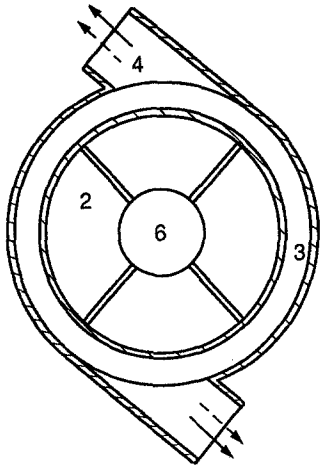

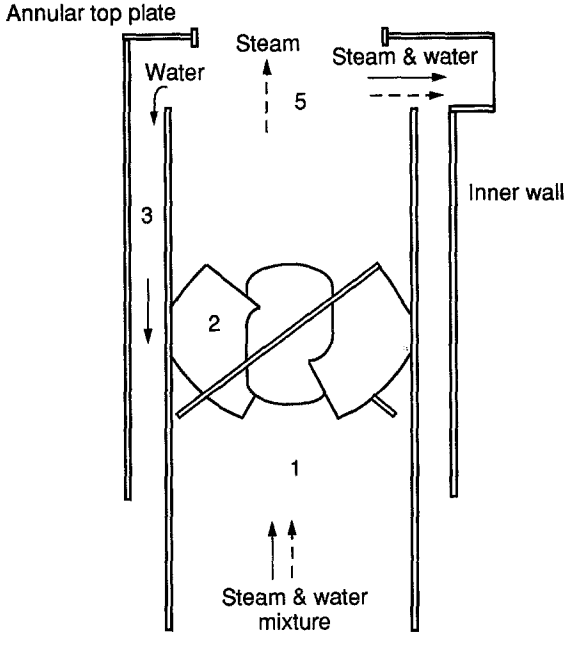

Figure 23. (Part 2). Westinghouse separator.

The types of cyclone separators are reviewed briefly. Later, the development of a new type of separator will be discussed in some detail:

(1) Curtis–Wright separator (figure 23—Part 1)—the steam water mixture enters the riser from the bottom and passes through the swirl passsages mounted at the top. The water is separated and flows to the downcomer and the steam exits between the swirl tubes into the next stage of separation.
(2) Westinghouse separator (figure 23—Part 2)—the steam water mixture passes through swirl vanes which cause the liquid to flow as a film on the cylinder wall, and is then skimmed off at the top. The steam passes through the hole in the center of the top plate, to the secondary separators. The efficiency of this device has been calculated to be about 75%.
(3) General Electric separator—is made up from a series of swirlers and skimmers, which operate in a similar fashion to the previous ones. This type of separator has

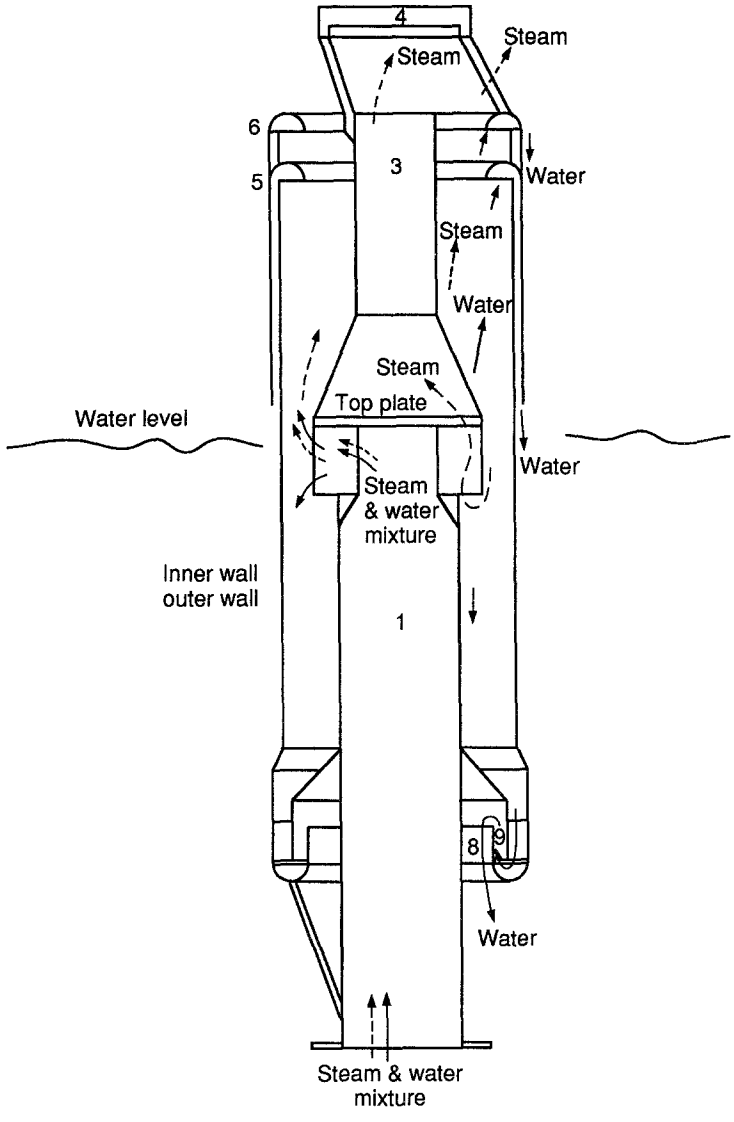

Figure 23. (Part 4). KWU steam separator (Carson & Williams 1980).

deterioration in performance for low steam flows and low liquid flow rates, unlike the other separators.

(4) KWU separator (figure 23—Part 4)—the steam water mixture flows through a tortuous path, losing water at several stages. This is quite a complicated separator, compared with the other ones.

(5) CE separator (figure 23—Part 5)—the two-phase mixture enters the swirl vane at the bottom, and the liquid is caused to flow towards the perforated wall, where it is continuously removed. Steam is exiting through a screen assembly at the top. This is quite a simple separator which operates well until critical water level is reached, at which point a rapid deterioration occurs.

The carryover in all these separators is mostly due to reentrainment of water from the surfaces. The other kind of carryover occurs when the device reaches a critical load, after which there is a rapid deterioration of separation efficiency. This can also be a result of high water level around the separator.

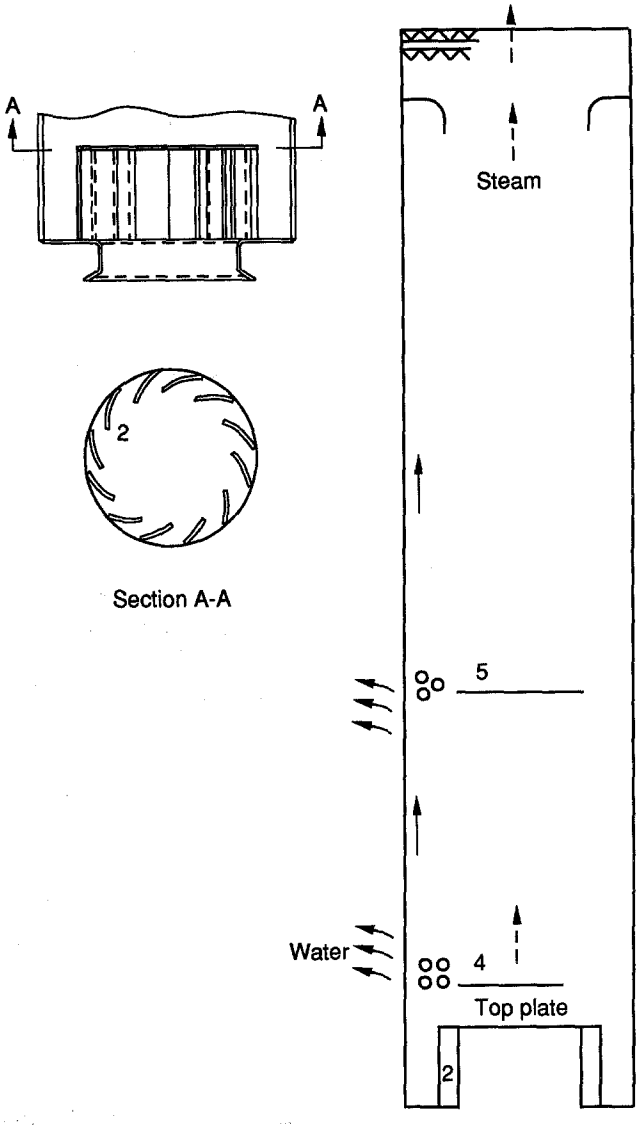

Figure 23. (Part 5). Combustion Engineering steam separator.

4.2. Experimental

There were a number of experimental efforts spent to develop steam separators. In recent years there has been an experimental program in France (see e.g. Bouchter *et al.* 1984 and Wyatt *et al.* 1981).

These programs were initiated in 1977 and lasted about 7 years, with their main objective to develop a 0.5 m diameter centrifugal separator to equip the new French 1300 MWe plants.

The experimental means included:

—RAMSES: air–water global tests (EdF)
—TOPASE: air–water swirl vane characterization tests (CEA)
—ARGUS: Water–Freon 13B1 global tests (ordered by Framatome to Technicatome)
—EVA SEP.SEC full-scale 3.5 MPa steam–water tests (ordered by Framatome to Technicatome)
—MB1 reduced scale 7 MPa steam–water tests (Westinghouse)
—CYCLOPE reduced and full-scale Freon 114 tests including global and local measurements, in particular velocity and void fraction profiles downstream of the swirl vanes (CEA).

Major benefits were:

—The design of a separator which is actually producing less than 0.1% carryover in the 1300 MWe French plant
—The demonstration (based on both local and global measurements) that separators with appropriate lowered swirl vanes work much better
—A much better understanding of the separate effects of the governing parameters of centrifugal separators (riser diameter, swirl vane geometry and location, skimmers' size, deck plate transparency...).

Here we describe briefly another experimental program which was carried out in Italy with the purpose of developing a new, improved moisture separator. This program is unique in as much as it was published in the open literature and because tests are described both in a low pressure air–water loop and in a high pressure steam–water loop.

In the program described herein, a methodical approach was adopted: initial developmental work was done on a small water–air loop, LARA, until promising geometries and features were identified. In particular, a new swirl vane was designed (similar to the one developed by Dementéu *et al.* 1972), a conical perforated riser was developed (similar to the one used by Allis-Chalmers) and other features were optimized such as riser perforation, skimmer, tangential slots and outlet nozzle. The promising designs were then constructed and full-scale tests were conducted in a large air–water loop, ARAMIS (after the proper scaling laws were established). In this loop a wide range of variables were tested and the final design was chosen. Finally, the end product was tested under prototypical conditions, and the results were compared to the air–water results, in order to verify the scaling laws, and qualify the final design (Mauro *et al.* 1990).

4.2.1. Preliminary tests

The preliminary tests were conducted on a small air–water loop, LARA, where scaled down models (0.23 of full size) were tested. The tests were primarily based on visual observations and measurements of pressure drop and flow rates. After a considerable number of tests, the following geometrical features have been identified as having a major effect on the performance:

- the riser geometry
- the outlet orifice geometry
- the geometry and location of the swirling vanes.

All the resulting configurations have the common characteristic of a perforated riser with a skimmer which is located downstream from the swirl vane.

Riser geometry: both cylindrical and conical risers were tested, both having closed ends with lateral slots. These risers were tested, while maintaining the same vane geometry, and the performance curves (i.e. moisture carryover and air carryunder, with water level as a parameter, versus the mass flow rates) and pressure drops were examined and compared. It was concluded that the conical riser resulted in superior performance, and it was chosen for the final geometry (figure 24).

In a similar fashion, the outlet geometry was optimized and fixed. The geometry which was chosen included the closed end of the perforated riser (figure 24) with tangential slots for the steam outlet, and the outlet orifice.

The most crucial component of the separator is the swirl vane. Earlier geometries of separators included straight blades such as those depicted in previously (figure 23), which resulted in high pressure drops and poor separation performance. Therefore, it was decided to adopt a design where the blades are curved and the hub is streamlined. The parameters which were varied were the hub diameter and the number of the blades and their angles. The best performance (i.e. lowest pressure drops and best separation efficiency) was achieved with a hub of 40 mm in diameter and 6 blades with 25.6° overall angle—30° at the hub and 20° at the rims. There were other geometries which yielded either lower pressure drop or better separation efficiency, but this geometry was judged to have the best overall performance characteristics.

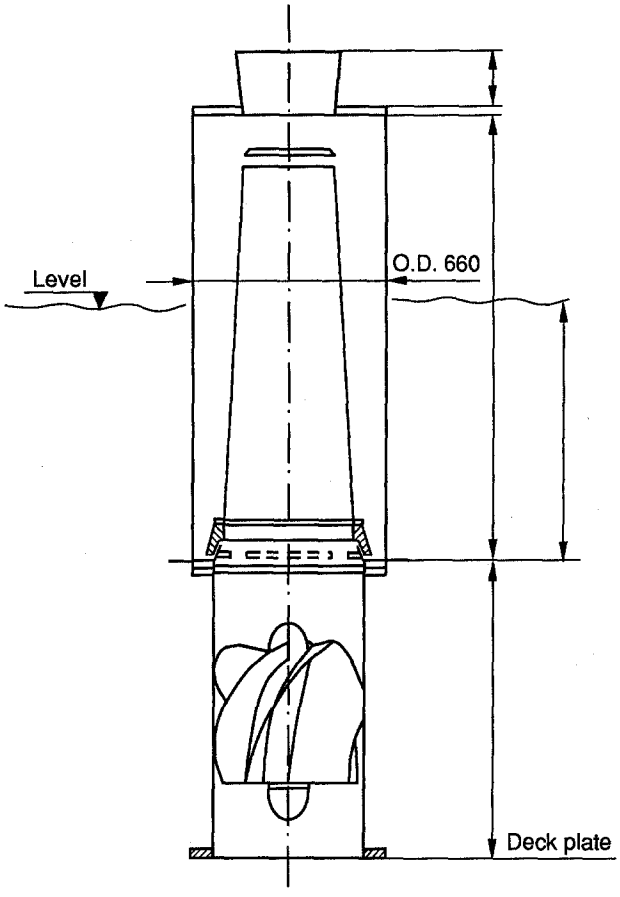

Figure 24. Schematic of the new design 500 mm improved Italian moisture separator (IIMS) (Mauro *et al.* 1990).

Another very important feature is the relief area in the deckplate. Enough relief area in the deckplate for water to drain is provided, in order to prevent considerable deterioration in the performance of the separators.

4.2.2. Scaling considerations

The main problem associated with tests which are conducted under non-prototypical conditions is the lack of proven scaling laws. Scaling laws are necessary in order to conduct model tests, rather than full size components; or in order to conduct tests in non-prototypical conditions (i.e. not a steam–water mixture at 7.0 MPa)—both cases allow for tests at much lower costs than full-scale ones. The costs of developing a product experimentally under prototypical conditions are, of course, prohibitive. Therefore, scaling laws were developed and used in order to define the experiments for the air–water ARAMIS loop. In order to ascertain adequate coverage of all the test range in the steam–water tests, the range of the air–water tests was expanded to cover more than the minimal necessary ranges.

After considering the effect of the flow parameters such as flow patterns, quality, void distribution etc. on the postulated separation mechanisms (centrifugal forces, drag forces and surface tension) it was decided that the scaling criteria for the primary separators are:

- volumetric two-phase fluxes in model and prototype should be maintained
- flow patterns, according to the Taitel–Dukler (see Hetsroni 1982) map, should be maintained
- dynamic head as calculated by homogeneous two-phase flow model should be maintained in model as in the prototype.

In retrospect, by comparing data from the air–water low pressure ARAMIS loop to data from the high pressure steam–water GEST-SEP loop, the first of these, i.e. the volumetric flux criterion,

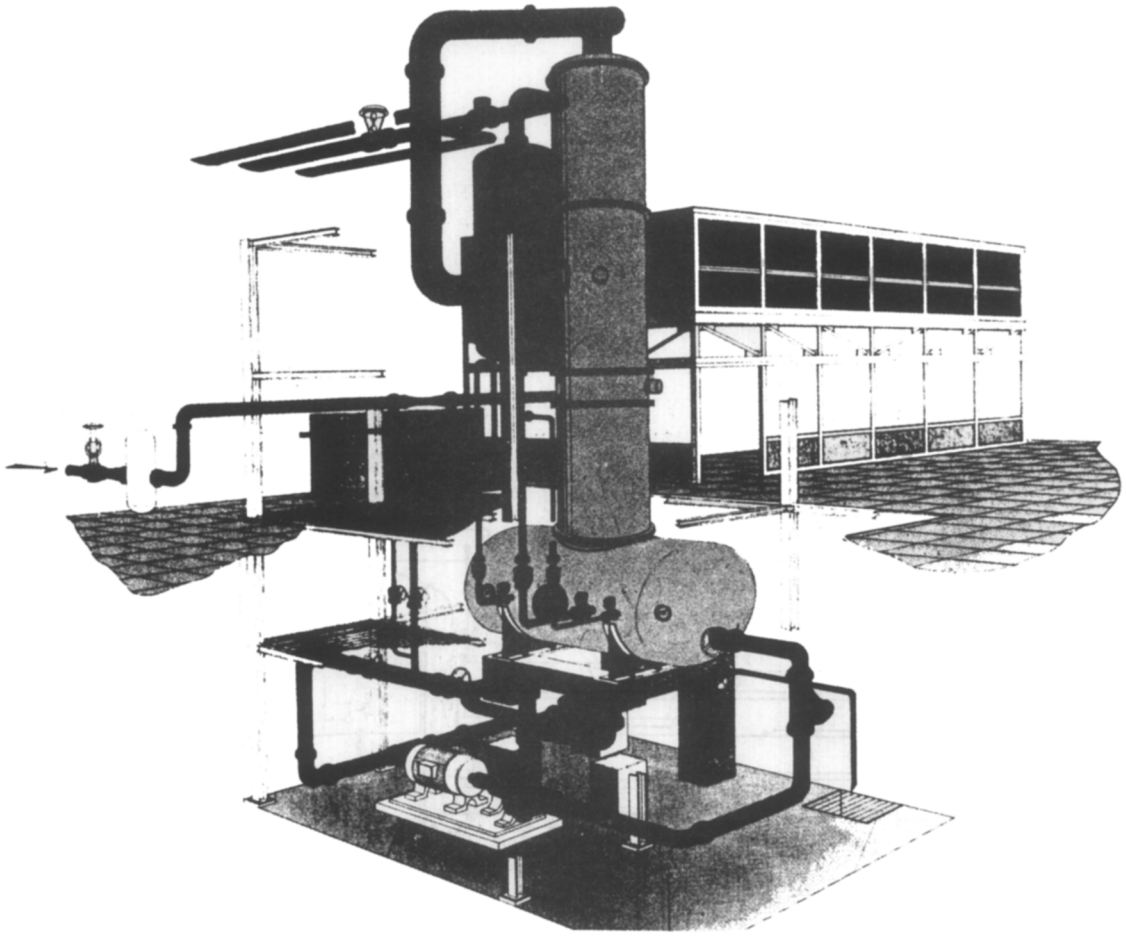

Figure 25. The ARAMIS loop.

proved to be most important for maintaining similarity between the model and the prototype, which was tested later. The resulting values for the air–water test matrix, corresponding to loads of 60–140% of nominal load under prototypical conditions were:

water mass flow rate	60–195 kg/s
air mass flow rate	0–4.5 kg/s
separator water level	0–1 m
system pressure	0.1 MPa.

The simple scaling procedure worked because the flow regime was about the same, friction and form loss pressure drop were about the same, water level was the same, while other scaling parameters were of secondary importance.

4.2.3. The ARAMIS loop

The ARAMIS (ARia Acqua MIScela) is, as its name implies, an air–water loop, capable of full-scale testing of separators or other two-phase flow equipment (figures 25 and 26 and table 6). The ARAMIS test rig, 15 m high, is installed at the ENEA Laboratories Thermal Reactor Department in the Energy Research Center at Casaccia. It is an experimental facility, normally

Table 6. Some characteristics of ARAMIS

Separator diameter	up to	0.5 m
Separator length	up to	2.5 m
Operating pressure	up to	0.4 MPa
Water mass flow rate	up to	250.0 kg/s
Air mass flow rate	up to	4.5 kg/s

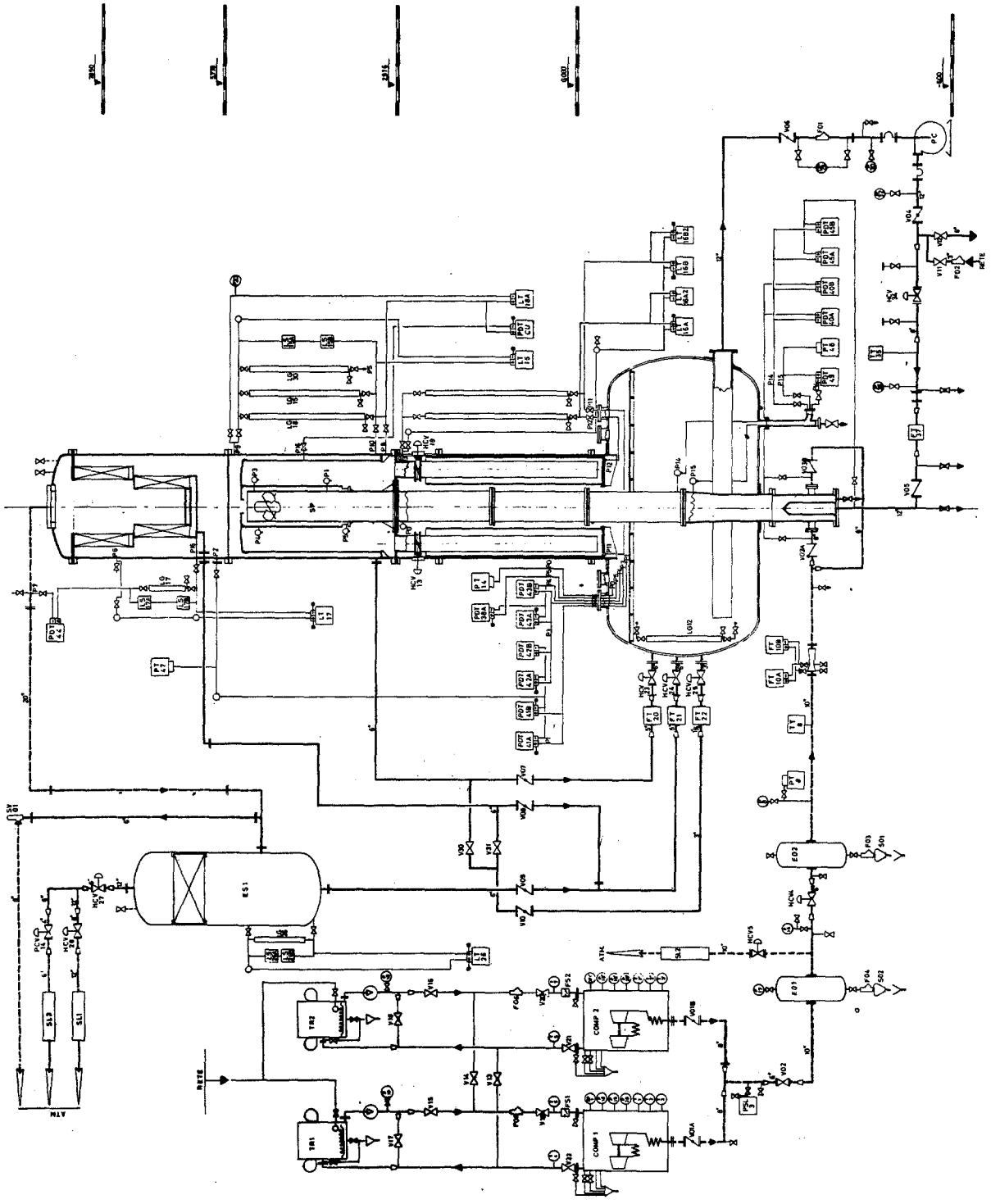

Figure 26. Schematic of the ARAMIS loop (Mauro *et al.* 1990).

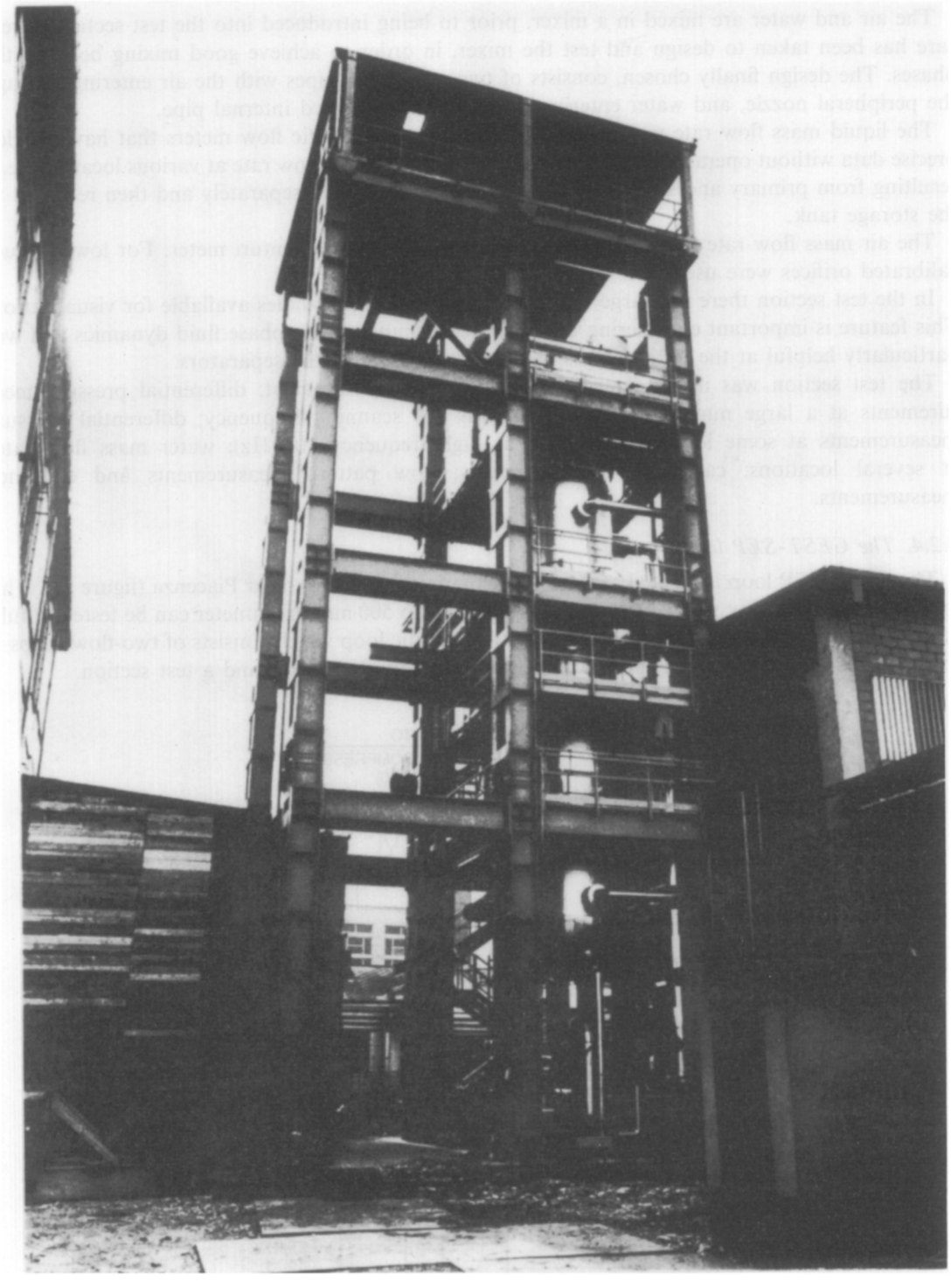

Figure 27. The GEST-SEP loop.

operating at about 0.3 MPa, with a built-in flexibility to test, with slight hardware modifications, various components, such as steam separators.

The ARAMIS test loop consists of two flow loops—the air loop and the water loop—which have in common a mixer and the test section. The water loop is a closed circuit loop, driven by a centrifugal pump of 300 kW and cooled by two cooling towers. Air is fed into the loop by two double-stage compressors of 1.5 MW. The air, after passing through the test section, is released to the atmosphere through silencers.

The air and water are mixed in a mixer, prior to being introduced into the test section. Great care has been taken to design and test the mixer, in order to achieve good mixing between the phases. The design finally chosen, consists of two concentric pipes with the air entering through the peripheral nozzle, and water entering through the perforated internal pipe.

The liquid mass flow rate was measured by means of magnetic flow meters that have yielded precise data without operational problems. The separated water flow rate at various locations (e.g. resulting from primary and secondary separation) was measured separately and then returned to the storage tank.

The air mass flow rate was measured, for higher values, by a venturi meter. For lower values calibrated orifices were used.

In the test section there is a large number of transparent port-holes available for visualization. This feature is important considering the intrinsic difficulty of two-phase fluid dynamics and was particularly helpful at the initial stages of the development of the separators.

The test section was instrumented for temperature measurement; differential pressure measurements at a large number of locations, with low scanning frequency; differential pressure measurements at some locations, scanned at high frequency (100 Hz); water mass flow rates at several locations; carryunder measurements; flow pattern measurements and efficiency measurements.

4.2.4. The GEST-SEP loop

The GEST-SEP loop is located at the CISE experimental facility near Piacenza (figure 27). This loop is a unique facility where moisture separators up to 500 mm in diameter can be tested at full-scale and under prototypical conditions. It is an adiabatic loop which consists of two-flow-loops—the steam loop and the water loop, which have in common a mixer and a test section.

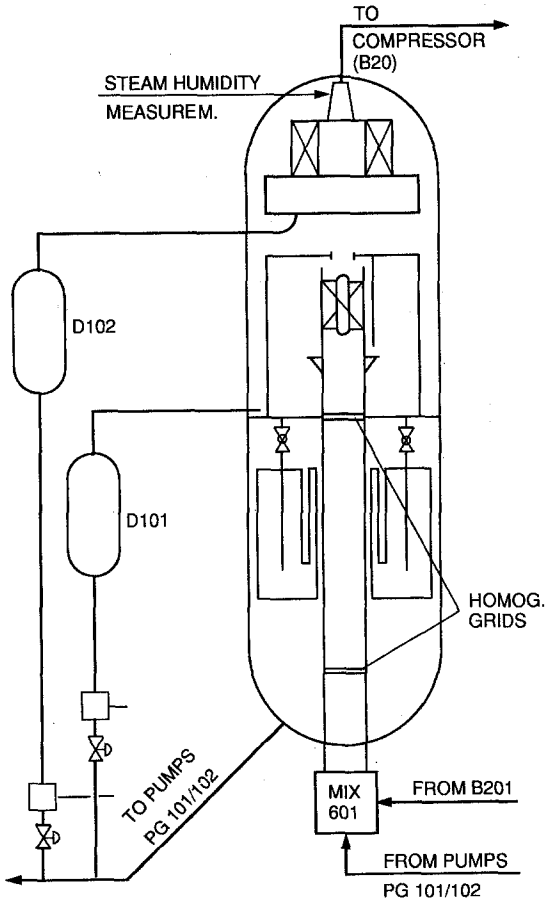

Figure 28. The test section in the GEST-SEP loop.

The water loop consists of two pumps, a control valve and a flowmeter. The two vertical centrifugal pumps are each driven by a 200 kW motor and are capable of delivering 250 kg/s each with a pressure head of 0.67 MPa at a pressure of 18 MPa and a temperature of 340°C. The flow rate is controlled by means of a 300 mm globe valve driven by a pneumatic actuator and measured by means of a turbine flow meter with a range of 20–200 kg/s with an accuracy of 0.5% of actual value.

The steam loop consists of a compressor, control valve, flowmeter and condensate separator. The variable speed centrifugal compressor (Franco Tosi) can deliver 44 kg/s steam with a pressure head of 0.30 MPa, at a design pressure of 10 MPa and temperature of 300°C. The minimum permissible steam quality is 95%. The steam flow rate is controlled by a 250 mm globe valve, driven by a pneumatic actuator, and measured by means of two 250 mm nozzles. The nozzles were built according to ASME PTC 19, 5/4 standard and are designed to cover the flow rate range from 3.7 to 35 kg/s with an accuracy of 1.5% of full scale.

The condensate separator is located at the outlet of the test section and is a 2 m high, cylindrical vessel of 890 mm i.d. The separator is designed to ensure residual humidity less than 0.1%, at a design pressure of 10 MPa and temperature of 310°C.

The test section (figure 28) consists of a 13.4 m high cylindrical vessel of 2.1 m i.d., with internal collecting tanks and weirs. In this vessel one can install a riser, swirl vane primary separator up to 500 mm in diameter and a secondary separator.

In the test section, the water which is separated by the separator, is collected in a separator tank (3.3 m high) equipped with two butterfly valves. These valves, placed in the lower part of two 400 mm pipes control the water level around the separator. From the separator tank the water is conveyed to the lower part of the vessel and then to the pumps.

Above the primary separator a gravitational separation and a secondary separation take place. The water collected by either of these stages is collected into a separate tank and metered externally to the test section by means of a turbine flow meter for normal range and by means of a system of bottles for integral measurements in the low flow range (less than 10%).

Level measurements were performed in the bottom vessel, collection tanks, separator tank, downcomer, gravity separation region and dryer tank. Density was measured through measurements of differential pressures at the collection tanks and in the separator tank.

The residual wetness in the steam at the outlet of the separation package was measured by means of lithium salts. The lithium, which was introduced in a hydroxide form (LiOH), has the desirable features of high solubility in water and a negligible vapor pressure in steam.

This technique is based on extracting steam samples from the outlet nozzle region by means of an isokinetic probe (ASTM D-1066-82). The steam samples are condensed and the concentration of Li^+ ions in the sample determined by chemical analysis. This concentration is then compared to a similar analysis of a water sample taken upstream of the mixer. The moisture content (CO) in the outlet steam is then

$$CO = \frac{\bar{C}_G}{\bar{C}_{L,in}} \times \frac{F_1}{F_2} \times 100,$$

where $\bar{C}_G$ is the lithium concentration in the condensed steam (mean value of four or more samples); $\bar{C}_{L,in}$ is the lithium concentration in the saturated water flow rate F_1 entering the separator (after mixing), obtained from the concentration $\bar{C}_L$ measured in the subcooled water flowrate F_2 at the mixer inlet, by means of the following equation:

$$\bar{C}_L F_L = C_{L,in} F_1$$

An error analysis was performed to establish the relative error (in the form of standard deviation) associated with various data points. The detailed analysis indicated that the relative standard deviation for the primary separation efficiency is less than 0.2%, for the gravity region is less than 15%, for the dryer region is less than 28% and for the moisture carryover the relative standard deviation is less than 10%. The relative standard deviation associated with the irreversible pressure losses is less than 6%.

4.2.5. Experimental results

The experimental program was aimed at developing a high performance separator with low pressure drops. Therefore, the results are discussed in terms of separation efficiency, carryunder and pressure drops. The separation efficiency is defined as the ratio between the separated mass flow rate and the total mass flow rate, i.e.

$$\eta = \frac{\dot{M}_L - \dot{M}_R}{\dot{M}_L}$$

where $\dot{M}_L$ is the total liquid mass flow rate at the inlet of the separator (kg/s) and $\dot{M}_R$ is the mass flow rate of the unseparated liquid (i.e. the mass flow rate of water at the outlet) (kg/s). The separator performance is sometimes expressed in terms of carryover CO, i.e. the ratio of $\dot{M}_R$ to the total mass rate at the outlet expressed in percent

$$CO = \frac{100\dot{M}_R}{\dot{M}_{GO} + \dot{M}_R},$$

where $\dot{M}_{GO}$ is the gas mass flow rate of the outlet of the separator. The separation efficiencies for the steam water tests are depicted in figure 29.

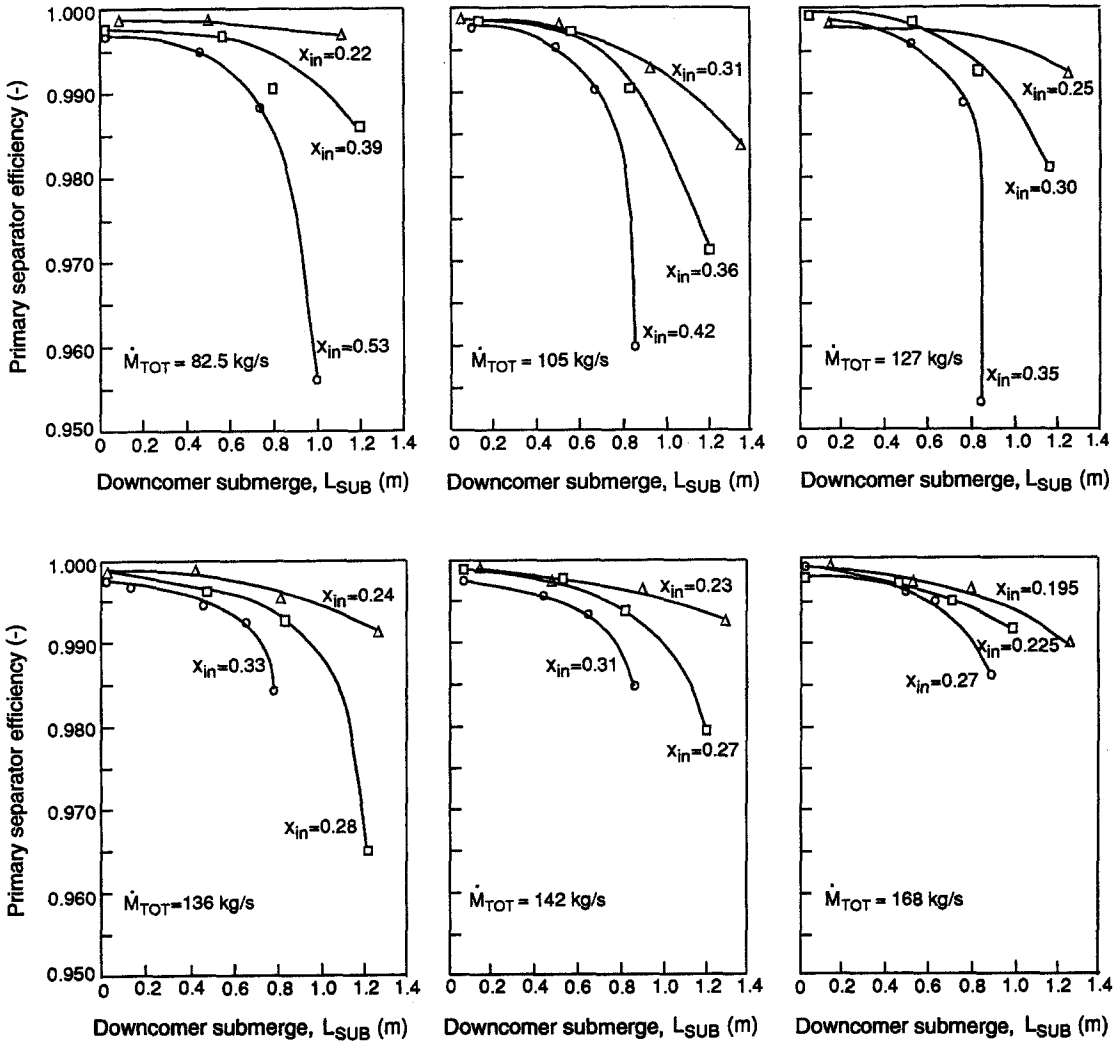

Figure 29. Primary separator efficiency vs downcomer water level for various total mass flow rates. Data from steam–water tests, at 6.9 MPa, of 500 mm IIMS (Mauro *et al.* 1990).

Table 7. Air–water to steam–water comparison for the separator loss coefficient

Air–water (ARAMIS $P \sim 0.3$ MPa)		Steam–water (GEST-SEP $P \sim 6.9$ MPa)	
L_{sub} (m)	K_G (—)	L_{sub} (m)	K_G (—)
0.0	5.8		
		0.0–0.5	~10.4
0.5	6.2		
0.75	7.3		
		⩾8.0	~11.2

The irreversible pressure losses were obtained from the measured differential pressure across the separator. The resulting values were expressed in terms of the loss coefficient K_G and following quantities:

$$\Delta p = K_G \frac{G^2}{2\rho_L}\left[1 + x\left(\frac{\rho_L}{\rho_G} - 1\right)\right]$$

where G is the total mass flow rate of the mixture at the inlet to the separator (kg/s), ρ_L is the density of the liquid (kg/m^3) and ρ_G is the density of the gas (air or vapor) (kg/m^3).

Experimental results of the pressure drops as were measured in the air–water, 0.3 MPa tests in the ARAMIS loop are compared in table 7 with the pressure drop measurements as obtained from the steam–water 6.9 MPa tests in the GEST-SEP loop. The pressure drops are compared in terms of the loss coefficient K_G: an increase of the loss coefficient is observed with the system pressure. Also, in all the tests it was observed that the loss coefficient increases with the downcomer submergence (L_{sub}).

4.3. Chevron Dryers

Chevron dryers are used extensively as the last separation stage in steam generators. There are a large number of configurations of these separators, e.g. figure 30. Mostly louvers with projections and corners are employed, such that the water droplets impinge on the chevron and are drained.

The design of the chevron dryers is mostly based on a cut-and-try procedure, and then on experimental testing. The aim of the design is to obtain a high efficiency, low pressure drop separator, which is reasonably easy to manufacture, install and replace.

Table 8. Description of various chevron separators with their characteristics (from McNulty *et al.* 1987)

	V_{cr} at inlet loading			
	2.04 (m/s)	$17 \times 10^{-4} \frac{m^3}{m^2 s}$ (m/s)	ΔP (kPa)	Eu (—)
(1) Four-pass, zig-zag wtih hooks, 5 cm spacing, 45° angle to flow	0.95	0.91	23.8	32.6
(2) Four-pass, zig-zag, no hooks, 5 cm spacing, 45° angle to flow	0.91	0.85	12.3	17.8
(3) Corrugated sheet metal packing, 1.25 cm corrugation height, 30 cm thick, 45° angle to flow	1.25	1.10	30.3	13.1
(4) Corrugated sheet metal packing, 2.5 cm corrugation height, 30 cm thick, 30° angle to flow	1.30	1.19	32.5	5.4
(5) Corrugated sheet metal packing, 2.5 cm corrugation height, 30 cm thick, 45° angle to flow	1.13	1.02	11.5	7.1
(6) Corrugated sheet metal packing, 12.5 cm corrugation height, 15.25 cm thick, 45° angle to flow	0.98	0.85	15.2	8.5

V_{cr} = the critical velocity above which re-entrainment occurs and performance deteriorates (m/s).
ΔP = the pressure drop in kPa.
Eu = $2\Delta P/\rho U^2$ = the Euler number.

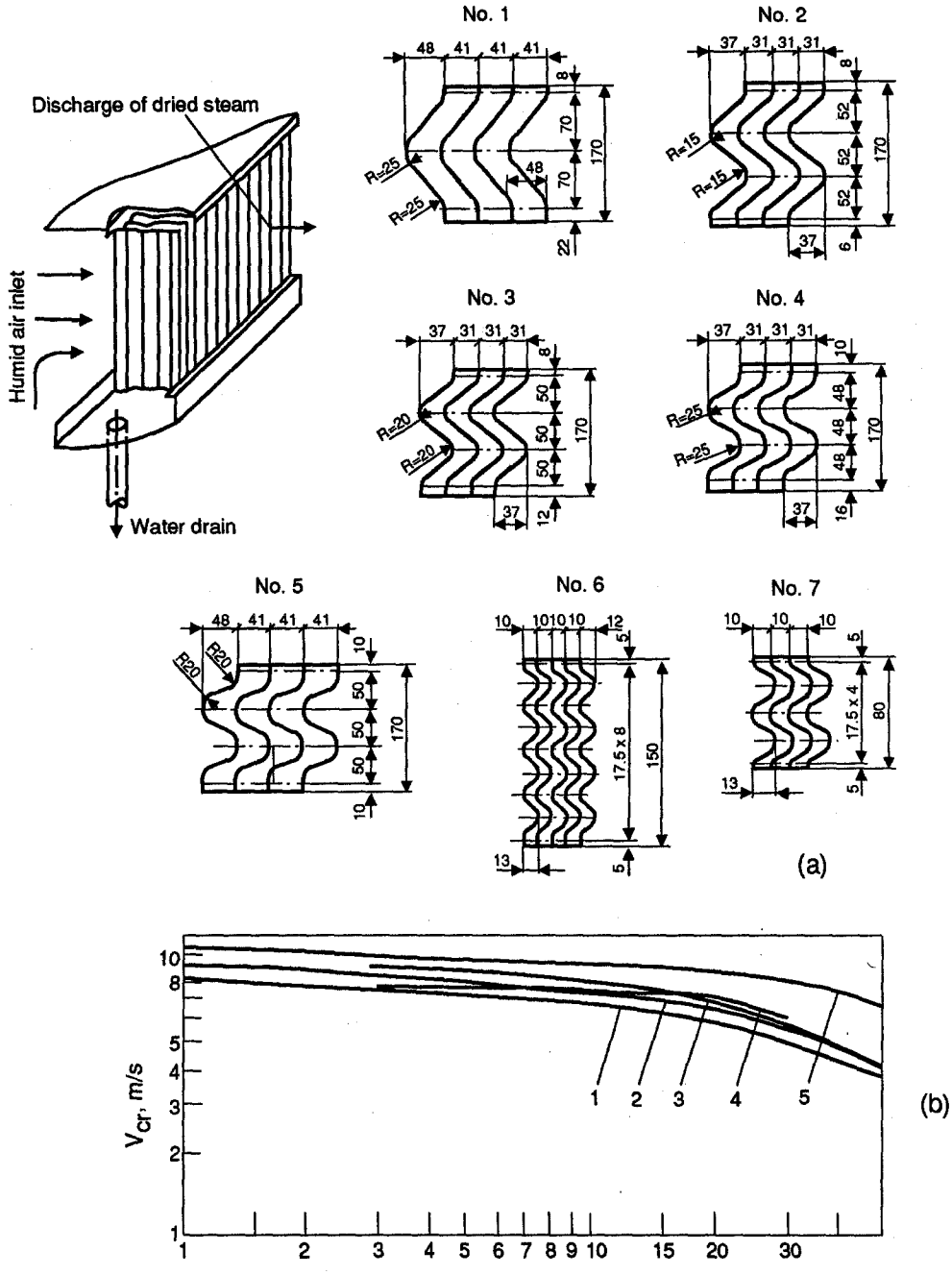

Figure 30. Separator unit, louvered elements (a) and values of critical velocities for the first five stacks (b) as a function of the initial humidity of the air (the numbers of the curves correspond to the number of stack) (Styrikovich *et al.* 1987).

Most of the information needed for the design of chevron separators is included in McNulty *et al.* (1986), Monat *et al.* (1986) and Moore *et al.* (1976). Sheet metal or plastic are formed into corrugations such as in figure 30. These corrugated sheets are then stacked in a vertical or horizontal direction. The separated water flows down due to gravity.

Also shown in the figure is the maximum allowable gas and liquid velocity before degradation in effectiveness becomes severe. The experiments were performed with air–water at atmospheric pressure. The degradation in performance is much like flooding and can probably be extrapolated to steam–water flows using flooding parameters.

It is clear that removal efficiency is quite good for drop sizes encountered in steam generators. The removal efficiency increases with velocity for all drop sizes until the point of reentrainment occurs.

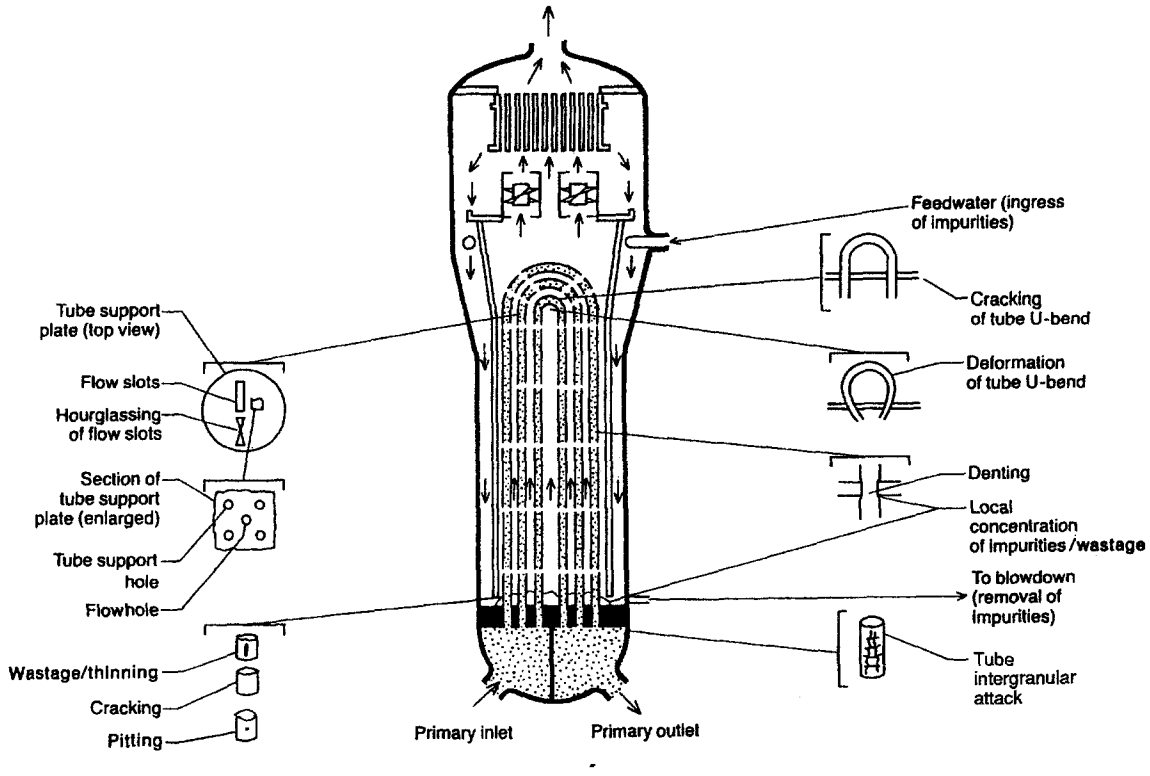

Figure 31. Sketch of recirculating steam generator (UTSG) with indicated problems.

Pressure drop is one of the important considerations when selecting a chevron geometry. Pressure drop characteristics of 6 separators are given in table 8.

5. PROBLEMS WITH STEAM GENERATORS

5.1. General

A schematic outline and problem areas of a UTSG is depicted in figure 31. The problem areas are associated with tube denting, intergranular attack (IGA), wastage and corrosion, flow-induced vibrations (FIV), cracking and deformation of U-tube bend, cracking of tube support plates, carryover and carryunder. IGA can occur in sludge piles above the tube sheet or at the tube support plate regions (Nordman *et al.* 1989; Campan & Shoemaker 1987).

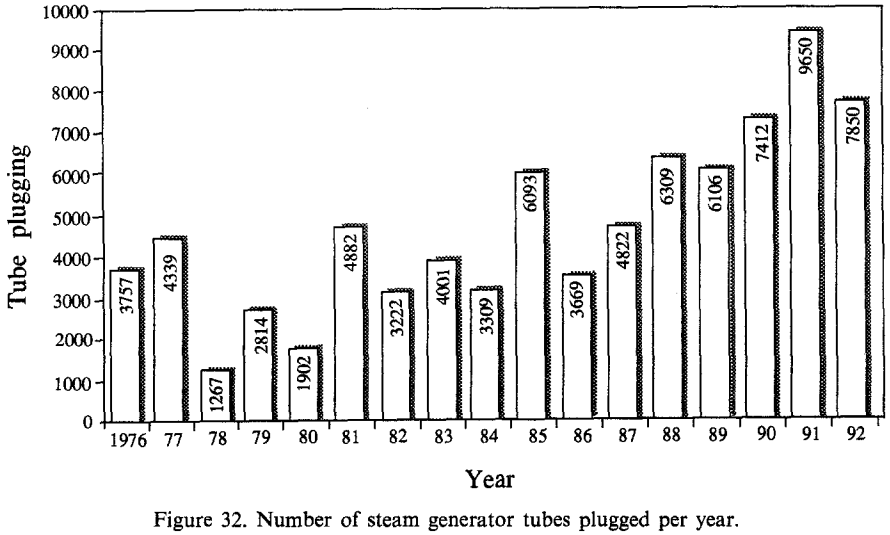

Figure 32. Number of steam generator tubes plugged per year.

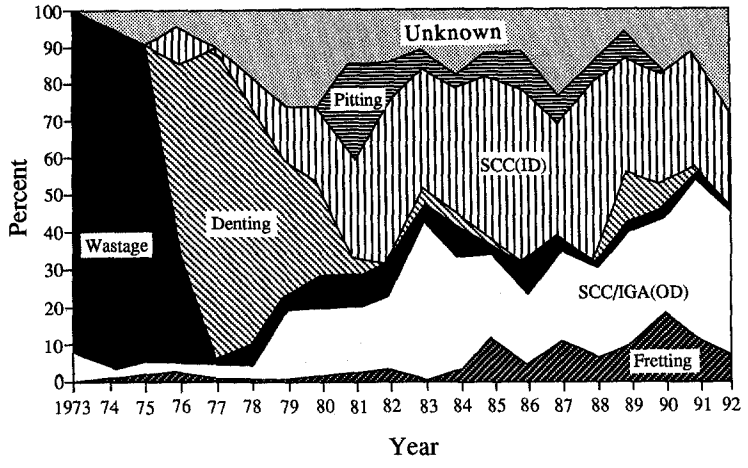

Figure 33. Causes of tube plugging worldwide.

In figure 32 are shown the number of tubes which have been removed from service (this is done by inserting a metal plug at the two ends of the tube, thus preventing primary flow from flowing through that tube—which removes this tube from service and reduces the heat transfer area) per annum, worldwide from 1976 through 1992.

In figure 33 are illustrated the reasons for removing the tubes from service, over the years. These are discussed in the following sections.

5.2. Tube Wastage (Thinning)

Tube wastage or thinning was one of the first corrosion problems that occurred in recirculating steam generators operating with sodium phosphate as a secondary water treatment. Phosphate wastage was first observed in commercial PWR plants when phosphate treatment was changed to a low sodium-to-phosphate molar ratio control, in which the Na/PO_4 molar ratio was maintained at about 2.0.

The phosphate wastage in PWR steam generators of the Westinghouse design occurred, for the most part, at the interfaces between hot-leg tubes and the tops of sludge piles that accumulated on top of the tubesheet. Where the sludge pile was deep, the zone of wastage extended about 2.5 cm into the pile; in most cases, it did not penetrate appreciably into the tube/tubesheet crevice.

As recognition grew that this new phenomenon was widespread and of a generic nature, major laboratory investigations were launched by the two U.S. vendors of recirculating-type steam generators. It was demonstrated in pot boilers that the location of attack was related to the concentration of aggressive species at steam–water interfaces.

The above difficulties led the vendors of the affected plants to recommend that the operators adopt an all-volatile water treatment (AVT) based on the use of ammonia and hydrazine. This recommendation was universally followed in the U.S. except for two plants.

Thus, the cause of wastage was determined to be an aggressive environment, and the corrective action involved a change in the environment for operating units from a phosphate chemistry to an AVT. However, as discussed below, this change led to another corrosion problem, namely denting.

5.3. Denting

Denting was discovered in 1975 when eddy current probes were prevented from passing through tube/tube support plate intersections by tube diameter restrictions. Denting is a term used to describe the localized tube diameter reduction that occurs when the hole of a carbon steel tube support plate corrodes to the point where the corrosion products deform the steam generator tubing (figure 34). The cause of denting is best explained by Potter–Mann-type linear accelerated corrosion (Paine & Green 1981), in which a non-protective oxide layer is formed as the corrosion progresses. These corrosion products, which have a bulk volume considerably larger than the

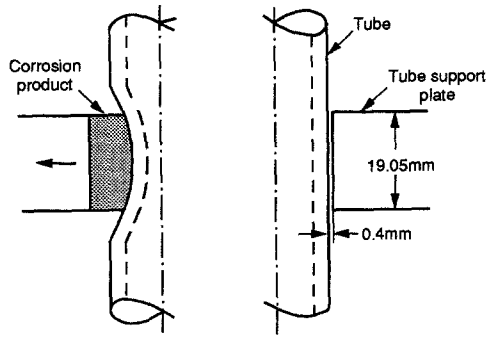

Figure 34. Denting at tube–support-plate intersection.

volume of metal corroded, fill the original tube-to-tube support plate crevice and deform the tube and the tube support plate simultaneously.

It is now obvious that denting occurs due to inadequate chemistry control of the water in the steam generator and of the feedwater. The most common source of ingress of impurities is from leaks in the condenser. Therefore, it is also obvious that cooling water leakage control is the key to steam generator chemistry control.

Some of the parameters affecting denting are as follows:

(a) Chlorides—denting occurs in crevice areas when high concentrations of acidic chloride species are present. Sample intersections of tubes and tube support plates (TSP) removed from dented steam generators have shown local chloride concentration of over 4000 ppm in the dented region. A contributing factor to this high local chloride concentration is inadequate local thermal–hydraulic conditions in the crevice between the tube and the TSP, causing a concentration of the aggressive species. In particular, it is hypothesized that alternate wetting and drying of the crevice, due to some instability of the two-phase fluid, can cause the observed increase in concentration.

Denting has been successfully reproduced in the laboratory indicating that non-protective magnetite (NPM) cannot be produced by neutral chlorides alone, but that the presence of reducible metal cations introduces NMP formation and the presence of oxygen induces NPM in neutral chloride solutions.

(b) Oxygen, copper and nickel—the roles of oxygen, copper and nickel in denting is not fully understood. In some laboratory tests they seem to have accelerated the denting—but these results are yet inconclusive. Oxygen in laboratory tests has been shown to produce an acid environment. If a large amount of neutral chloride is present, a small amount of oxygen can produce an acid chloride environment.

(c) Sulfates—the role of sulfates as a cause of denting must be evaluated since they are used to treat cooling tower water and in demineralizers. Preliminary tests are yet inconclusive, but it is possible that sulfate behavior would be similar to the behavior of chloride, thereby causing denting-type corrosion.

(d) Thermal–hydraulic power, level and local thermal–hydraulic conditions seem to play a significant part in the denting corrosion process. As indicated above, local instability of the two-phase flow can cause alternate wetting and drying in the crevice—a process which leads to local concentration of chemicals. Concentration of at least 20,000 times has been calculated for some laboratory experiments.

Tube support plates have various designs to support the tubes which penetrate them. These designs include drilled (cylindrical) holes, broached holes and lattice or eggcrate strips (figure 5). The broached hole design may have three (trefoil) or four (quatrefoil) flow regions adjacent to the tube. Calculations showed that in the drilled flow holes, only 3–8% of the flow passes through the tube–TSP crevice, while the remaining flow passes through the flow holes. Furthermore, any buildup of chemical solid deposits in the crevice will increase the resistance to flow and even less fluid will go through it. This may lead to high temperatures in the crevice and indeed, initial results from laboratory tests show that the tube wall superheat in the crevice is significantly higher than

the superheat existing away from the crevice. Values of 22°C superheat have been observed, with heat flux of about 315 kW/m^2 (figure 35). Local concentration processes are discussed in more detail in section 5.6 below.

All data thus far indicate that high tube wall superheating (most likely indicating dryout) occurs at the point where the tube is in contact (or close to it) with a concave surface of the TSP. On the other hand, where the tube contacts a flat or convex TSP, no indications of dryout have been detected. This suggests that TSP with flat or convex landing are superior to concave landing, and thus flat or convex landing TSP should be used in the future. The contact zone (lands) in broached designs now installed are generally flat.

Denting control: experience indicates that steam generator corrosion has been limited with rigorously controlled all-volatile-treatment (AVT) chemistry. In addition, limitation of the ingress of cooling water impurities, especially chlorides and dissolved oxygen, helps minimize local concentration of aggressive chemicals. Boric acid is also being used to inhibit the acidic chloride attack.

The major methods of the boric acid inhibitor application are the soak, the on-line application or a combination of the two. The soak application is defined as a short and intermittent application of the inhibitor to the steam generator, while at low power conditions. Another mode of soaking considers off-line, hot shutdown conditions for the steam generators. On-line addition of boric acid, when coupled with good chemistry control has been effective in arresting denting. Also frequent soaks (i.e. boric acid soak) help in returning chemicals from hideout. There have been very significant returns observed. For example, a unit operating at full load with chloride level at ~0.05 ppm, had an increase of chloride concentration to 5 ppm (a factor of 100!) when the unit was shut down to zero load.

5.4. Primary Side Stress Corrosion Cracking

Primary side stress corrosion cracking (SCC) of alloy 600 steam generator tubing evolved from a laboratory prediction during the 1950s and 1960s to a major degradation mechanism of the 1970s and 1980s in operating steam generators. As early as 1959, Coriou *et al.* (1959) reported on the cracking of high-nickel alloys in "high-purity" water at 350°C. During the following years numerous laboratory tests were performed in different environments in an attempt to duplicate and explain the Coriou observations. This work was summarized by van Rooyen (1975), Serra (1981) and Garud & Gerber (1983).

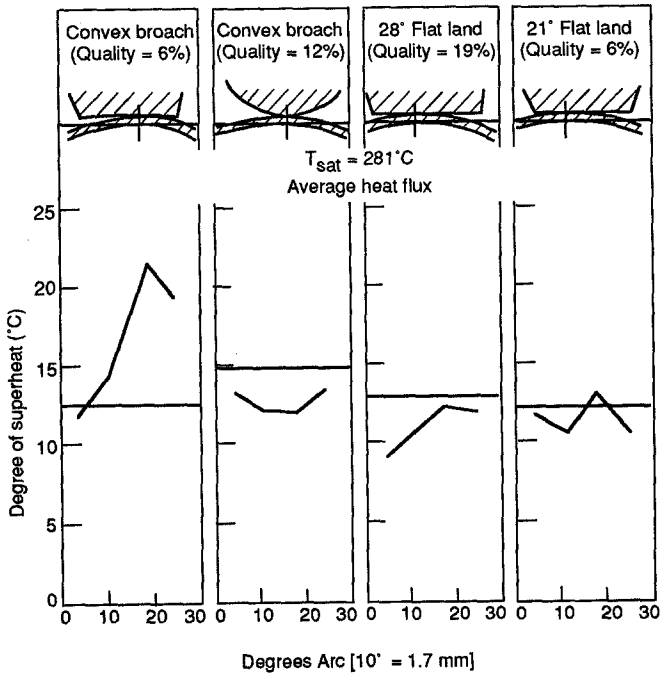

Figure 35. Tube wall superheat vs circumferential position.

Table 9. Plants affected by primary side cracking

Type of primary side attack†	No. of plants affected (as of 1985)
U-bend tangent cracks	16
Roll transition cracks	16
Roll expansion cracks	10
Explosive expansion transition cracks	1
Total number of plants affected‡	29

†Plants may be affected by one or more of these phenomena.
‡Excluding those caused by denting.

In 1971 the laboratory cracking phenomenon in high-purity water became an in-service degradation mechanism with the first confirmed primary side cracking of hot-leg roll transition regions at the tubesheet and suspected primary cracking in U-bends (Schenk 1976). U-bend leakage was experienced in Obrigheim steam generators, manufactured by Kraftwerk Union, after only 2 years of operation.

In recent years, cracking of alloy 600 tubes from the primary side has become a problem of increasing importance. As of early 1985, this type of cracking has been experienced by a number of plants (table 9) of some steam generator designs. Cracking in the U-bend has occurred mainly on the inner row at the apex and at the tangent points. Cracks have also occurred in the tubesheet in transition expansion and roll expansion regions. Primary side cracking is a form of intergranular stress corrosion cracking (IGSCC). This type of IGSCC, in common with other forms of stress corrosion cracking, occurs when tensile stress, certain environmental and material susceptibility factors are sufficiently severe.

Preventive measures against stress corrosion cracking, discussed by Frederick & Hernalsteen (1985) include reduction of temperature in the inner row U-bends. By orificing the inlet, the flow to these tubes is reduced, which would cause the primary coolant temperature to reach the cold-side temperature at the apex and thus reduce the time to crack by factors of about 2–3. For operating plants and for plants already built but not operating, reduction of tensile stresses by stress relief heat treatment and peening of the inner diameter (i.d.) surface are the most practical approaches.

Sleeving is a repair method. Sleeves up to 1 m long have been installed in the region between the lower face of the tubesheet and the first support plate as a corrective measure against pitting and intergranular attack at the outer surface. In some cases, even longer sleeves have been installed. The sleeves bridge the damaged area and are attached to unaffected material beyond either end of the damage. The ends of the sleeves are expanded hydraulically or explosively and are in most cases sealed by rolling, welding or brazing.

For recent plants, the corrective action has been to use tubing made of thermally treated alloy 600. Extensive tests (Airey 1983) have shown this material to be superior to mill-annealed alloy 600 with respect to primary side stress corrosion cracking. More recent steam generators are being fabricated using thermally treated alloy 690. Intergranular carbide precipitation reactions have been known to increase the stress corrosion cracking (SCC) resistance of nickel–chromium–iron alloys in nuclear steam generator environments for some time. However, even after a carbide precipitation thermal treatment, alloy 600 was still susceptible to SCC in the secondary side high purity water environments. The SCC of alloy 600 led to the development of a more resistant alloy, INCONEL(R) alloy 690, which has 60% Ni and 30% Cr compared with 72% Ni and 15.5% Cr for alloy 600 (Sedriks *et al.* 1979). It has been reported that this alloy is superior to thermally treated alloy 600 from the standpoint of resistance to stress corrosion cracking (Theus & Emanuelson 1983; Berge & Donati 1981; Smith *et al.* 1985).

In particular a workshop was held to collect available metallurgical and corrosion data on thermally treated (TT) alloy 690 and to compare these data with those for other candidate tube alloys for nuclear steam generators. The data indicate that TT alloy 690 is the most corrosion-resistant tube alloy. It is immune to stress corrosion cracking (SCC) in primary water, chlorides and sulfates. The TT improves its corrosion resistance to caustic, the most corrosive environment (Shoemaker *et al.* 1986). Manufacturing parameters for alloy 690 tubing are little different than for alloy 600 except that higher mill-annealing temperatures are required.

5.5. Sludge and Secondary Side Cracking

Sludge and secondary side cracking is found in tubes which show extensive intergranular corrosion in the tube/tubesheet crevice region (figure 36), mostly in the hot leg of the steam generators. In this crevice caustic deposits have been found, together with other deposited materials. The factors on which deposition depends have not yet been clearly defined. However, tube corrosion in the tubesheet crevice region has been witnessed in a number of plants, preferentially on the hot side of the steam generator. It is postulated that concentration of chemicals occurs in the region where alternate wetting and drying takes place. The presence of sludge on the tubesheet undoubtedly accelerates this process. The most corrosive region is judged to be the intermediate region, where alternate wetting and drying occurs.

Another mechanism of chemical concentration that has been postulated to operate involves the ability of any solute to raise the boiling point of water. The water is postulated to migrate into the device until it is heated to its boiling point, as determined by its, say, sodium hydroxide concentration. At this point vaporization takes place, and the caustic begins to concentrate in the remaining water, which raises the boiling point even further and allows further migration of the water. Through this process the temperature of the solution can ultimately reach that of the hot primary fluid ($\sim$325°C) and the concentration of sodium hydroxide in the solution can reach a maximum value of about 660,000 ppm. Thus, it is possible for a highly concentrated solution of sodium hydroxide to penetrate the entire length of the tubesheet crevice and cause substantial corrosion.

The copper content of the sludge can vary significantly, depending on the materials of the balance of the plant. Copper seems to primarily affect the morphology of the sludge, thus changing the thermal–hydraulic characteristics. Interestingly enough there is little difference in sludge morphology between plants converted to AVT operation and those always on AVT operation.

It is quite clear that lower heat flux (or lower temperature in the crevice) may mitigate the occurrence of the tube corrosion in the tubesheet crevices. Since this may mean reduced power of operation, other means were sought to alleviate the problem. One process, developed in Japan, is crevice flushing. This involves filling the crevice with water and depressurizing the steam generator to cause bubble nucleation in the crevices which forces the liquid containing dissolved chemicals out of the crevice top.

In one case the steam generator was filled with water up to 60 cm deep and the system was brought to a temperature of 120°C, with the main steam isolation valves closed. The pressure in the steam generator reached the saturation pressure of about 0.2 MPa. The reactor coolant pumps were stopped and the unit was allowed to remain in this condition for a short time to allow for dissolution of deposits in the crevices. The water on top of the tubesheet was then subcooled by adding cold water and the relief valves were opened and the generator was rapidly depressurized

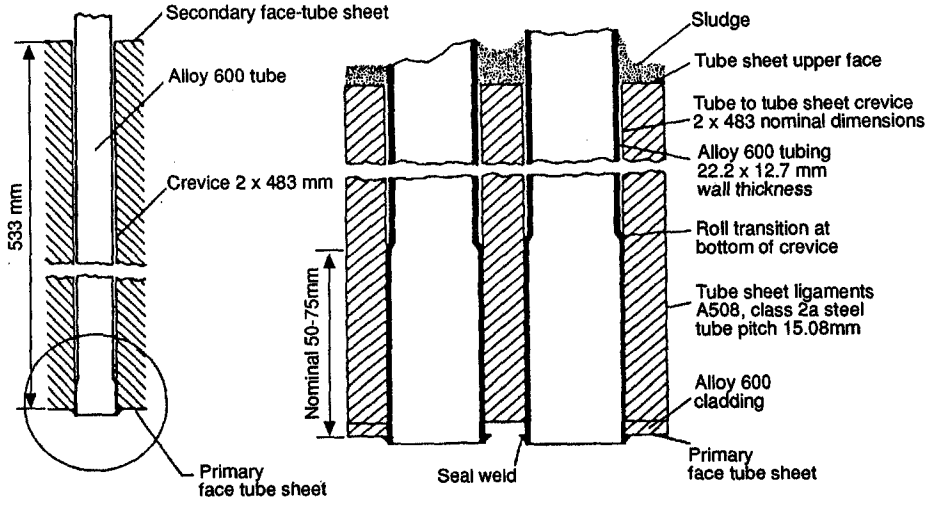

Figure 36. Typical steam generator tube–tubesheet annular crevice.

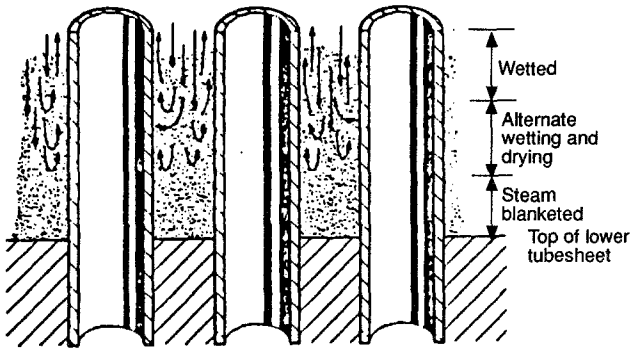

Figure 37. Sludge deposited on top of the tubesheet.

for about 8–15 min. The tubesheet was then cooled and the generator was drained. The cycle, which took about 6 h, was then repeated. Results of these procedures were very encouraging.

The mechanisms of concentration of chemicals in the sludge are similar to the mechanisms which control the phenomenon in the crevices. It is postulated that the liquid flows down in the center of the space between the tubes (see figure 37), and reaches the region of alternate wetting and drying). There, vapor is chugging and bubbles are rising to prevent the liquid from penetrating the lower part of the sludge pile, which therefore stays dry, at a temperature which is close to the temperature of the primary coolant. There is further discussion of this concentration mechanism in section 5.6 below.

A recent study by Beal & Chen (1986) developed a mathematical model of sludge behavior in a pressurized water reactor steam generator. This model included the differential equations that describe the buildup of sludge in various places in the steam generator and also the means of determining the rates associated with the processes that govern the behavior of the sludge.

The sludge behavior was modeled by representing the liquid mass in the steam generator by a number of regions. For example, one might have two regions, one for the liquid on the hot side of the tube bundle and one for the liquid on the cold side. Each liquid region has associated with it horizontal and vertical deposit subregions representing the tubes, tubesheet or support plates. By writing a mass balance equation for the concentration of sludge in each liquid region and the mass of sludge in each deposit subregion, the time behavior of the sludge can be described as it deposits on the surfaces and is reentrained back into the liquid.

The computer program that calculates values for all the rate coefficients and solves the mass balance equations is called SLUDGEM. It is written in FORTRAN and can be run on a personal computer.

SLUDGEM results have been compared to actual measurements and estimated values of sludge deposit weights, concentrations and amounts removed by a blowdown and the agreement has been good (table 10). The available data are very sparse, however, and do not provide complete confirmation that the model predictions are accurate. Nevertheless, it is judged that the model is sufficiently well versed to be used to estimate the effect of differences in design or the effectiveness

Table 10. Comparison of calculated and observed sludge distributions

Sludge location	Calculated	Observed
Tubes (g/cm^2)		Deposited mass per unit area is not known
Hot side	0.0005	
Cold side	0.0007	
Tubesheet (g/cm^2)		Deposited mass per unit area is not known with any precision. Anecdoctal evidence indicates small deposits at periphery, increasing in thickness toward center, with two crescent-shaped regions of very large deposits (up to 30–38 cm deep, or about 100 g/cm^2) on either side of the tube lane. Anecdotal evidence indicates very small deposits. Beal (1970) gives 250–1400 ppb with a mean of about 800 ppb. Beal (1970) gives 6–34% removed with a mean of 20%
Outer half	0.0009	
Inner half	20	
Stagnant		
Hot side	100	
Cold side	80	
Support plates (g/cm^2)	2.E-4	
Bulk concentration (ppb)	700	
Blowdown (%)	20	

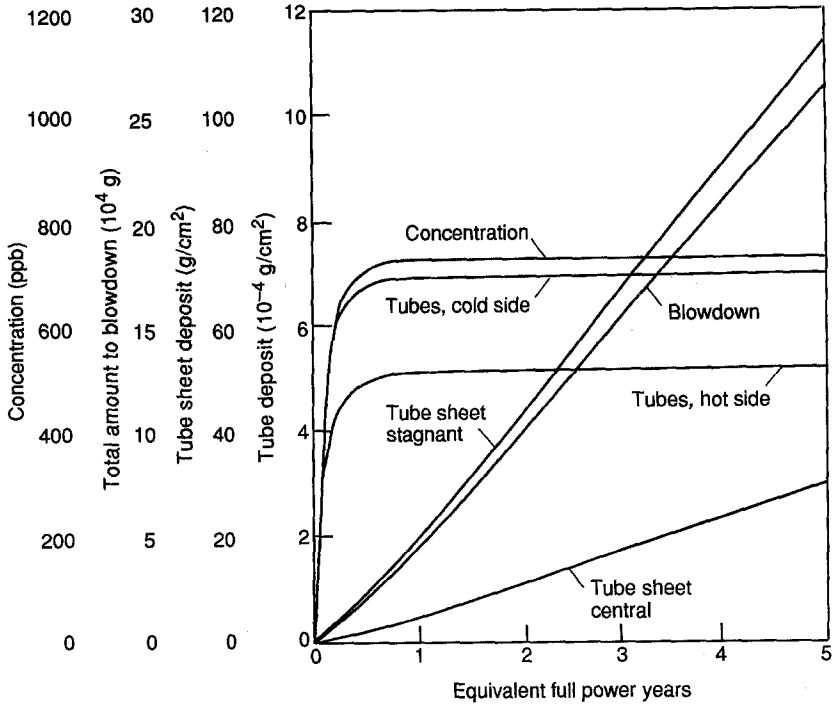

Figure 38. Calculated time behavior of sludge.

of a sludge trap, provided one is mindful that it could produce misleading results. The model predicts that the sludge deposits on the tubes and support plates build up fairly fast but level off and become constant after about 6 months (figure 38).

The rate of magnetite deposition on the tubesheet is estimated by the use of a particle flux (Wazzan *et al.* 1987) derived from the conservation equation of the particles and by the method of Thomas & Grigul (1984), which assumes that when a fluid volume evaporates, its entire particulate content will deposit on the tubesheet. Table 11 compares measured values of magnetite deposition at Bugey 4 plant to the two methods, assuming values of magnetite concentration from 10 to 1000 ppm. Order of magnitude agreement is reached. The distribution of sludge on the tubesheet of Tricastin 1 is also reported. In general, the maximum deposits occur where the horizontal velocity across the tubesheet is less than 0.49 m/s and where simultaneously the quality is high.

Sludge control: the presence of large quantities of sludge indicates clearly that blowdown is inefficient for corrosion product removal in current design and at current rates. It is also expected that demineralizers, and proper treatment of feedwater can reduce sludge buildup by a factor of 2–10. Demineralizers also reduce ionic levels during condenser in-leakage. It has also been demonstrated that there is a relationship between air in-leakage and sludge accumulation. The air in-leakage occurs at subatmospheric locations in the secondary plant including the low pressure turbines, the condensers, and the inlet end of the condensate pump.

Table 11. Computed and measured magnetite/sludge deposit on tubesheet; Bugey 4

	Magnetite weight W (kg/year)		
	Computed		
Magnetite concentration, c_a (ppm)	Particle flux	Thomas & Grigul (1984)	Measured at Bugey 4
10	9	550	Actual, 256 kg Estimated to be lost, 66 kg Total, 323 kg
100	90		
1000	900		

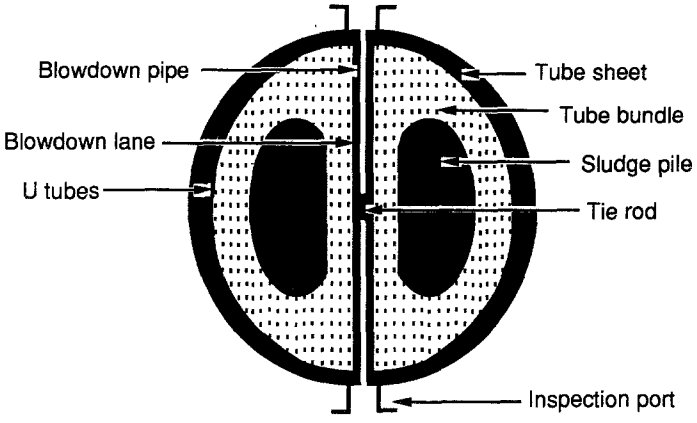

Figure 39. Sludge forms in the U-tube bundle of a steam generator in an irregular pile, which distorts the inspection signal of an eddy-current probe.

Increasing the pH of the feedwater to 9.4 (9.3–9.6) in an all-ferrous system can reduce the total iron transport to the steam generators by about one third. Also, recent use of morpholine chemistry has reduced the iron (sludge) input to the steam generator. Morpholine is less volatile than ammonia and produces a high pH in the balance of plant piping which leads to reduced corrosion (and reduced erosion–corrosion). In these cases, where sludge has accumulated on the tubesheet (normally in kidney shape as in figure 39), it may be extremely difficult to remove, because it becomes hardened and is very tenacious. The amount and location of the sludge can be monitored by various means of NDE techniques such as eddy-current testing (ECT), elementary visual probes and, most recently, remotely operated robots. Sludge removal can be achieved, with various degrees of success, by chemical cleaning or by mechanical removal. Chemical cleaning can be used in UTSG and OTSG (see below). Various methods were developed by the Steam Generator Owners Group, EdF, KWU and others. The EdF method (use of gluconic acid) was applied to the Tihange steam generators.

The three most common mechanical methods are blowdown, gas pressure and lancing (Lee 1989).

The blowdown method, only for recirculating steam generators, makes use of a draining system built into the steam generator. This is the blowdown pipe which is located across the tubesheet in the non-tubed region (the blowdown lane) between the two legs of the U-tube bundle. The blowdown typically removes only the sludge that exists as suspended particulates. Specifically, deposited sludge is not removed. This sludge removing operation has quite a low efficiency, and it is ineffective in removing hardened sludge.

Two gas pressure methods: are used for removing magnetite deposits and sludge from the flow passages and top surfaces of tube support plates: the "water slap" and "pressure pulse" methods. Both of these methods are considered proprietary by their developers. Both techniques utilize devices with quick acting valves which release large volumes of nitrogen gas at approximately 60 bar below the water surface in partially filled generators. The rapid release of gas produces a large bubble which violently displaces the surrounding water. The displaced water surges back and forth through the flow holes, dislodging deposits which have formed in and around these orifices and flushing the loosened deposits, as well as sludge which has collected on the top surfaces of the tube support plates, into suspension. Once in suspension, the particles of magnetite deposits and sludge are removed from the generator by various methods. The principal method incorporates a closed loop recirculation system for the water and suspended sludge. Filters in the loop extract the sludge before the demineralized water is returned to the generator. Other extraction methods include the use of special draining procedures, and sludge lancing for the particles which settle on the tubesheet after being dislodged and flushed from high elevations.

These gas pressure methods have been applied to once-through steam generators with varying degrees of success.

Lancing methods: the most common technique is sludge lancing which uses high-pressure water jets to remove sludge from generators. The basic process involves inserting a device with water

Table 12. Lancing practices of nine vendors

Vendor code	1	2	3
Equipment characteristics			
Lance location	Periphery	Two heads in blowdown lane	Blowdown lane, periphery
Extraction nozzle location	Blowdown lane or annulus	Two nozzles per BD lane hand hole	Annulus
Auxiliary flushing nozzles	—†	—	—
Number of lance jets	Three per head	Four per side	Two per side (BD), 9 per side (periphery)
Angle of attack	Variable	90° to blowdown lane	30° and 150° with adjustable heights
Jet pressure (psig)	Adjustable to 3000	Adjustable to 2900	Adjustable to 2900
Scanning mode	Continuous, oscillating	Continuous, oscillating	Continuous, oscillating
Tube lane indexing	Manual	Automatic	Manual
Recirculating water filter size	1 μm	0.5 μm	0.5 μm
System experience			
RSG tube bundle pitch	Square and triangular	Square and triangular	Square
OTSG tube bundle pitch	Under development	Under development	Yes
Type of sludge	Soft, clay	Soft, hard	Soft
Inspection and control			
Prelancing	Video camera	None	Fiber optics
In-process	Video camera	Sight glass in extraction line	Video camera
Postlancing	Video camera	None	Fiber optics
System qualification			
Generator mockups	CE, W.51	OTSG	—
Type of modeled sludge	Soft, clay-like	Flakes	—
Tube abrasion-recirculating water	Yes	Yes	—
Tube abrasion-entrained debris	No	No	—
Water droplet erosion	No	No	—

†Utility identities are on file at EPRI.

nozzles into the interior of the generator through an inspection port (hand hole) in the shell. High-pressure jets of water are then directed down the rows between the tubes. The high-pressure jets dislodge the sludge from around the tubes and flush it towards an extraction device. Extraction nozzles suck up the sludge–water mixture, which is then piped out of the generator through flexible hoses to a surge tank. The sludge and water mixture is next pumped through a series of filters to remove the suspended sludge particles.

A survey of lancing service vendors was conducted (Chick *et al.* 1988). Table 12 shows a summary of these lancing practices for nine vendors. The lancing jet pressures range from 50 to 270 bar. Each vendor offers similar, but unique, services relevant to equipment characteristics, system experience, inspection and control and system qualification.

A summary of the combined survey responses of the service vendors and utilities indicates that sludge lancing has demonstrated a capability to remove soft and, to a lesser extent, sticky sludge accumulations from the tubesheet of both RSGs and OTSGs. As the sludge becomes more cohesive, systems which lance in multiple directions appear to be more effective than those which lance in only one direction. It is doubtful that the surveyed techniques remove hard (consolidated) sludge deposits to any significant degree. The efficiency of the various vendor processes is uncertain. The surveyed sludge lancing systems do not address sludge deposits above the tubesheet. Radiation exposure of personnel is potentially higher for those systems which require more frequent manipulation of equipment located at the hand holes. To improve the lancing capability, joint research was undertaken by EPRI and Con Edison to develop a remote-controlled device—CECIL.

The problem of access to locations deep within the tube bundle was solved by producing a flexible belt, or flex-lance, which could be inserted into the lanes between columns of steam generator tubes. Two flex-lances were designed which carry a miniature color video camera for high-resolution inspection of the interior of the tube bundle and observation of the subsequent cleaning process; a high-pressure conduit to release water close to sludge deposits; and a core-drill bit to retrieve hard sludge samples.

As shown in figure 40, the flex-lance is introduced into the intertube lane by a riding, curved side located in the steam generator's central blowdown lane. Repeatable, accurate access to selected sites in the tube bundle is realized by installing this curved guide in a robotic carrier which can:

- Position the outlet of the curved guide at the entrance to any intertube lane;

Table 12. *(Continued from opposite page).*

4	5	6	7	8
Blowdown lane Annulus	Blowdown lane Annulus	Blowdown lane Annulus	Blowdown lane Annulus at blowdown lane hand holes	Blowdown lane Annulus
Annulus Two per side	Annulus Three per side	Annulus Four per side	— Four per side	— Three per side
90° to blowdown lane	Adjustable	30°, 90°, 150° to blowdown lane	90° to blowdown lane	90° to blowdown lane
1350 and pulsed Continuous, rotating Automatic 1 μm	2000 Continuous, rotating Automatic 1 μm	4000 Height adjustment Automatic 1 μm	1500 Continuous, rotating Automatic 1 μm	750 Manually rotated Manual 1 μm
Square No Soft	Square, triangular No Soft, hard	Square, triangular No All types	Square No Soft	Square No Soft
Water balance None Fiber optics	None Pressure drop across filters None	None None Fiber optics	Fiber optics None Fiber optics	Fiber optics None Fiber optics
— —	No No	Yes Hard phosphate, magnetite, hematite	W.51, W.D3 Magnetite in plaster of paris	No No
— — —	No No No	Yes Yes Yes	Yes No No	No No No

- Extend or retract the flex-lance once the curved guide has been positioned correctly; and
- Rotate the curved guide along its longitudinal axis to accommodate varying sludge pile heights.

The first field trial of CECIL successfully demonstrated its capabilities for high quality inspection and improved sludge removal, with reduced personnel radiation exposure. Use of CECIL is growing.

5.6. Local Concentration Processes

Most of the corrosion problems encountered in nuclear steam generators can be attributed to the concentration of non-volatile ionic impurities (hideout) in local regions. Hideout is a result of heat flux-driven concentrating processes. It occurs in semi-isolated locations that have restricted access to free circulating bulk water and within which the temperature is higher than the saturation temperature of pure water at steam generator pressure. Typical locations are the crevices between tube and tube support plates, crevices within the tubesheet, sludge piles surrounding active steam generator tubes and porous scale deposited on active tubes. The temperature elevation above the secondary water saturation temperature at these locations is referred to as the local superheat. For a PWR steam generator, this is limited to the difference between the local primary coolant temperature and the saturation temperature (T_{sat}) at the steam generator pressure.

Boiling action draws bulk water into these locations and expels steam or a mixture of steam and water. Some of the non-volatile dissolved substances that are drawn in along with bulk water remain behind to accumulate, initially as an increased concentration in the liquid within the occluded, semi-isolated region. If the concentration increases to the solubility limit for a solid substance, solids will precipitate to block or alter access and escape paths. Highly water-soluble substances can concentrate to the extent that the boiling point of the local fluid is significantly increased over the boiling point of pure water at steam generator pressure. Boiling action will stop wherever concentration increases to the extent that the boiling point elevation equals the local superheat.

Concentrating processes that reach the ultimate concentration at which boiling stops are "thermodynamically limited". The thermodynamic limit on achievable concentration is determined by local superheat, the boiling point elevation characteristics of dissolved substances and their solubilities. However, the rates of input and output for dissolved substances may become equal

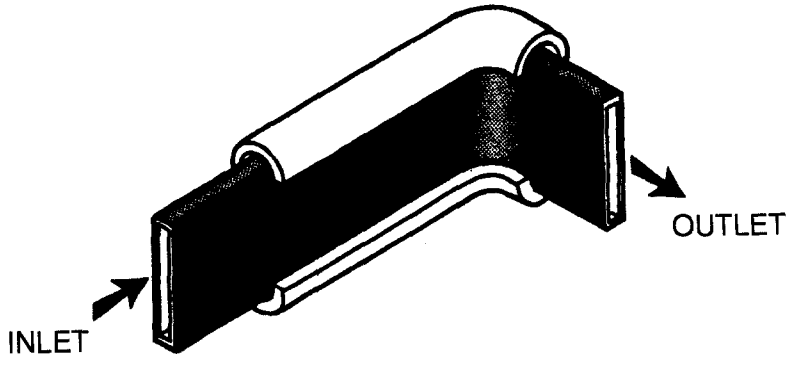

Figure 40. Flexible intertube lance concept.

at some concentration that is less than the thermodynamic limit, resulting in a steady state for which no further net accumulation occurs. This is known as a "kinetically limited" concentrating process. Whether the concentration at a particular location is kinetically limited or thermodynamically limited depends on many factors. These include the geometric configuration of the location itself and of the pathways connecting it to the bulk water, the local temperature and heat flux and the boiling point and other characteristics of the fluid. Laboratory data (Solomon 1977) indicate that both thermodynamically limited and kinetically limited situations do occur, possibly in close proximity to each other, but the interacting dynamics of heat and mass transfer with boiling on a microscopic scale are complicated and difficult to predict. Further, the concentration processes are also affected by the crevice dilution that occurs during power reduction (hideout return). This dilution during shutdown may be a limit on concentration for some application. The ultimate concentration in a thermodynamically limited process is independent of the bulk water concentration, while in a kinetically limited process the ultimate concentration increases with increasing bulk water concentration. This is schematically illustrated in figure 41, adapted from Solomon (1977).

The tube wastage near the top of the tubesheet in steam generators operated with phosphate chemistry was recognized in the early 1970s and is considered to be caused by concentration phenomena in the sludge pile on the upper face of the tubesheet. Figure 37 illustrates the heat transfer regimes postulated to exist in the sludge. Near the top of the sludge there is a fully wetted region, where the vapor that is generated by boiling is fully replenished by liquid. Further down the sludge there is a region of alternate wetting and drying, where the liquid flow is not sufficient to fully replenish the vapor formed by boiling. Finally, the lowest part of the sludge is a

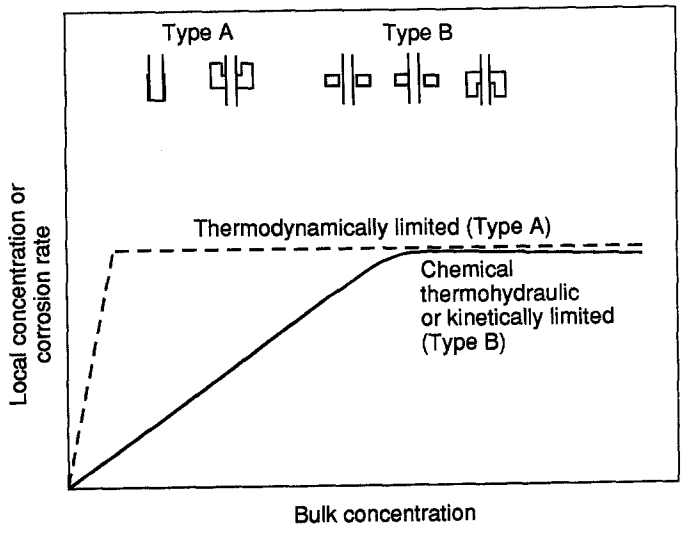

Figure 41. Behavior of concentrating devices (Solomon 1977).

Table 13. Sludge characterization data

Sludge	Void fraction			Surface area/volume ($m^2 cm^3$)	Nominal void diameter‡ (μm)	Nominal particle size (μm)	Copper content (wt%)	Permeability§ (darcy)
	Based on bulk density	Based on tap density	Measured†					
Indian Point 3	0.71	0.56	0.69	5.91	10	8.7	26	0.15
Indian Point 2	0.66	0.53	0.62	6.41	3.5	15	14	0.10
Tihange	0.75	0.64	0.72	2.56	1.7	13	1.42	0.25
San Onofre	0.78	0.66	0.71	3.84	1.5	15.5	18	0.47
H. B. Robinson	0.73	0.58	0.72	4.44	8.5	24	19.6	0.09
Point Beach 1	0.75	0.58	0.72	4.92	7.5	11	49	0.05
Zion 1	0.75	0.57	0.62	3.23	0.8	12	5.8	0.31
Trojan	0.72	0.59	0.70	4.55	10	—	32	0.37
Metallic sinter	0.35	—	0.32	—	28	—	—	1.98
1-mm spheres	0.39	—	0.37	—	402¶	1000	—	420

†Measured by mercury porosimeter.
‡Between particles only.
§Based on tap density.
¶Calculated.

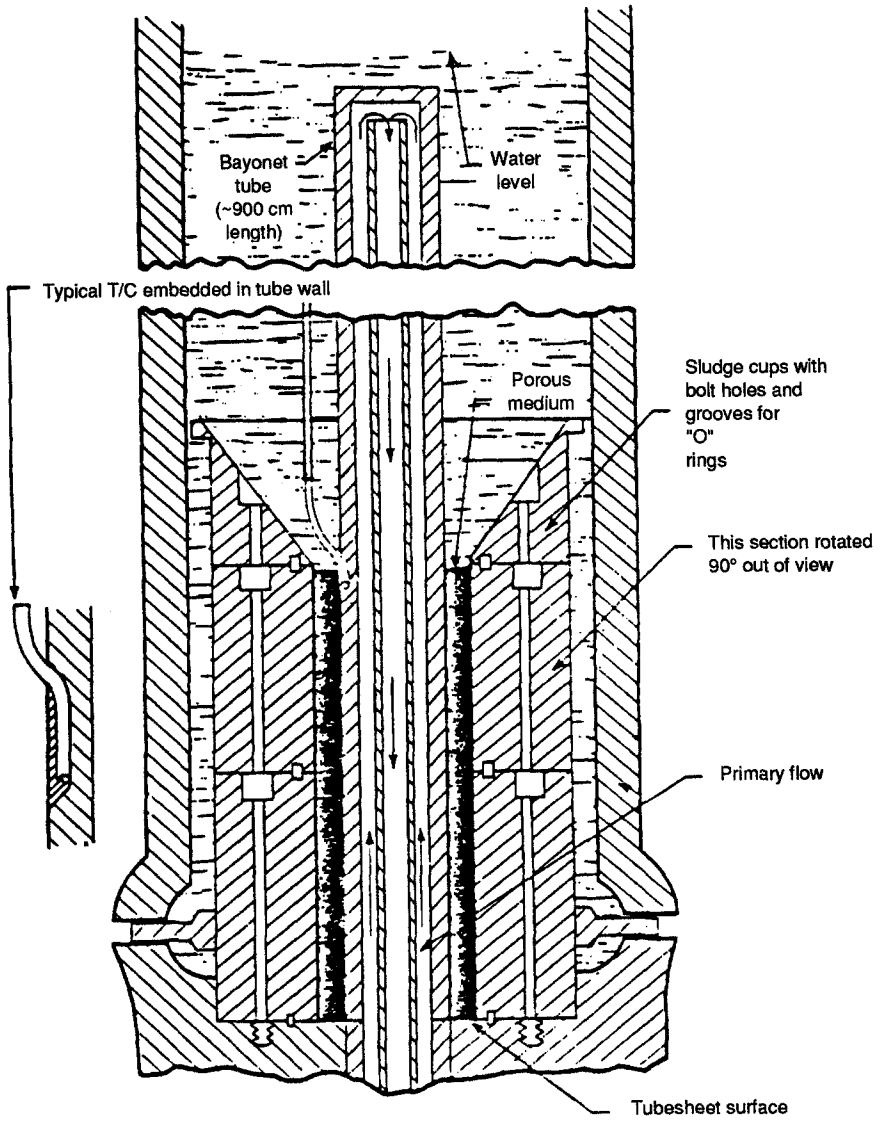

Figure 42. Sludge pile model boiler.

steam-blanketed region, which no water penetrates. The highest concentration of chemicals probably occurs in the intermediate region of alternate wetting and drying. At first thought, the sludge would be expected to contain mainly dry steam at the primary temperature, but a completely dry region would not lead to chemical deposition. However, if the boiling point was raised by soluble chemicals such as NaOH and NaCl, more of a liquid phase would exist in the crevice. These or other chemicals may reach saturation concentration and precipitate out as solid deposits within the crevice. These higher concentrations can lead to corrosive attack on the tubing. Further details on the chemical concentrating aspects of steam-generating systems may be found (Cohen 1977, 1980).

Programs were conducted to evaluate the phenomena (Baum & Gearney 1981). Samples of eight plants' sludges and several sludge stimulants were identified in preparation for thermal and hydraulic tests. Additional properties of the plant samples and the sludge simulants, which may be related to their thermal–hydraulic behavior, are presented in table 13 (Becker & Esposito 1981).

The thermal–hydraulic test program conducted on the Tihange and Indian Point 3 samples and the two sludge simulants was performed in the sludge pile model boiler (SPMB), depicted in figure 42. The boiler was connected to primary and secondary flow loops such that representative steam generator thermal and hydraulic conditions were produced at the bottom of the boiler. The internals of the boiler consisted of the heat transfer tube and segmented sludge cups containing the sludges. The heat transfer tube was fabricated from a second of 19.05-mm o.d. alloy 600 tubing

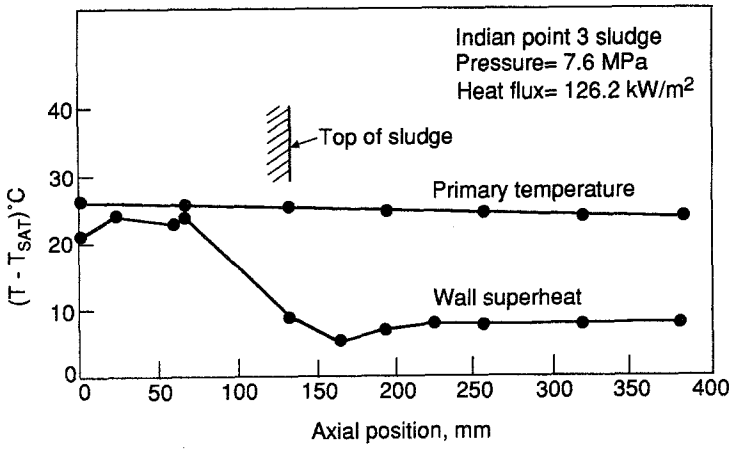

Figure 43. Sludge heat transfer studies.

having a 1.09-mm wall thickness. Sheathed 0.50-mm o.d. thermocouples were embedded in the tube in order to identify the wetted and non-wetted regions on the tube surface. The primary tube penetrated the boiler in the bayonet tube configuration indicated in figure 42.

The sludge cups were designed to simulate a unit cell around one steam generator tube. The lower and intermediate sludge cups were fabricated in removable cylindrical segments to accommodate a variety of sludge fill heights. The top cup had a conical upper surface so that fluidized sludge would be returned to the sludge pile.

A series of tests without sludge were initially performed in order to obtain reference nucleate boiling wall superheat data. The testing was performed over a range of nucleate boiling heat fluxes of 56.8–420 kW/m^2 and secondary pressures of 5.5–75 MPa. One typical run (figure 43) shows that dryout occurs about 2.5 cm below the top of Indian Point 3 sludge at a heat flux 126 kW/m^2. Least-squares fits to the wetted length versus heat flux data are plotted in figure 44 for all the sludges tested. The first observation to be drawn from figure 44 is that the wetted length showed a light dependency on the heat flux for the sintered sludge simulant and the two actual sludges, but was strongly dependent on the heat flux for the 1-mm spheres. This observation is probably associated with the large pores and the very high permeability of the 1-mm spheres as opposed to the small pores and the low permeabilities of the other three sludges as shown in table 13. The second observation is that the 9.5 mm wetted length for the sinter was shorter than the wetted lengths of the 1-mm spheres. This was expected from a comparison of the characterization data for the two simulants. Since the permeability of the 1-mm spheres was greater than that of the sinter by a factor of about 200 (see table 13), liquid should be able to penetrate the 1-mm balls further than the sinter.

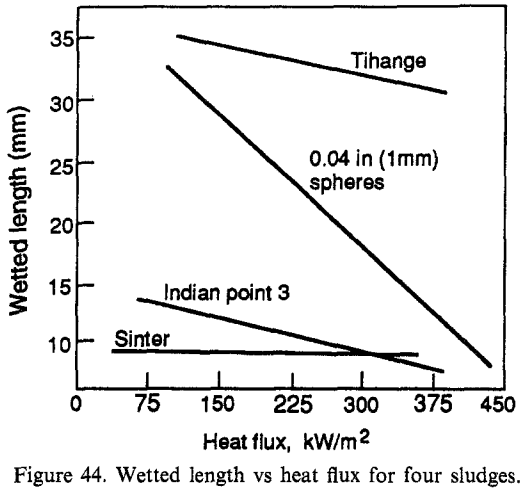

Figure 44. Wetted length vs heat flux for four sludges.

The third observation is that the wetted lengths of the two plant sludges were considerably longer than would be expected solely on the basis of the permeability measurements. Exposure of the actual plant sludges to the boiling environment may have produced significant increases in the sludge permeabilities. Evidence of changes in the sludge morphology were found for both sludges tested. In addition, the absorbing action from capillary forces was probably quite strong for the sludges compared to the sludge simulants.

Finally, it was observed that the wetted length of the Tihange sludge was considerably greater than that of the Indian Point sludge. This is attributed, in part, to some fluidization near the top of the Tihange sludge bed. Such fluidization is consistent with flow visualization studies reported. The Indian Point sludge, on the other hand, became hard and adherent to the tube wall during the course of the testing.

The analytical modeling of Baum & Gearney (1981) provides a fairly generalized methodology for determining the liquid and vapor flow distributions within porous media. The model simulates the qualitative trends in the test data quite well, although perhaps because of the peculiarities of the test data, it does not always reproduce the wetted length.

Visualization studies and temperature measurements were made in a granular bed of nickel or copper particles. The granular bed filled an annular space between two concentric glass tubes or the space inside a square array of nine tubes. Water filled the voids and the space above the bed and was brought to boiling by a heat flux through the wall of the tubes. It was found that counterflow between the liquid and the vapor escaping through the voids of the bed can be established over a certain height of a wetted region only. The boiling process increases this height by the creation of horizontal cracks and vertical channels, through which the vapor can escape. A dryout region is established when the total height of the bed is larger than the height of the wetted region. Corrosion is expected in the dryout region or at its border with the wetted regions by concentration of aggressive chemical species dissolved in the water.

Additional analytical studies of boiling in a porous bed are reported in Abe *et al.* (1982).

Concentration in tube/tubesheet crevices (closed end)

As mentioned above, concentration processes are either thermodynamically or kinetically limited. Concentration processes in single-end open (one-end closed) crevices tend to be thermodynamically limited. That is, the solution will concentrate in the crevice until the boiling point elevation equals the available superheat ($T_w - T_{sat}$ for the pressure) or until the solution is saturated with respect to some solute, which will then precipitate. However, these crevices do not always act as concentrators. The conditions under which concentration will or will not occur are described below.

Tubes in some PWR steam generators are mechanically expanded and welded only at the bottom (i.e. the primary face) of the tubesheet, which is approximately 56 cm thick. This results in a deep crevice approximately 0.18 mm wide between the tube and the tubesheet. Some manufacturers have eliminated most of this crevice by fully expanding the tube (figure 45).

Bulk steam generator water containing soluble chemical impurities will enter the crevice at the top and begin to penetrate along its length as a result of capillary and gravitational forces. Because

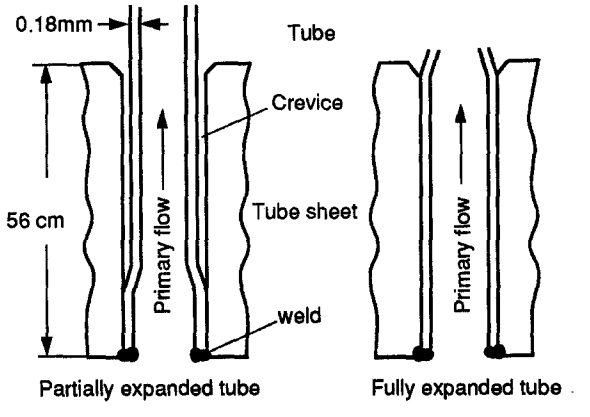

Figure 45. Tube–tubesheet joint geometries of steam generators used in PWRs.

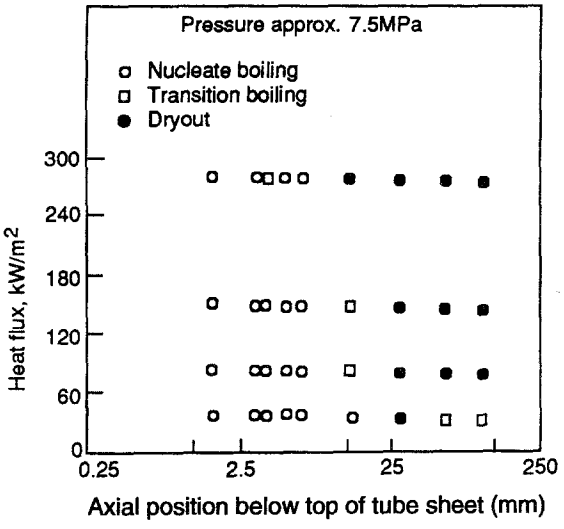

Figure 46. Concentric crevice boiling regime distribution at 7.5 MPa.

of the heat supplied by the tubesheet and the tube, this water starts to vaporize as soon as it enters the crevice. At the point of dryout, the soluble chemical will precipitate on the tube and/or the tubesheet surface. This dryout position may not remain stationary, so alternate wetting and drying occurs. The deposited salts are alternately moistened and dried, which increases their corrosive effect.

On the other hand, if sufficient liquid is present to redissolve the chemical deposits, this washing action may prevent significant amounts of precipitate from accumulating in any location along the crevice for a considerable period of time. But as the steam produced must exit through the top of the crevice (i.e. must flow in the opposite direction to the water), a flow regime may develop in the crevice that tends to stabilize the liquid–vapor interface and thus prevent any significant washing action. Aggressive chemicals may then precipitate and concentrate at the liquid–vapor interface, eventually corroding the tube and/or the tubesheet.

Simple calculations show that during normal operation small crevices should be vapor-blanketed over most of their length. To verify this conclusion, a test program (Baum & Steininger 1982) investigated the boiling heat and mass transfer processes in these crevices. Heat was transferred from the primary to the secondary side through a single alloy 600 tube 19.05 mm in diameter and 1.09 mm thick. The crevice was formed at the bottom of the boiler, adjacent to the primary tube penetration. The crevice boiling regime distribution was inferred by interpreting the readings of 0.5 mm sheathed thermocouples, which were embedded in the tube wall at several locations.

Tests performed with pure water show that for a tube concentric with the tubesheet hole, dryout will occur from 2.5 to 25 mm below the top face of the tubesheet, depending on circumferential position. Representative boiling regime distributions for the concentric crevice testing are presented in figure 46. There is a gradual transition from nucleate boiling to transition boiling and then to vapor blanketing as the distance into the crevice increases. As expected, the region in nucleate boiling decreases in size with increasing heat flux. The size of the transition boiling region appears to increase with decreasing pressure. There is also clear evidence of circumferential variations in the boiling regime progression with elevation. Evidently, small variations in the local geometry can alter the axial flow distribution.

Testing with the tube eccentrically located within the tubesheet hole produced significant circumferential variation of the boiling zone, but dryout developed within approximately 25 mm from the top of the tubesheet.

The crevice heat and mass transport processes were interrelated by a test in which sodium sulfate was added to the secondary fluid and permitted to concentrate in the crevice. The rate of sodium sulfate accumulation was found to reach a maximum immediately following the start of the test, after which the rate steadily decreased until an equilibrium between the crevice and the bulk concentrations was reached. A post-test examination of the tube surface indicated that the deposit

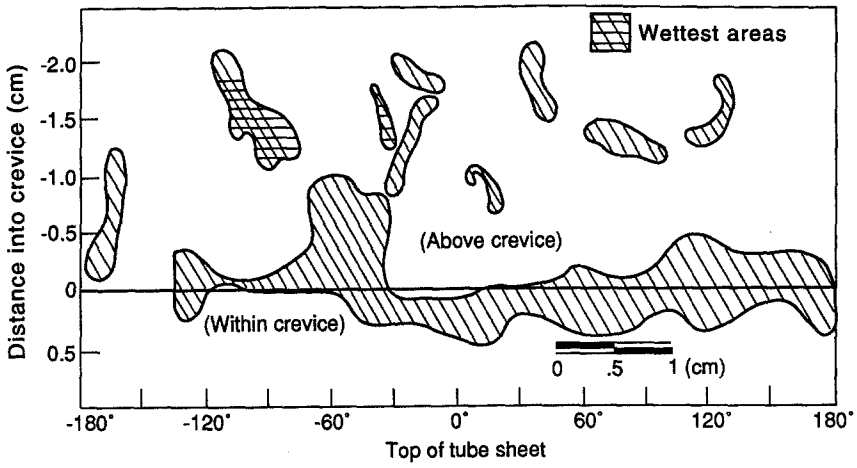

Figure 47. Sketch of Na_2SO_4 precipitate pattern.

was confined to the top of the crevice and preferentially located in regions that were in nucleate boiling (figure 47).

The test results indicate that the range of boiling regimes found in an annular crevice can result in the concentration of chemicals within and adjacent to the crevice to levels far higher than are found within the bulk fluid outside the crevice. A concentration factor of 20,000 is required for precipitation of the sodium sulfate. However, the flow patterns within the crevice appear to result in the transport of concentrated solutions away from the crevice regions having the greatest potential for concentration and into regions in which the potential for significant concentration should be reduced. The interactive role played by the overall crevice flow distribution and the effect of the confined geometry in the tightest crevice regions in restraining the local liquid flow requires further investigation in order to fully interpret the meaning of the test results.

The concentric crevice heat transfer results were also compared to the predictions of a number of analytical models based on flooding criteria. This comparison required an extrapolation of the models to smaller hydraulic diameters than were used in the development of the models. It was found that the crevice region in nucleate boiling could be adequately predicted by the simplest superficial velocity flooding model, while more complex flooding models based on the Kutateladze number were found either to be inappropriate or to give a poorer prediction of the wetted length.

To simulate a tubesheet crevice narrow-gap boiling heat transfer has been investigated for the geometry of a plate-shaped crevice (Kozawa & Aoki 1982). The experimental results are summarized as follows: (1) there exist spatially three kinds of boiling configurations in the crevice. Near the entrance region of the crevice (A), water is replenished easily, but the water penetration and discharge occur periodically. At the intermediate elevation of the crevice (B) are scattered water droplets, which are produced at the time of water discharge in the upper region. In the lowest region of the crevice (C), water is rarely supplied, so the heat transfer wall is always blanketed by steam. In the region from the boundary of A and B to B, the alternate drying and rewetting occurs cyclically, and it has been confirmed that the water treatment and impurities are apt to be deposited profusely on the heat transfer wall. (2) The water penetration is mainly dominated by the surface tension, whose magnitude is determined by the gap, while the water discharge is governed by the inertia force of the penetrated water and by the rise in pressure due to the generated steam in the crevice. (3) The generation of water droplets is caused by the Taylor instability of the boundary between the penetrated water and the steam. Since the generation and dissipation of droplets occur intermittently on the heat transfer wall, the temperature fluctuation is much larger than in regions A and C and is large enough to be observed even on the primary side surface.

Concentration in tube/tube support crevices (double-ended)

Double-ended open crevices exist in the tube/tube support structure intersections. The various designs of these intersections are depicted in figure 5. The thermal and hydraulic aspects of these

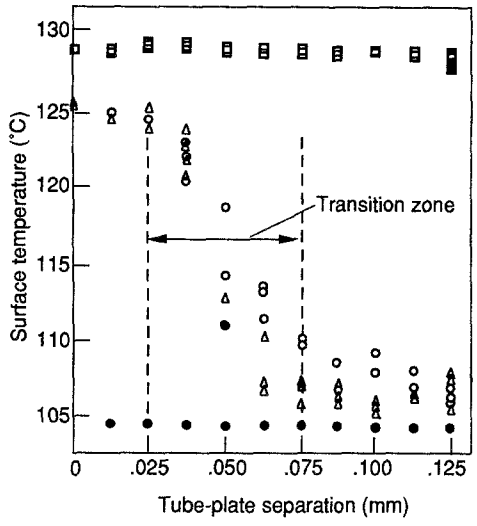

Figure 48. Effect of crevice gap on dryout. Pressure, 0.177 MPa; mass velocity, 555 kg/s/m; inlet quality, 0; diametral gap, 0.2 mm; □, primary temperature; ●, saturation temperature; △, surface temperature—approaching; ○, surface temperature—receding.

tube/tube support intersections and their relationship to chemical concentration have been studied extensively, both experimentally and analytically.

The investigations similarly indicated that for the drilled hole configuration, no superheat was developed as long as the tube was concentrically located in the hole. It was determined that this condition prevailed as long as the minimum gap exceeded 0.050 mm for heat fluxes in the range of interest (figure 48). However, it is recognized that there will be tube/tube support contact in most. For the drilled hole configuration with contact, superheat was developed near the contact locations over the entire range of heat flux and flow. Wall superheat in the vicinity of contact between tube and support is not strongly dependent on flow rate, quality, or pressure. Three regions were identified in the crevice:

- A steam-blanketed dryout region adjacent to the contact area.
- A nucleate boiling region in the wide part of the crevice where heat transfer was the same as that experienced on the open tube surface.

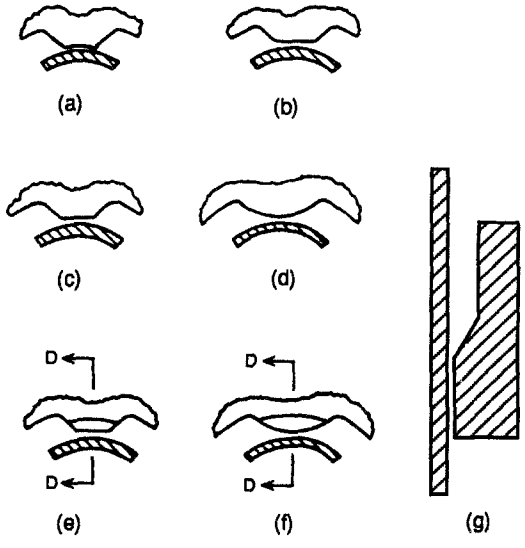

Figure 49. Support plate holes—land geometries tested. (a) Concave land; (b) 21° flat land; (c) 21 + ° flat land; (d) convex land; (e) 21° flat land, counterbored; (f) convex land, counterbored; (g) section D.

- A transition boiling region between the dryout and nucleate boiling regions, which is variously described in the different studies. Whether the region is described as thin-film boiling or as alternate wetting and drying, it is clear that any chemical concentration that occurs will happen in this region.

Figure 49 illustrates the variety of land geometries that were tested. A broached hole design with concave lands (trefoil or quatrefoil) shows heat transfer characteristics similar in many respects to those of the drilled hole configuration. Figure 50 shows tube wall superheat versus circumferential position around a quatrefoil, with the tube in contact with one land at the location shown on the figure. In figure 50, the amount of superheat at the point of contact (e.g. approximately 22°C for a heat flux of 315.5 kW/m^2) is higher than at regions away from the contact point; the lowest temperature around the tube circumference is essentially the same as the nucleate boiling free-steam value. This temperature difference between the free-steam value and the contact point is a measure of the heat transfer dryout or alternate wetting and drying conditions. These conditions are believed to lead to local concentration and precipitation of chemicals and subsequent corrosion and denting.

The difference in superheat between drilled hole designs and the quatrefoil design (with one land in contact with the tube) is in some cases substantial. For example, at a heat flux of 315.5 kW/m^2, the tube wall superheat in one drilled hole crevice exceeded the free-steam value by about 11°C; in the quatrefoil crevice, the superheat exceeded the free-stream value by only about 6°C in one test, although the data of figure 50 indicate about an 11°C difference for that particular crevice.

Cassell & Vroom (1983) showed that a concentration factor of 20,000 was achieved by precipitation of an added chemical (Na_2SO_4) in the crevices in the drilled hole configuration. After approximately 3 weeks of operation the test device was disassembled and the support plates examined for chemical deposition. Sodium sulfate deposits were found at all locations where tubes were in contact with support plates. The deposition pattern observed and a pattern predicted from thermal–hydraulic considerations, are shown schematically in figure 51.

These results imply that under certain conditions, the quatrefoil broached hole design will have some tendency to dryout in the land regions, thereby allowing chemicals in the steam generator bulk water to concentrate. These results also apply, in a qualitative sense, to the OTSG broached trefoil design since the land dimensions and clearances are comparable. Results show that the OTSG broached trefoil will exhibit dryout at prototypical heat fluxes of approximately 95 kW/m^2

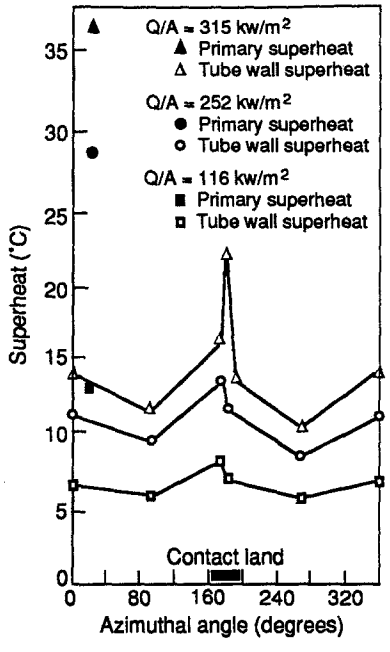

Figure 50. One-land-contact quatrefoil support plate–wall superheat azimuthal angle (secondary pressure, 6.5 MPa; secondary flow, 0.1 kg/s; local quality, 20%).

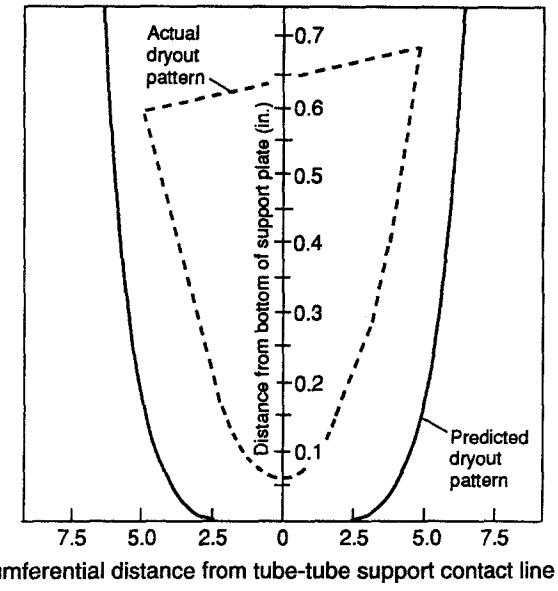

Figure 51. Predicted and actual deposition patterns. Flow straightener (cylindrical hole support plate); pressure drop = 2.7 kPa, Heat flux = 350 kW/m^2.

for inlet qualities to the trefoil of 0.9–0.95. These results are consistent with design expectations for OTSGs.

Even though the quatrefoil and trefoil broached hole designs have a tendency to dry out in the land regions, the large flow area presented by the flow lobes may minimize the dryout. The dryout zone has been substantially reduced, and the lobe flow could provide some degree of washing action at the boundaries of the transition zone. This would further confine the extent of chemical concentration.

Data (Curlee & Baum 1983) on egg crate or Breda-type tube support geometry show that dryout does not occur for heat fluxes up to 695 kW/m^2 over a range of local qualities of 4–15%. Figure 51 illustrates similar results for a flat-land broached hole configuration at a heat flux of 350 kW/m^2. Other tests (Cassell 1983) show that inlet quality to the egg crate could be increased to 0.88 before dryout occurred.

All these data suggest that high tube wall superheat indicating dryout will occur at the point where a tube is in contact with or is close to (e.g. within 0.050 mm) a concave surface of a tube support—even if the surface is narrow, as is the case with broached holes. On the other hand, for cases where the tube is in contact with a flat or convex tube support surface, no indications of dryout have been detected under conditions representative of recirculating steam generators. As a caution, it is noted that reduced contact area, as in the flat land and convex land designs, is more conducive to wear. Qualification for this design is required before these configurations are accepted for specific applications.

It also seems interesting to mention the tests performed in the CEA Clarinette facility (12 model boilers operating at actual primary–secondary conditions with adjustable chemistry) in which both sequestration and desequestration rates (during power reduction) were monitored by a gamma-ray technique following the concentration of the isotope Na^{24} used as a dye.

One major conclusion was that the quantity of sodium, which deposits inside the crevice, was found to depend on the integrated pollution (time × concentration) and also that the desequestration remains partial during power reduction periods.

5.7. Corrosion in OTSG

Operators of OTSG have observed an increase in the pressure drop in the lower part of the bundle over a number of years. The increased pressure drop was traced to buildup of corrosion products inside the gap between the tubes and the tube support plates (TSP), e.g. Oconee 1 and 2. The pressure drop is caused by two different mechanisms: (1) corrosion products which are

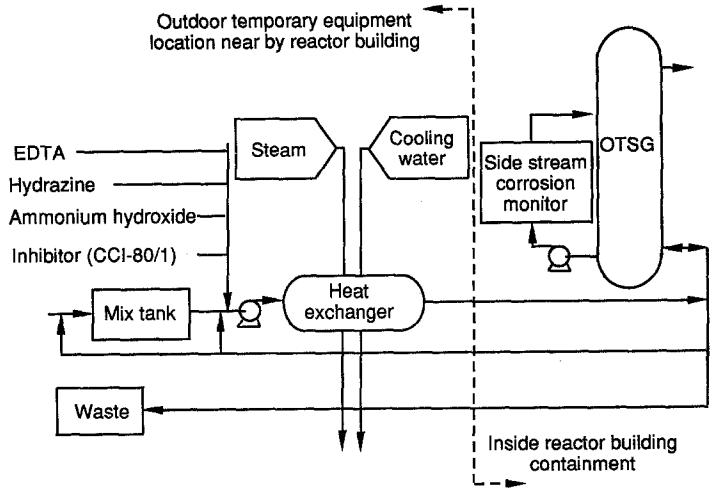

Figure 52. Chemical cleaning process flow chart.

predominantly magnetite collected in the TSP flow openings restricting the flow and (2) flake-like deposits spall from the tubes and wedge themselves in the flow openings. The first mechanism can result in a gradual increase in pressure drop while the second can result in a large rapid increase.

The pressure drop increase caused the OTSG downcomer level to increase to a point where main feedwater nozzles and preheating aspirator ports could become flooded. This situation can cause unacceptable OTSG thermal stresses and thermal–hydraulic instability. Therefore, before the flooding occurred, reactor power level was reduced to lower the downcomer level. Oconee Unit 1 was originally power limited in October 1986. Power was reduced about 1% per month until the September 1987 outage to account for increasing pressure drop. In the past, utility personnel have used a mechanical process to remove spalled flakes and magnetite deposits from the broached openings.

In 1978 the Steam Generator Owner's Group, under the management of the Electric Power Research Institute (EPRI), initiated a series of programs designed to develop generic magnetite and copper solvents for chemically cleaning any pressurized water reactor steam generator. Additionally, a process that used these solvents was to be developed and qualified on a generic basis (Schneidmiller & Stiteler 1983; Fink *et al.* 1983; Cleary & Cockley 1983; Coponer *et al.* 1984; Hildebrandt *et al.* 1987; Eaker *et al.* 1988).

The chosen process application was a fill/soak/drain method limited to a magnetite solvent step only: the Oconee units do not contain any copper alloys in their secondary systems. The fill/soak/drain method was selected because it would allow the solvent to be mixed, heated and replenished outside the steam generator (figure 52).

The most important system design considerations included reducing/minimizing system leakage, controlling temperature and steam generator level, maintaining operational flexibility and redundancy and ensuring personnel safety (considering chemical, thermal and radiological hazards). Additionally, the design allowed for installing the system's major components outside the reactor building prior to the unit's outage with installation and removal of piping inside the reactor building occurring during a normal refueling outage (approximately 60 days).

The solvent chosen was:

Magnetite solvent:	15% EDTA
	1% hydrazine
	1% CCI-80/1 corrosion inhibitor
	pH 7.0 (ammonium hydroxide)
Rinse/passivation:	300 ppm hydrazine
	pH 10.2 (ammonium hydroxide)

The cleaning removed approximately 1600 kg of magnetite from each SG, returning the downcomer level to original startup values and permitting continued operation at 100% power (from the previous 86% power limit).

In figure 53 the effect of chemical cleaning on the pressure drop through the OTSG, is demonstrated. One can observe that the pressure drop increased by about 64% over the period of about 13 years, and was restored to the original value after the chemical cleaning.

5.8. Tube Fretting and Wear

5.8.1. Flow-induced vibrations

Tubes, either single or in bundles, when exposed to external flow, vibrate. The mode of vibrations and their amplitude depend on the geometry of the structure, velocity, direction and properties of the fluid, etc. The flow-induced vibration (FIV) may result in structural damage and may compromise the integrity of the tube, due to fretting and wear and due to tube fatigue.

There is voluminous literature written on FIV, fretting and wear, which we cannot cover in this exposition. Instead, the points which are most relevant to steam generators will be covered.

Steam generator tubes, being long and slender cylindrical structures with very thin walls, must be supported along their length to maintain their separation. The tube support plates (TSP) serve to support the tubes—but these supports are rather loose (this is necessary for manufacturing reasons), and the tubes can vibrate in their TSP penetration. When the tubes vibrate, they also impact against the TSP and fret against it—which causes tube wear. The degree of wear determines whether the loss of material from the tube wall will be small enough not to affect the expected lifetime of the SG, or whether this wear will result in weakening of the tube wall and its premature failure.

In addition to the detrimental effects of tube metal loss, fretted regions are highly sensitive to fatigue cracks. Under fretting conditions, fatigue cracks can be initiated close to the material surface at very low stresses, well below the fatigue limit of non-fretted tube test material. If the nominal cyclic stresses on the tube produced by the induced vibration is sufficient to cause these fretting-induced cracks to grow and propagate, early failure of the tube can occur. Furthermore, if there is impacting of the tube on the tube support plate, then it is possible to get local grain boundary slippage, which is then more sensitive to corrosion attack.

Mechanisms. There are normally three mechanisms which cause FIV. These are: turbulent excitation, vortex shedding and fluid–elastic instability. It is also possible that two-phase flow has a parametric effect on the FIV.

Turbulence-induced random vibration of a tube bundle, frequently referred to as subcritical vibration, is usually of a much smaller amplitude than that experienced in fluid–elastic instability. Through fretting and wear, turbulence-induced random vibration can still determine the long-term reliability of the SG tube bundle. Of particular importance is the case of cross flow-induced random vibration, often referred to as buffeting.

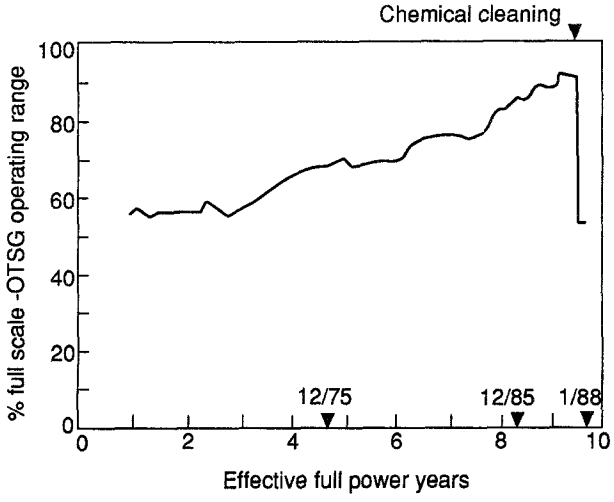

Figure 53. Ocone 1B OTSG; typical pressure drop vs time as measured by OTSG operating range level (Eaker *et al.* 1988).

The second mechanism is associated with vortex shedding or with the von Karman vortex sheet downstream of a cylinder. When the natural frequency of the cylinder coincides or "locks in" with the frequency of the shed vortices, large amplitude and violent motion of the tube can result. The significant feature of synchronized vortex shedding is a large magnification of fluctuating forces on the oscillating cylinder in comparison with those measured on a stationary one. These forces will cause significant tube motion and may result in tube fretting and wear and in fatigue.

For tube pitches and diameters normally found in steam generators, the tube-to-tube gap is believed to be sufficiently small to mitigate the occurrence of vortex shedding. It is theorized that the tight tube spacing limits the ability of a vortex to form and naturally evolve and sweep downstream of the cylinder. Chen (1977) indicates that vortex shedding is generally not important for a tube bundle unless the tube spacing is larger with a pitch-to-diameter ratio greater than 2.0. Gorman (1976) reports a vortex shedding-type tube response of an inlet tube in an in-line array with a pitch-to-diameter ratio of 1.57. However, in two-phase flow, it is doubtful that vortex shedding is an important mechanism.

The third mechanism, which is the most dangerous, is the fluid–elastic instability—since it may cause tube damage after only a few hours of operation. The detailed process leading to this instability is not yet well understood. Phenomenologically the process involves a tube displacement and the resulting imposed force in a resonant condition. The amount of energy expended by the tube motion through damping is less than the energy input to the tube. This energy input occurs from the tube motion itself. Fluid–elastic instability associated with a tube row was first modeled semi-empirically by Connors (1970) and has subsequently been the subject of a considerable number of investigations, both experimental and theoretical (Tanaka *et al.* 1982; Soper 1983; Yeung & Weaver 1981; Chen & Wambsganss 1977; Blevins 1974; Goyder 1980; Paidoussis 1981; Chen 1987; Lever & Weaver 1982; Pettigrew *et al.* 1985, 1989, 1989).

It is believed that many of the tube failures in heat exchangers and steam generators that have been attributed to other causes could be explained by this fluid–elastic mechanism. Paidoussis (1980) and Pettigrew & Campagna (1980) are excellent reviews of some past heat exchanger tube failures attributed to flow-induced tube vibration. Some of these cases appear to have foretold the tube vibration problems that have recently occurred in some recirculating-type steam generators. In simple terms, if a blunt body is immersed in fluid flowing perpendicular to its axis, the body vibrates. The midspan peak-to-peak amplitude of the displacement increases in a mild fashion, until the critical velocity is reached. As the velocity increases further (figure 54) the magnitude of peak-to-peak vibrations increases much more rapidly.

The displacement of one cylinder in an array alters the flow field, upsetting the cylinder itself and the neighboring cylinders and causing them to change their displacements. If, during a cycle of oscillation, the energy extracted from the flow by the cylinders exceeds the energy dissipated by damping, an instability will occur as a result of the interaction between the flow field and cylinders.

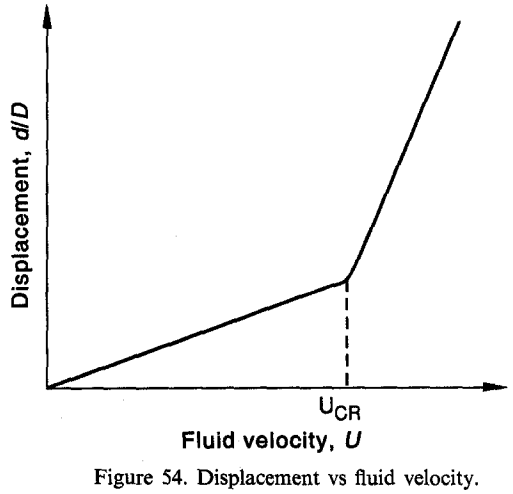

Figure 54. Displacement vs fluid velocity.

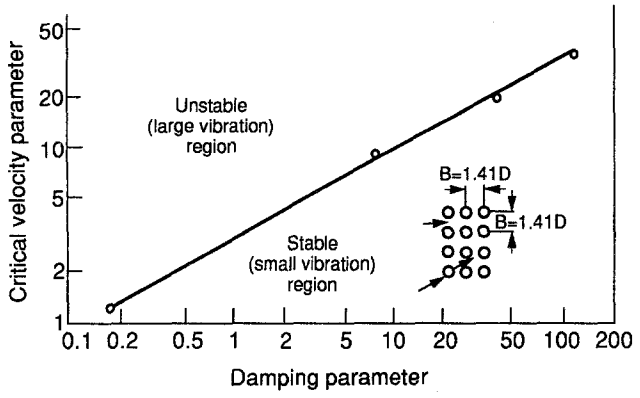

Figure 55. Dimensionless critical velocity vs the damping parameter.

Connors (1970) developed a simple stability criterion based on the quasi-static theory; the critical velocity U above which large-amplitude cylinder vibration initiates is given by

$$\frac{U}{fD} = \alpha\left(\frac{2\pi\zeta m}{\rho D^2}\right)^{0.5},$$

The left-hand side of this equation is a dimensionless flow velocity, where f is the frequency of oscillations and D is the tube diameter. On the right-hand side is the product of mass ratio $m/\rho D^2$ and the log decrement $2\pi\zeta$. Here m is the mass of tube per unit length and ρ is the density of the fluid. ζ is the damping, which includes structural and fluid damping and α is a coefficient, to be determined experimentally for various geometries, flow directions etc.

The threshold of instability is plotted in a dimensionless form—as the critical velocity parameter vs the damping number (figure 55).

The line separating the unstable from the stable regions in figure 55 is somewhat dependent on the geometry and maybe other parameters. Any reasonable design should be well within the stable region, taking into account all design uncertainties. A state-of-the-art on FIV in heat exchangers, in particular on the fluid–elastic instability, was recently reviewed by Weaver & Fitzpatrick (1987).

There are a variety of theories correlating the amplitude Y of the turbulence-induced vibration in circular cylinders to the flow parameters.

$$Y = K\rho^i U^j d^k D^e m^m f^n \zeta^o$$

where K is a constant and the powers are summarized in table 14 (Blevins 1979). As can be seen there is a wide variation of exponent in the table, and one can hope to achieve an accuracy in predicting vibration of perhaps an order of magnitude.

The fourth probable mechanism for FIV may be associated with two-phase flow—perhaps with flow regime. Although some progress has been made in the last 3 years, the available information on vibration in two-phase cross-flow is still scarce. Vibration experiments were made on small tube bundles partially exposed to two-phase (air–water) cross-flow (Pettigrew & Gorman 1973). Heilker & Vincent (1981) have also studied air–water cross-flow for a limited range of bundle geometries and flow conditions pertaining to their nuclear steam generator design. Remy (1982) studied

Table 14. Comparison of exponents in theories of parallel flow-induced vibration of cylindrical structure

Theory	ρ	U	d	D	m	f	ζ
Baisle	0.25	1.5	0.5	−0.5	−0.25	−1	0
Burgreen	0.385	2.3	1	0.77	−0.65	−2.6	0
Y.N. Chen	1	2	0	1	0	−2	0
Paidousis	0.8	2.4	0.8	0.8	−0.66	−2	0
Reavis	1	1.5	0.4	1.5	−1	−1.5	−0.5
Wambsganss	1	2	1.5	1.5	−1	−1.5	−0.5

d = hydraulic diameter; D = cylinder diameter; f = natural frequency (Hz); m = mass per unit length including added mass; ρ = fluid density; ζ = damping, including fluid dynamic damping.

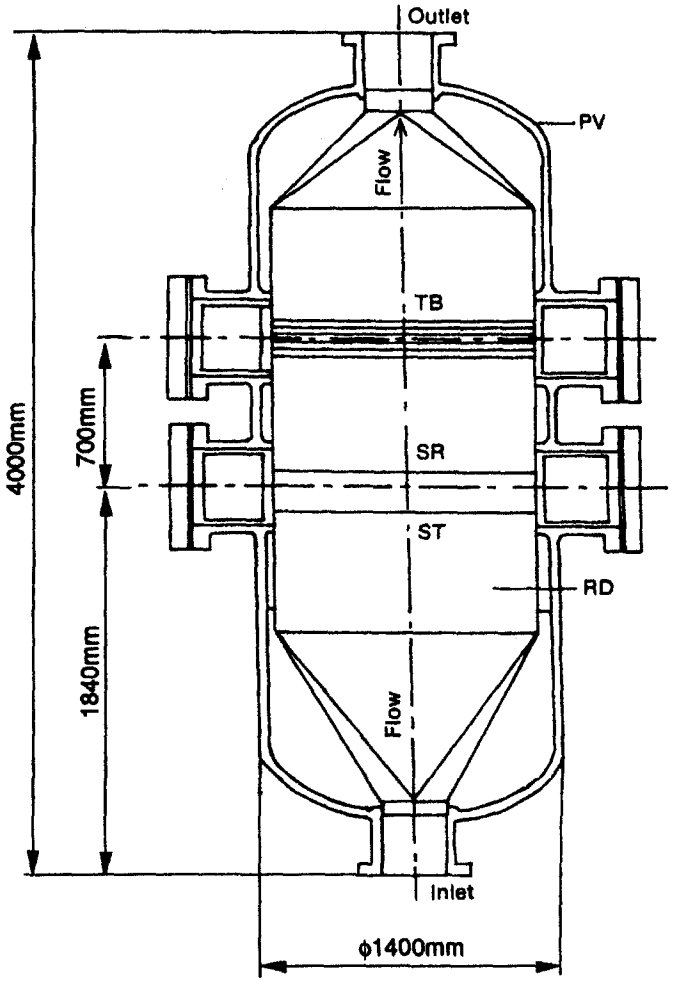

Figure 56. EVA I test section: straight tube model 1. PV, pressure vessel; RD, rectangular duct; ST, single tube; SR, single row; TB, tube bundle.

vibration for a multispan tube bundle of normal-square configuration simulating their condenser design. Nakamura *et al.* (1982) measured random forces on bundles of normal-square and rotated-square configurations subjected to air–water cross-flow. They have investigated, in particular, the frequency content of the random excitation forces and the effect of slug and bubbly flow regimes. Hara (1982) has studied random turbulence excitation forces on a single cylinder in cross-flow at homogeneous void fractions of 0–60%. Axisa *et al.* (1984) were the first to present results on the fluid–elastic instability of a tube bundle subjected to both air–water and steam–water cross-flow. They tested a normal-square tube bundle of $p/d = 1.44$. They found that the simulation of steam–water flow with an air–water mixture is reasonable for fluid–elastic instability. Since these measurements were the first of their kind we will elaborate on them below. Subsequently, they studied fluid–elastic instability of normal-square, normal-triangular and parallel-triangular tube bundles, all of $p/d = 1.44$ in steam–water cross-flow (Axisa *et al.* 1985). Recently, Taylor *et al.* (1986) presented random turbulence excitation data for flexible tube rows of $p/d = 1.5$ and 3.0 in air–water cross-flow. Goyder *et al.* (1986) discussed preliminary results on the measurement of random turbulence excitation forces on a flexible tube installed in a rigid triangular tube bundle of $p/d = 1.25$. A single span tube bundle, with a square array $p/d = 1.44$, was exposed in its central part to air–water cross-flow. Void fraction measurements were performed between the tubes, and the damping was evaluated from the measurements of the displacements (Remy 1982). Remy & Bai (1982) compared flow-induced vibrations in various tube bundles and fluids combinations. In particular, tests were presented on vapor flow across a multispan tube bundle (triangular array $p/d = 1.37$ and 1.42). These data were then compared with the previous reference.

Gay *et al.* (1988) compare the effects of two types of two-phase mixtures (air–water and water–freon) on fluid–elastic instability with different support conditions (drilled holes, trefoil holes). The tube bundle studied in these tests is a normal-triangular array with reduced pitch equal to 1.44. The tests were performed for the same qualities of air–water and water–freon mixture.

The experimental program studied flow-induced vibration in straight and U-tube bundles subjected successively to air–water and steam–water two-phase cross-flow (Axisa *et al.* 1984). The test program utilized two mock-ups called EVA I and EVA II, which represent a full-scale straight and U-bend portion of an inverted U-tube (the FRAMATOME model 68/19, the equivalent of Westinghouse Model F). The EVA I model, shown in figure 56, includes three distinct sets of identical straight tubes; a single tube, a row of 10 tubes and a rectangular bundle with square pitch involving 6 rows of 10 tubes each.

The EVA II model, shown in figure 57, consists of a bundle of 80 U-tubes with square pitch representing the innermost central portion of the SG bundle. It includes 10 tube layers with a distinct radius of curvature, the 7 more external layers being secured by a set of antivibration bars. Straight spans of each U-bend pass through quatrefoil broached plates acting as intermediate supports. To date, EVA II has been tested only in the feedwater loop.

Flow rate measurements of each separate phase and void fraction measurements using gamma-ray densitometry were made to identify the flow parameters inside the test sections. Tube variations were measured by using biaxial accelerometers (BAs) and strain gages (SGs). EVA I uses a set of 28 SGs and 4 BAs fitted inside 16 selected tubes to measure motion in the lift and drag directions. EVA II uses a set of 18 SGs and 3 BAs fitted inside 9 tubes located in the 3 innermost

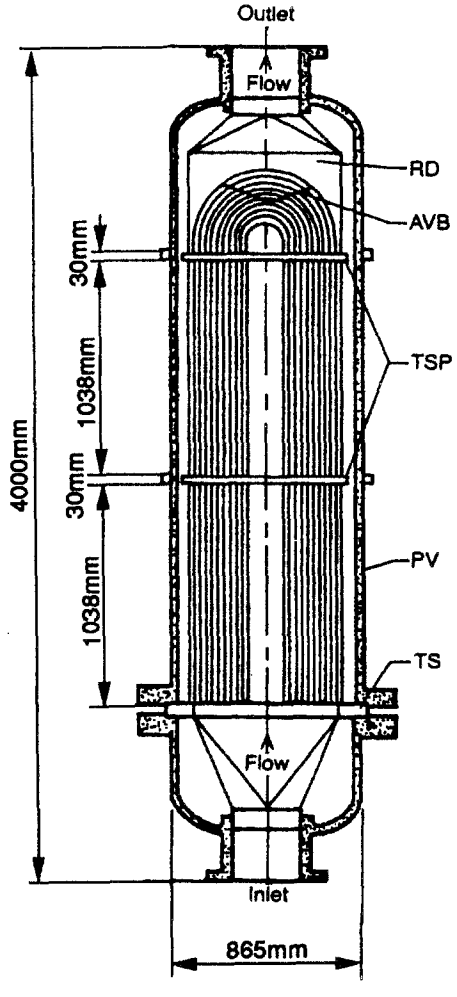

Figure 57. EVA II test section: U-tube bundle model. AVB, antivibration bar; PV, pressure vessel; RD, rectangular duct.

Table 15. Flow parameters of the EVA vibration tests

Tests	Quality, X	Void fraction,† ϵ	Density,† ρ (kg/m^3)	Tube gap velocity range, V† (m/s)
EVA I, air–water	1	1	1	12–36.5
	0.285	0.997	4.1	20–38.5
	0.16	0.994	7.5	6–35‡
	0.1	0.990	11	14–28
	0.077	0.987	16	13.5–23.5
	0.05	0.981	25	13.5–20
	0.025	0.963	45	8–14
	0.01	0.902	120	5.5–8.5
	0.0	0	1000	0.8–1.2§
	1	1	10	1.9–7.2
EVA I, steam–water	0.186	0.953	52	10.9–12.6‡
	0.117	0.921	80	5.7–9.9
	0.09	0.897	100	5.0–10.3
	0.059	0.847	145	4.4–10.3
	0.03	0.732	240	4.0–11.7
	0.012	0.517	430	4.8–6.9
	0.0	0	890	0.9–2.5§
EVA II, steam–water	1	1	12	6.7–38.7
	0.34	0.976	35	8.8–40.0‡
	0.20	0.952	58	5.2–40.3
	0.13	0.925	85	6.3–36.6
	0.1	0.898	111	5.8–32.7
	0.05	0.805	194	6.1–17.1
	0.0	0	953	5.3–15.2

†ϵ, ρ and V are calculated according to the homogeneous flow model.

‡The U-bend region of a Westinghouse Model F steam generator experiences the following flow conditions: (1) tube gas velocity range of 6–9 m/s, (2) homogeneous void fractions ranging from 0.80 to 0.90 and (3) homogeneous qualities ranging from 0.20 to 0.30.

§The entry region to the bundle from the downcomer of a Westinghouse Model F steam generator experiences saturated single-phase flow with tube gap velocities at the peripheral tubes approximately equal to 2 m/s.

tube layers, which are not secured by an antivibration bar. Motions are measured in and out of the U-tube plane.

Flow conditions are summarized in table 15. An example of these data is given in figure 58, where peak-to-peak midspan displacements are plotted vs the gap velocity, for various qualities. These are from the EVA I steam–water data. Data reduction and analysis have produced the following:

(1) power spectral densities (PSDs) of tube displacements and PSDs of the turbulent forces per unit tube length,

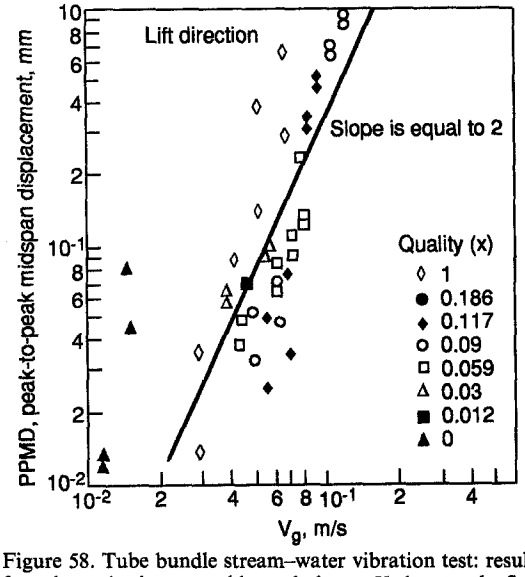

Figure 58. Tube bundle stream–water vibration test: results for tube excitation caused by turbulence. V_g denotes the flow velocity in the gap between adjacent tubes.

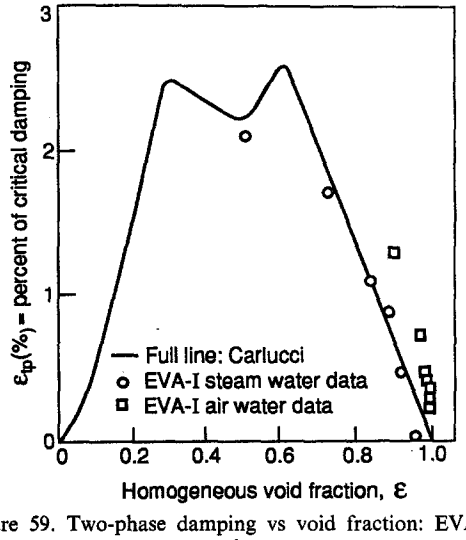

Figure 59. Two-phase damping vs void fraction: EVA I results.

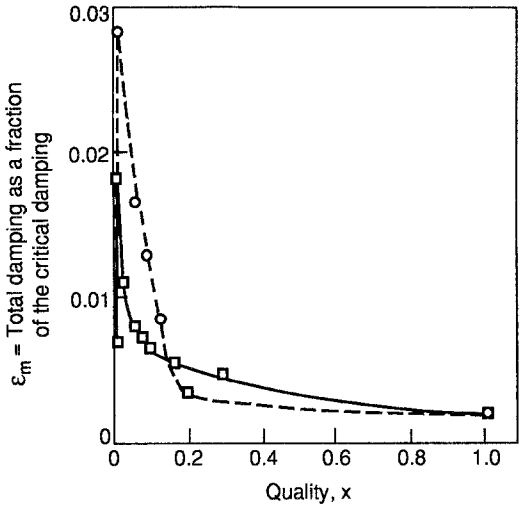

Figure 60. Damping in two-phase flow: EVA I results.

(2) cross power spectral densities (CPSDs) of tube motions for selected pairs of adjacent tubes with results given in terms of coherence and phase functions,
(3) damping factors of the tubes (figures 59 and 60), and
(4) critical flow velocities for fluid–elastic instability (figure 61).

Other experiments were conducted to characterize the steam generator tube-to-tube support interaction behavior over a wide range of simulated cross-flow excitation conditions (Haslinger *et al.* 1987; Haslinger & Steininger 1984). The test stand and instrumented drilled hole support are shown in figures 62 and 63. Several tube alignment and support clearance conditions were considered. First, the vibration response behavior of a prototypically supported multispan tube was identified for sinusoidal and random-type excitations. Typical responses to a series of sinusoidal excitations in a water environment are shown in figure 64. Then the tube contact forces and the tube sliding distances at each support during sinusoidal dwell and random excitations were recorded. These signals were digitally processed in terms of peak, rms and mean values. Tube contact percentages and total sliding distances per time unit were also determined, as were, most importantly, the integrated product of contact force times sliding distance (wear-work). Test results are to be used as input to single-span tube, autoclave wear tests, which are described later.

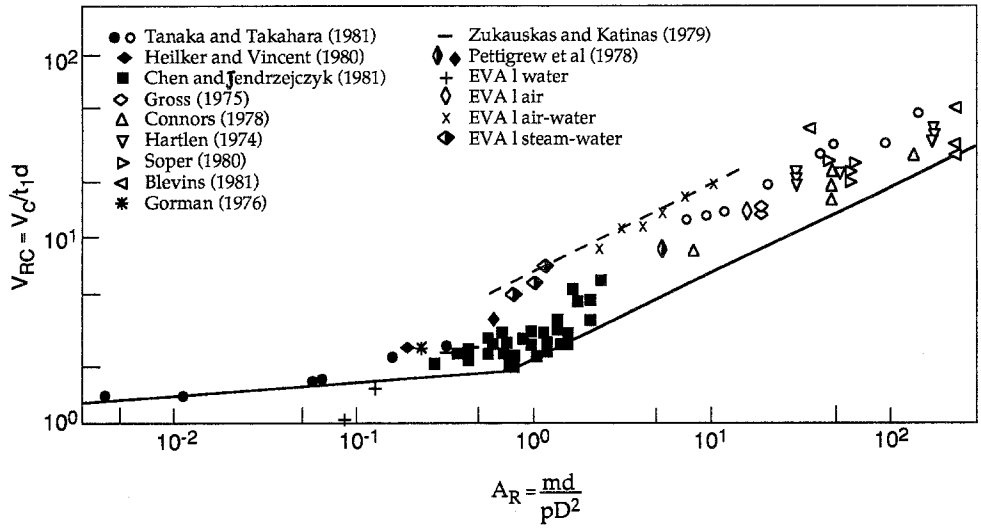

Figure 61. Stability diagram for the tube bundle; comparison with literature results.

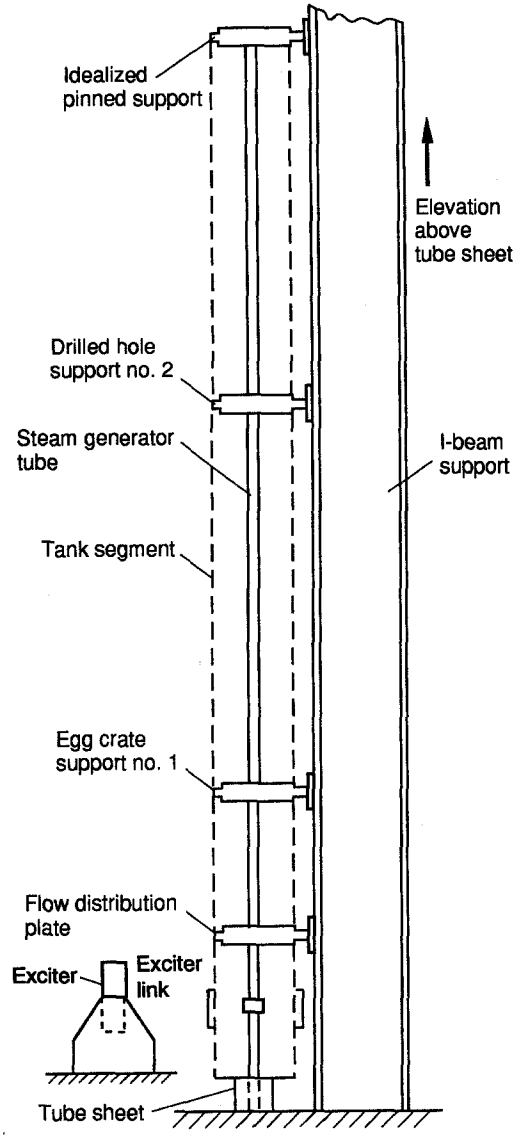

Figure 62. Multispan tube vibration test stand, general arrangement

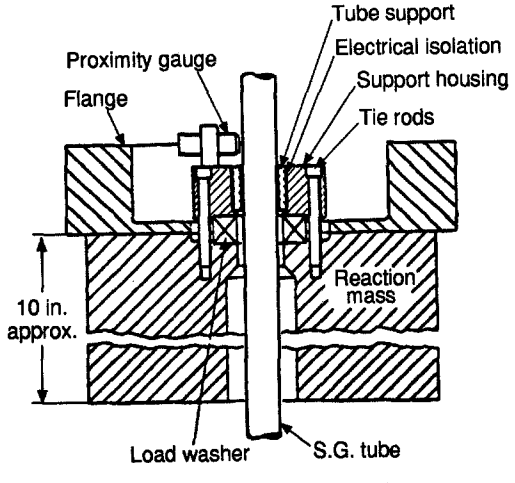

Figure 63. Schematic instrumented drilled hole support.

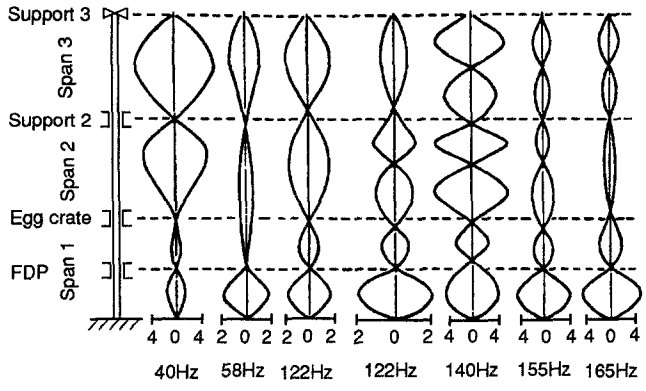

Figure 64. Experimental mode shapes; offset condition 2, water environment, 0.5 kg excitation.

Tube alignment within the various support plates was found to significantly influence the tube's vibrational behavior and also the tube-to-tube support plate interaction parameters. Double-span (i.e. one inactive support) and triple-span (i.e. two inactive supports) behaviors were observed during the tests for certain support plate alignment conditions. Depending on the tube support alignment, manufactured tube/tube support crevice clearance and tube preload conditions (i.e. tube straightness or support plate positioning), one, two or even three supports may be inactive. That is, the support does not participate in determining the tube dynamic response. Once the vibration amplitudes exceed available crevice clearance, impacts occur at the support, which increase damping and restrict tube amplitude buildup. At this point, the tube response may shift to a different resonance frequency and mode shape, or the tube may vibrate at several frequencies superimposed on each other. Complementary work indicated that damping is also a strong function of support plate axial position along the tube length. This effect is due to the relative position along the tube length and to the relative position of a support plate and a nodal point of the particular structural mode being excited. In addition, it was found that relative tube-to-tube support plate positions could be constructed such that damping would increase with increasing vibration amplitude, but only up to a point, and then sharply decrease to a low level at higher vibration amplitudes. This complicates one's effort to define a damping value for use in tube vibration analysis.

Methods for accurately accounting for inactive support plates in tube vibration and wear analysis are not fully developed. If tube excitation is due to fluid–elastic phenomena, wear prediction is difficult. Work performed at Argonne National Laboratory (Chen *et al.* 1983) indicates that for loosely held multispan tubes non-classical fluid–elastic phenomena appear to occur. For low-amplitude tube vibrations with a flow velocity less than a specific value, tube motion occurs with some of the tube supports inactive as identified in the tests described in Haslinger *et al.* (1984). As the flow velocity is increased, an apparent instability is reached in this tube support plate inactive mode. The occurrence of this instability is identified by the first large rise in tube amplitude shown in figure 65 for a test with a 1.02-mm diametral gap. In this unstable mode the tube collides with the tube support plates that were previously identified as inactive. This condition results in a constant tube amplitude (equal to the tube/tube support plate clearance) at the inactive supports over a range of flow velocity, finally resulting in the tube becoming unstable in the tube support plate-active model. This is shown in figure 65 by the second significant increase in the tube amplitude with flow velocity.

Other experimental data are being collected from the Clotaire program, where two-phase flow profiles and tube vibrations are measured simultaneously in a 15 × 16 tubes U-bend region, with in-service adjustable gaps at the antivibration bars.

A prediction method of fretting and wear in steam generator tubes is also given by Axisa *et al.* (1989).

Turbulence buffeting. This is measured and simulated by computations. Experimental work has been done by Axisa *et al.* (1988), Taylor *et al.* (1989) and Granger (1990).

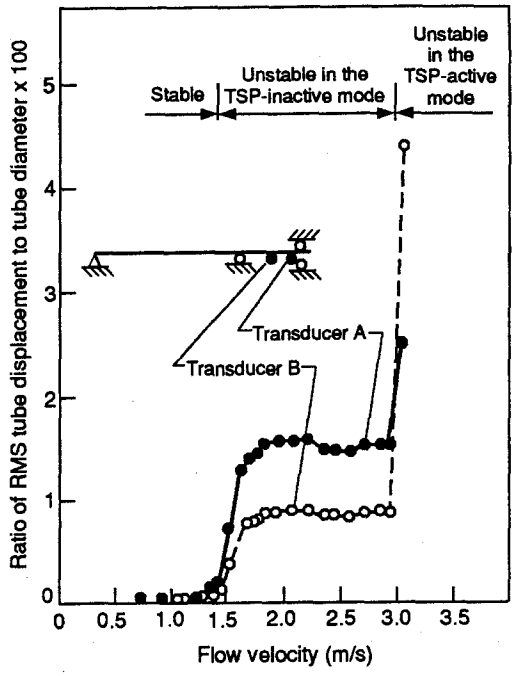

Figure 65. Fluid–elastic instability test showing effect of tube support plates on stability threshold and tube response characteristics.

The computations are done using various codes, such as GUST or ABAQUS-EPGEN (see, for example, Antunes *et al.* 1988; Fisher *et al* 1989; Fricker 1988). These simulations are performed by using the largy eddy simulation (LES) method, in order to predict turbulent buffeting of steam generator tubes which may be detrimental in the long term. The large eddy simulation uses solutions of the Navier–Stokes equation for predicting the large (low wave number) energy-containing eddies. For the smaller eddies, a sub-grid-scale viscous model is used—such as the Smagorinski model.

Time histories of fluctuating, two-dimensional forces experienced by individual tubes were obtained by integrating the instantaneous pressure distribution around the periphery of each tube (Chilukuri *et al.* 1987). Buffeting loads were obtained by multiplying the two-dimensional forces with typical correlation lengths along the tube axial direction. Correlation length was determined from LES results from upstream feedwater turbulence.

These results need further verification and experimental support since the turbulence intensity was found to be strongly dependent on the Smagorinski constant.

Fluid–elastic vibrations were simulated by using the ABAQUS-EPGEN finite element code (Rao *et al.* 1988), where the tube displacements were solved. The fluid–elastic forces were taken to be proportional to the tube vibratory velocities, with coefficients $K_x = K_y = 4.7$. One of the computations was that of a tube as shown in figure 66. The tube was partially exposed to flow. The results are shown in figure 67 and indicate a reasonable correlation between onset of the first instability

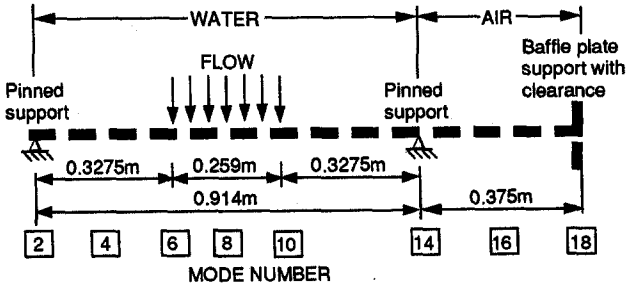

Figure 66. Finite-element model of test tube.

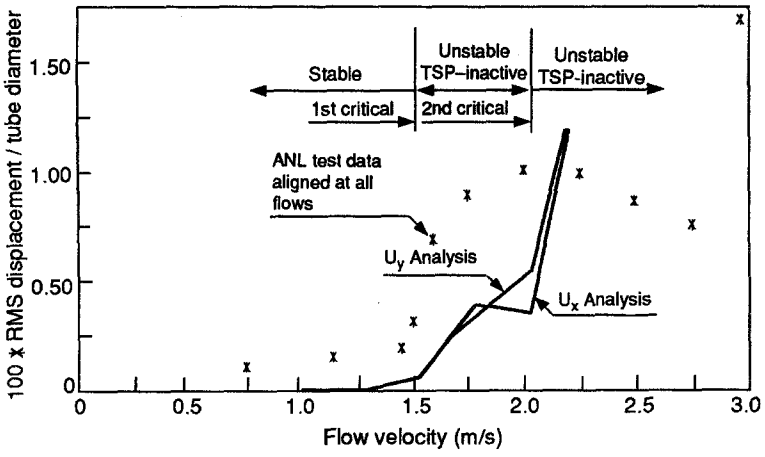

Figure 67. RMS tube displacements at node 16 as a function of flow velocity—analysis and ANL test data.

and that of the experiment. The study confirmed the existence of the typical behavior of a vibrating tube—multiple minor and major instabilities with several regions of tube impact and wear.

The results of the analysis showed that the fluid–elastic vibration of real heat exchanger or steam generator tubes with clearances at supports can be successfully simulated with a computer. Both qualitative and valuable quantitative data on critical velocities and tube wear can be obtained. Additional work, including further correlations with experimental data are necessary to improve the model and make it into a much-needed design tool (figure 68).

The study also showed that

- Clearance, contact stiffness and the squeeze film effect are important parameters when modeling the non-linear tube response, including tube-to-tube support interaction.
- Support misalignment generally increases support reactions and reduces vibration amplitude and impact forces.
- Structural damping has a strong effect on the dynamic response of the tube.

5.8.2. Fretting and wear

Numerous wear tests have been performed in the past (e.g. Ko 1979, 1985).

A detailed program to obtain tube wear data under prototypical operating conditions has been completed recently (Hofmann *et al.* 1986). The wear data were generated under controlled conditions of contact force and relative sliding distance between the tube and support structure.

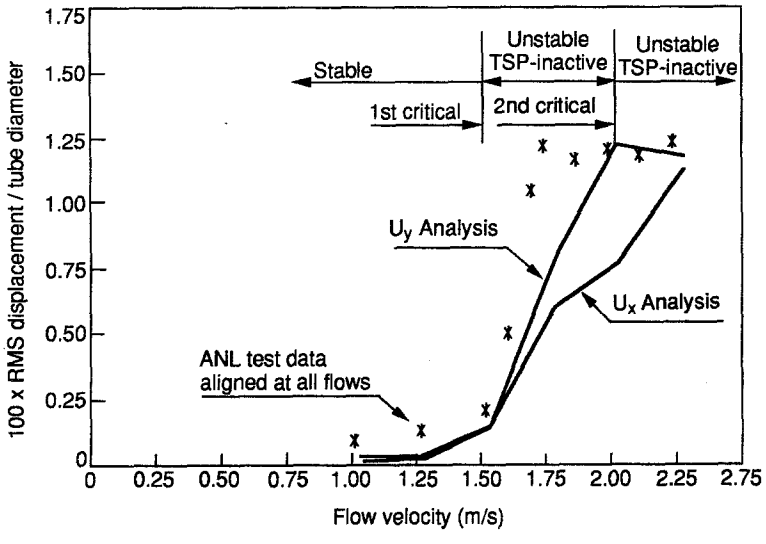

Figure 68. RMS tube displacements at node 18 as a function of flow velocity—analysis and ANL test data.

These controlled interaction characteristics were obtained from a complementary tube structural dynamic test using conditions of controlled tube excitation intended to simulate prototypical flow force excitation within a tube bundle.

Figures 69 and 70 show a schematic view and details of the test fixture. Test conditions of pure impact, impact plus sliding and pure oscillating sliding were covered. A wear rate representation was developed that includes the independent parameters of average tube/tube support structure contact time and work rate, where

$$\text{work rate} = \frac{\int_0^{t_1} [F_n(t)\dot{L}(t)]\,dt}{\int_0^{t_1} dt}$$

where F_n is the normal force, $\dot{L}$ the distance traveled and t the time.

Such a representation is believed to describe quantitatively the different combinations of impacts and sliding. Typical results are shown in figures 71 and 72.

These tube wear data, generated and reduced in the manner described, can be used in the design process once tube/tube support interaction characteristics are specified through experimental testing or analytical prediction. New tests on fretting wear are now being run at AECL to measure precisely the dynamic contact forces (Fisher & Ingham 1989).

Finally, determination of actual field tube motion within a support structure is possible by careful examination of the geometry of the worn surface of the tube and comparison of the topographical features of the worn surfaces of tubes obtained from tests performed in the manner described by Hofmann *et al.* (1986).

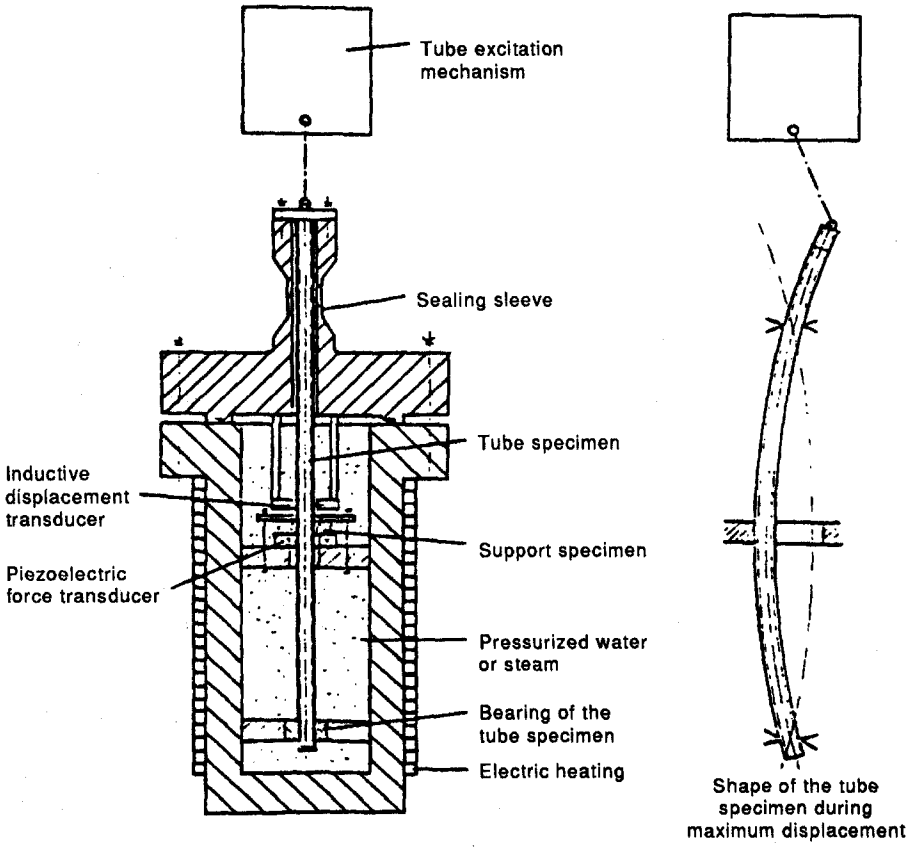

Figure 69. Schematic of the fretting wear fixture.

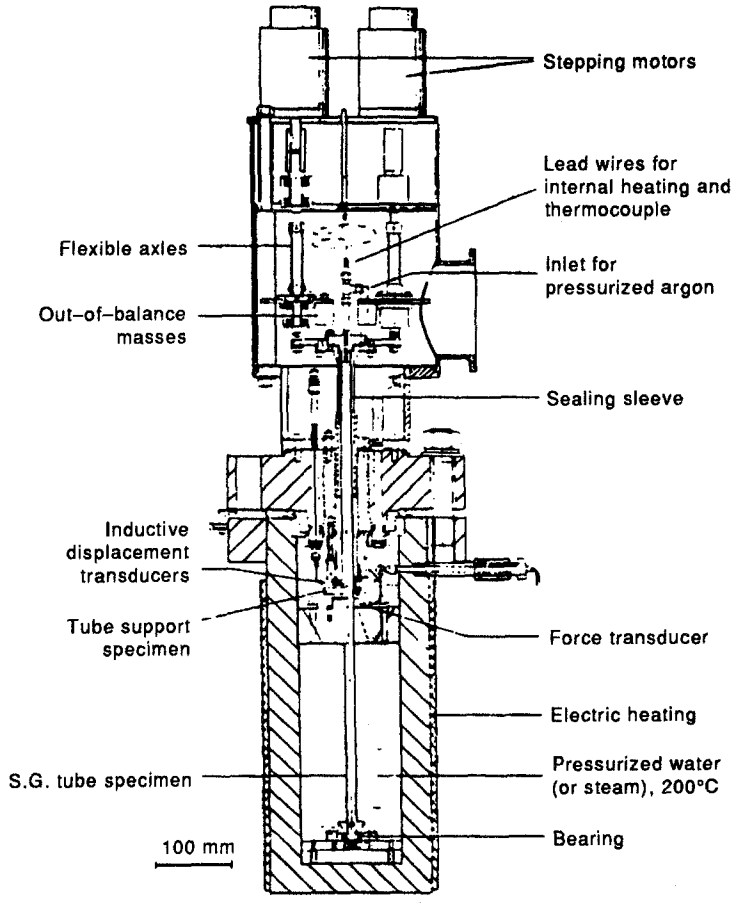

Figure 70. Details of the fretting wear fixture.

5.8.3. Operating experience

Antivibration bars. Antivibration bars are installed in the upper U-bend regions of recirculating steam generators to reduce the unsupported length of the tubes and resulting vibration. Extensive tube indications, typical of a wear mechanism, were identified at the antivibration bars in several steam generators at San Onofre Unit 1. This damage was attributed to the design of the antivibration bars, which were in point contact with the tubes; the design has now been changed and modification to the unit implemented. Antivibration bars of the new design provide a broader region of contact with the tubes.

U-bend indications on antivibration bars have recently been identified at a number of plants. Evaluations indicate wear as the principal contributor to the indications. The wall of one affected tube in the region of the antivibration bars of the Zion plant exhibited material loss of up to 22% of wall thickness (Aspden 1985). The flow-induced vibration mechanisms that may be the cause of this damage have not been identified. The existence of similar damage at other plants with the same steam generator design has not been confirmed by tube pull examination. But eddy current examination appears to indicate similar damage at other plants. Out-of-tolerance clearance between some of the U-bend tubes and their respective antivibration bars leads to lack of tube support at these critical locations and can result in tube vibration. If the vibrations are of significant magnitude they can lead to tube wear (Weaver & Schneider 1983). The antivibration bars in some of the affected plants have been replaced with wider bars that are designed to reduce the clearance between the bars and tubes.

It is clear that if there is a gap between the tubes and the antivibration bars, tube wear will result. In fact, tube wear at the antivibration bars has been detected in most operating Westinghouse Model F steam generators. The mechanism causing the wear is, most likely, fluid–elastic instability caused by the presence of inactive antivibration bars.

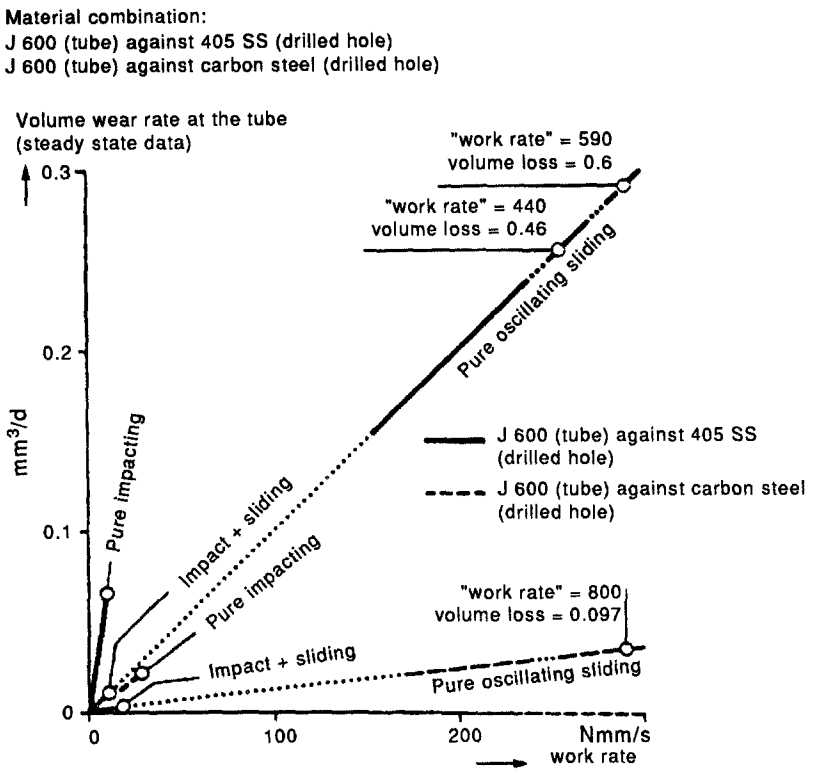

Figure 71. Comparison of tube wear rates and "work rates" for different support materials. Note: the points presented are steady data from long-term tests. To date, the assumed linear correlation between wear rates and "work rates" is hypothetical for the impact plus sliding condition.

Split-flow and counterflow preheat steam generators. In October 1981, Ringhals Unit 3 in Sweden, a three-loop plant with split-flow-type preheat steam generators, was shut down because a cold-leg tube had a small through-wall hole at the third baffle plate in the preheater. The unit had operated for approximately 2200 h at power levels of about 75% at the time of the leak. It was determined that an accelerated wear mechanism involving interactions between baffle plates and tubes was occurring. Eddy current testing performed on all three steam generators at Ringhals 3 and at a similar plant at Almaraz in Spain indicated that preferential wear was occurring in the other three rows of the tube bundle in the preheater section.

The two-loop Krsko plant in Yugoslavia contains counterflow preheat steam generators. The feedwater inlet flow geometries of the split-flow and counter-flow steam generators are different, as shown in figure 73. When tube wear in the Ringhals and Almaraz steam generators was detected, the steam generator vendor instituted a three-phase test program that included steam generator tube vibration measurements at the McGuire (in the United States), Almaraz and Krsko plants.

Data taken during the test program at Krsko indicated that tube/tube support plate impacts occur at power levels between 60 and 100%. In comparison with the tube results obtained at Almaraz, it was shown that, because of different tube support conditions (e.g. misalignment between tube and support plates, and/or different tube support hole sizes), the lowest natural tube frequency at Krsko was lower by approximately 42%. Root-mean-square (rms) tube displacement at Krsko for the lowest tube fundamental frequency and a plant power level of 70% was found to be comparable to typical Almaraz tube displacement at its higher frequency but at a power level of 50%.

On the basis of these results and the acceptable wear rate at Almaraz for the 50% power condition, it was concluded that the feedwater flow into the Krsko steam generators through the main nozzle should be limited to 50% of full flow to reduce tube vibration amplitude and the possibility of early tube wear.

Additional examination of tubes in the Krsko steam generators during plant modifications indicated that wear was occurring at three baffle plate locations within the preheater with the major

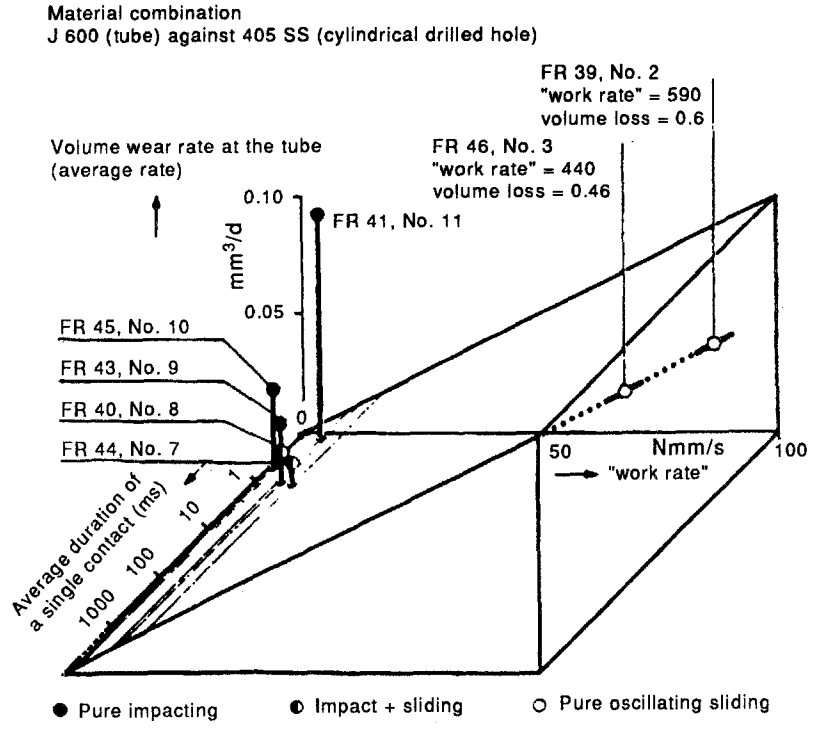

Figure 72. Average volume wear rate data vs "work rate" and contact time.

wear being 6% of the tube wall thickness. Since the feedwater flow through the main nozzle was limited to 70% at Krsko, 100% power was approached by feeding the remaining 30% flow through the auxiliary nozzle (located in the upper portion of the steam generator).

The cause of excessive tube vibration in model D2 and model D3 split-flow preheaters was investigated through the use of scale model flow tests, analytical modeling and in-field vibration measurements. It was concluded that excessive tube movement was dependent on position relative to the feedwater impingement plate location. Most of the field wear data for tubes located away

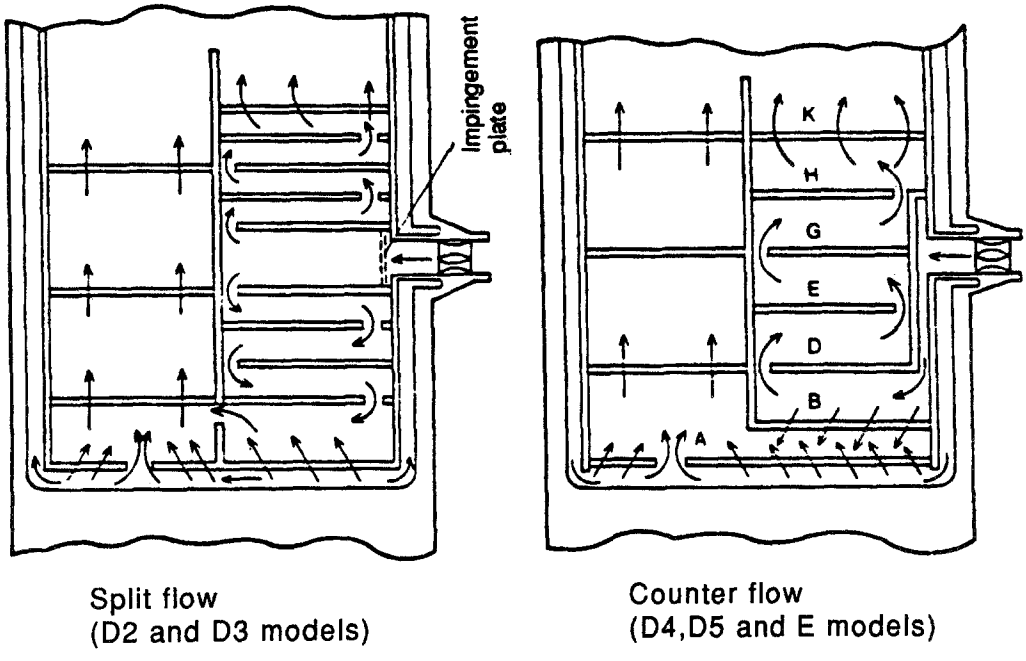

Figure 73. Preheat steam generator geometry.

from the impingement plate appear to be adequately described on the basis of turbulence-induced tube excitation with the use of a reasonable value of material wear coefficients. Some tubes that exhibit larger wear rates and are close to the edge of the impingement plate are considered to be, in part, under the influence of a fluid–elastic phenomenon, which is a fluid–structure interaction instability. Turbulence is probably also a component of the forcing function. This phenomenon is thought to result in more severe and violent tube vibration than that due to turbulence excitation alone. Besides reducing the flow to the main nozzle, a new impingement baffle, which distributes the flow more uniformly around the bundle, was installed.

The cause of the excessive tube vibration in the model D4, D5, and E counterflow steam generators is similar to that in the split-flow preheat steam generator case, although flow turbulence was thought to be the predominant tube vibration forcing function. The tube bundle area, where most of the flow energy for tube excitation occurred for both the split-flow and counterflow, was located at the entrance region. It appears that tubes located within the first two or three rows are predominantly affected. In the D4, D5 and E steam generators there exists a so-called T-slot (i.e. a T-shaped area within the preheater where tubes are absent). Some tubes located on the periphery of the T-slot also experienced unacceptable tube vibration. The tubes in the periphery were expanded at several of the tube support locations to reduce the vibration amplitude and resultant wear by reducing the annular clearance between the tube and the inside diameter of the tube support plate hole.

Batwing wear. In 1985 tube wear occurred in the steam generators of San Onofre 2 and 3 (figure 74) in the periphery of the central cavity region. It was concluded that this wear is a result

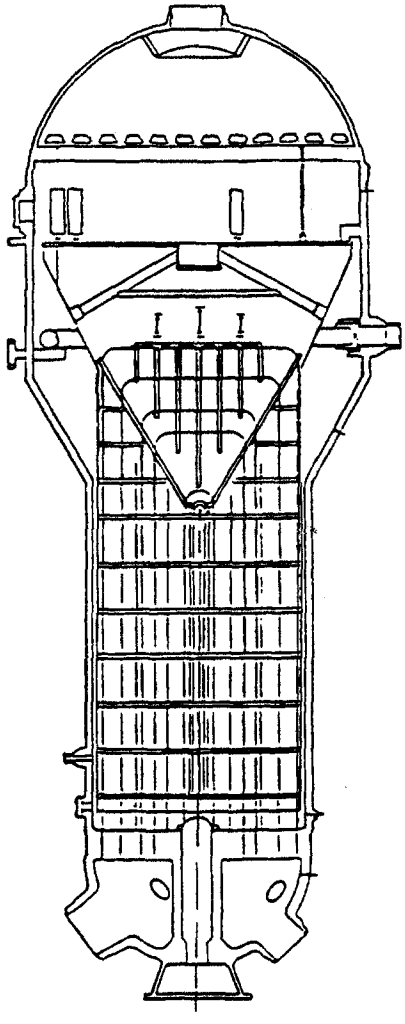

Figure 74. San Onofre Unit 2 and Unit 3 steam generators.

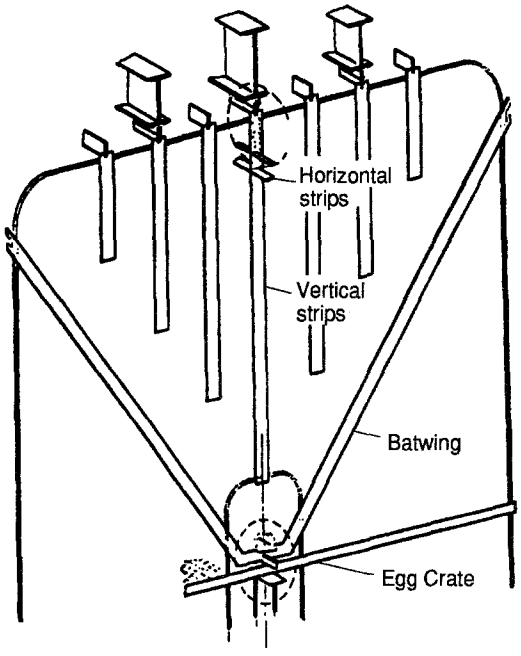

Figure 75. Upper tube bundle supports, San Onofre steam generators.

of flow-induced vibration in the cavity region caused by long unsupported spaces from the first tube contact point to the center of the bundle, where the tubes are partially held by a cross-plate (figures 75 and 76). This center support allows swinging and rocking or twisting modes of displacement and/or vibration. The strips of flexible flat (230 μm thick) plate have low natural frequencies and tend to pick up flow energy.

The tubes are also subject to flow-induced vibrations, and their motions include deflection in the plane of the batwing straps. Wear is caused by relative tangential motion between the vibrating tubes and straps. The volumetric rate of wear on each tube is proportional to the normal force acting between the tubes and straps and the relative tangential motions between them.

The steam generators at St Lucie 2, Waterford 3 and Palo Verde 1, 2 and 3 have comparable designs. The affected tubes were staked and plugged and no additional corrective action was taken, since it was judged that the tube wear damage was limited to one small region of the steam generator.

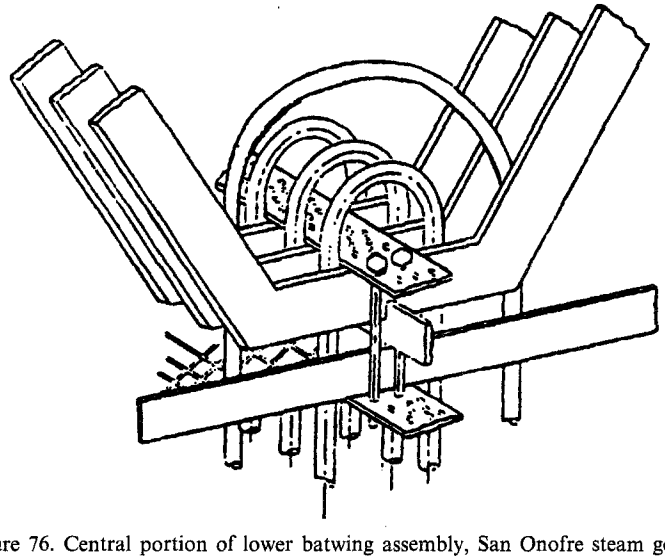

Figure 76. Central portion of lower batwing assembly, San Onofre steam generators.

5.9. Erosion–Corrosion

Wear has occurred in the J tubes of several steam generators due to erosion–corrosion. The J-tubes are connected to a feed ring used to distribute the feed uniformly around the bundle of the steam generator. The erosion–corrosion usually occurred in tubes that were fabricated of carbon steel due to the high velocities and change in direction. The problem was solved by replacement of the carbon steel tubes with a more resistant tubing, such as alloy 600 tubes.

REFERENCES

A full-range drift-flux correlation for vertical flows. EPRI Report NP-3989-SR, June 1985.

A model of sludge behavior in Nuclear Steam Generators. EPRI Report NP-4620, June 1986.

A study of the boiling processes in the sludge deposit of steam generators. EPRI Report NP-3018, May 1983.

An assessment of eight void fraction models for vertical flow. EPRI Report NSAC 107, December 1986.

Abe, J., Eckert, E. R. G. & Goldstein, R. J. 1982 A parametric study of boiling in a porous bed. *Waerme Stoffuebertrag* **16,** 119–126.

Airey, G. P. 1983 Optimization of metallurgical variables to improve corrosion resistance on Inconel alloy 600. EPRI Report NP-3051.

Airey, G. P. 1979 The effect of carbon content and thermal treatment on the SCC behavior of INCONEL alloy 600(R) tubing. *Corrosion* **35,** 129–136.

Airey, G. P. 1983 The stress corrosion cracking (SCC) performance of Inconel alloy 600 in pure and primary water environments. *Int. Symp. Environmental Degradation of Materials in Nuclear Power Systems—Water Reactors*, 22–25 August, Myrtle Beach, SC.

Antunes, J., Axisa, F., Beaufils, P. & Guilbaud, D. 1988 Coulomb friction modelling in numerical simulations of vibration and wear work rate of multispan tube bundles. *ASME International Symposium of Flow Induced Vibration and Noise*, Chicago, IL.

Aspden, R. G. & Pemento, F. W. 1985 Destructive examination of Zion Unit 1 tube and autovibration bar samples. EPRI Report NP-4375 LD.

ATHOS and FLOW-3, simulation of the FRIGG heated rod bundle experiments. EPRI Report NP-3514, May 1984.

ATHOS—computer program for thermal–hydraulic analysis of steam generators, Vol. 1: mathematical and physical models and method of solution. EPRI Report NP-2698-CCM, October 1982.

ATHOS—a computer program for thermal–hydraulic analysis of steam generators, Vol. 2: programmer's manual. EPRI Report NP-2698-CCM, October 1982.

ATHOS—a computer program for thermal–hydraulic analysis of steam generators, Vol. 3: user's manual. EPRI Report NP-2698-CCM, October 1982.

ATHOS—a computer code for thermal–hydraulic analysis of steam generators, Vol. 4: applications. EPRI Report NP-1698-CCM, August 1984.

Axisa, F., Villard, B., Gibert, R. J., Hetsroni, G. & Sundheimer, P. 1984 Vibration of tube bundles subjected to air–water and steam–water cross-flow: preliminary results on fluidelastic instability. *Proceedings of ASME*, Vol. 2, pp. 269–284, December, New Orleans, LA.

Axisa, F., Boheas, M. A. & Villard, B. 1985 Vibration of tube bundles subjected to steam–water cross-flow: a comparative study of square and triangular arrays. Paper B1/2, *8th International Conference on Structural Mechanics in Reactor Technology*, August, Brussels, Belgium.

Axisa, F., Antunes, J., Villard, B. & Wullschleger, M. 1988 Random vibration of heat exchanger tubes by cross-flow. *ASME International Symposium on Flow Induced Vibration and Noise*, Chicago, IL.

Axisa, F., Paurobally, A. & Remond, A. 1989 Predictive analyses of flow induced vibration and fretting wear in steam generator tubes. *International Symposium on Pressure Vessel Technology and Nuclear Codes on Standards*, pp. 2.57–2.75, Seoul, Korea.

Balakrishnan, P. V. 1980 Computation of chemical equilibria in steam generator water. *Proc. 41st Int. Water Conf.*, pp. 323–334.

Baum, A. J. & Curlee, N. J. Jr 1980 An experimental and analytical investigation of dryout and chemical concentration in confined geometries. ASME Paper 80 C2/NE-6.

Baum, A. J. & Gearney, P. K. 1981 Steam generator sludge pile model boiler testing. EPRI Report NP-1941.

Baum, A. J. & Gearney, P. K. 1981 An experimental and analytical investigation of boiling heat transfer in porous bodies. ASME Paper 81-HT-44.

Baum, A. & Steininger, D. A. 1982 A study of boiling heat and mass transfer in annular crevices. *7th Int. Heat Transfer Conf.*, September, Munich, Germany.

Bawden, R. J., Garnsey, R. & Martel, L. J. 1980 Calculations of steam generating chemistry. *Proc. 41st Int. Water Conf.*, pp. 318–220.

Beal, S. K. 1970 Deposition of particles in turbulent flow on channel or pipe walls. *Nucl. Sci. Engng* **40,** 1.

Beal, S. K. 1978 Correlations for the sticking probability and erosion of particles. *J. Aerosol Sci.* **9,** 455.

Beal, S. K. & Armstrong, R. C. 1981 A model to predict the particle size distribution in a system with corrosion fouling. *20th ASME/AIChE Heat Transfer Conf.*, 2–5 August, Milwaukee, WI.

Beal, S. K. & Chen, J. N. 1986 A model of sludge behavior in nuclear plant steam generators. EPRI Report NP-4620.

Becker, L. F. Jr & Esposito, J. N. 1981 Steam generator sludge pile model boiler—sludge characterization. Electric Power Research Institute.

Berge, Ph. 1971 *Proceedings on the Conference—Effects of Environments on Material Properties on Nuclear Systems*, Paper 6, BNES.

Berge, Ph. & Donati, J. R. 1981 Materials requirements for pressurized water reactor steam generator tubing. *Nucl. Technol.* **55,** 88–104.

Blevins, R. D. 1974 Fluid elastic whirling of a tube row. *Trans. ASME J. Pressure Vessel Technol.* 263–267.

Block, J. A. *et al.* 1977 An evaluation of PWR steam generator water hammer. Report by Creare Inc. for the Nuclear Regulatory Commission, NUREG-0291.

Blomgren, J. C. *et al.* 1988 PWR secondary water chemistry guidelines—Revision 1. EPRI Report NP-6259-SR.

Boiling heat transfer in narrow eccentric annulus. EPRI Report NP-2610, September 1982.

Boiling in narrow crevices in steam generators. EPRI Report NP-2638, November 1982.

Boivin, J.-Y., Bussy, B. & Pierotti, G. 1987 P.W.R. steam generators: a set of experimental programs for three dimensional code validation. *ASME Winter Mtg*, 13–16 December, Boston, MA.

Bouchter, J. C., Oceraies, Y. & Ferrand, F. 1984 *ANS Conference on Steam Water Centrifugal Separation—A Comprehensive Theoretical and Experimental Approach*, 11–16 November, Washington, DC.

Bouchter, J. C., Campan, J. L. & Gouirand, J. M. 1986 Verification test on three dimensional two-phase flow codes for PWR steam generators. *Proc. 2nd Int. Topical Mtng Nuclear Power Plant Thermal Hydraulics and Operations*, pp. 3-1–3-7, 15–17 April, Tokyo, Japan.

Bouecke, R., Odar, S. & Stellwag, B. 1986 Experience with KWU steam generator tubing corrosion phenomena and their prevention. *Proc. 2nd Int. Topical Mtng Nuclear Plant Thermal Hydraulics and Operation*, pp. 10-24–10-30, 15–17 April, Tokyo, Japan.

Bush, S. H. & Dillon, R. L. 1977 Stress corrosion in nuclear systems. In *Stress Corrosion Cracking and Hydrogen Embrittlement of Iron Base Alloys* (Edited by Staehle, R. W., Hochmann, J., McCright, D. & Slater, J. E.). National Association of Corrosion Engineers, Houston, TX.

CALIPSOS Code Report. EPRI Report NP-1391, Vol. 1, June 1980.

Campan, J. L., Pinard-Legry, G. & Vignes, A. J. 1983 Summary of denting mechanism and kinetic studies with seawater. *Nucl. Technol.* **63**.

Campan, J. L. & Castello, G. 1986 MEGEVE Program—verification and qualification of steam generator design on a 25 MW test loop. *Proc. 2nd Int. Topical Mtng—NUREG*, pp. 3-28–3-34, 15–17 April, Tokyo, Japan.

Campan, J. L. & Shoemaker, C. E. 1987 Sodium hideout studies in steam generator crevices. *Third Int. Symp. on Environmental Degradation of Materials in Nuclear Power Systems—Water Reactors*, August–September, Michigan, MI.

Campan, J. L. & Brunet, J. P. 1987 Caustic concentration in tube support plate crevices of steam generators. EPRI Report NP-5073.

Carlucci, L. N. 1980 Thermal–hydraulic analysis of the combustion-engineering system 80 steam generator. EPRI Report NP-1546.

Carlucci, L. N. & Brown, J. D. 1983 Experimental studies of damping and hydrodynamic mass of a cylinder in confined two-phase flow. *ASME J. Vibrat. Acoust. Stress Reliability Des.* **105.**

Carson, W. R. & Williams, H. K. 1980 Method of reducing carryover and reducing pressure drop through a steam separator. EPRI Report NP-1607.

Carter, H. R. & Promey, G. J. 1982 Measurement and THEDA code prediction of thermal, velocity, and pressure fields in a once-through steam generator heated air model. EPRI Report NP-2765.

Carter, H. R., Childerson, M. T. & Moshal, T. E. 1982 Model tests of a once-through steam generator for lance blocker assessment and THEDA code verification. EPRI Report NP-3042.

Carter, H. R., Promey, G. J. & Rush, G. C. 1982 Predictions and measurements of isothermal airflow in a model once-through steam generator. EPRI Report NP-2643.

Carver, M. B. 1982 Thermal–hydraulic analysis of the Westinghouse Model 51 steam generator. EPRI Report NP-2683.

Cassell, D. S. & Vroom, D. W. 1983 Thermal–hydraulic tests of steam generator tube support plate crevices. EPRI Report NP-2838.

Chan, K. C., Masiello, P. J. & Srikantiah, G. S. 1986 PORTHOS—a computer code for solving general three-dimensional, time-dependent two-fluid equations. ASME Paper 86-WA/NE-3.

Chapman, R. L. *et al.* 1982 Compilation of data concerning known and suspected water hammer events in nuclear power plants. Reported by EG&G Inc. for the Nuclear Regulatory Commission, NUREG/CR-2059.

Chen, S. S. & Wambsganss, M. W. 1977 Experiments on fluidelastic vibrations of tube arrays. Tech. Memo, ANL-CT-77-16, Argonne National Laboratory, Argonne, IL.

Chen, S. S. 1981 Instability mechanisms and stability criteria of a group of circular cylinders subjected to cross-flow, part I: theory. ASME Reprint 81-DET-21.

Chen, S. S. 1981 Instability mechanisms and stability criteria of a group of circular cylinders subjected to cross-flow, part II: numerical results and discussions. ASME Reprint 81-DET-21.

Chen, S. S., Jendzefczyk, J. A. & Wambsganss, M. W. 1983 Dynamics of tubes fluid with tube–baffle interaction. Argonne National Laboratory Report ANL-83-72.

Chen, S. S. 1987 *Flow Induced Vibration of Circular Cylindrical Structures.* Hemisphere, Washington, DC.

Chen, Y. N. & Young, W. C. 1974 The orbital movement and the damping of the fluidelastic vibration of tube banks due to vortex formation, part 3—damping capability of the tube bank against vortex excited sonic vibration in the fluid column. *J. Engng Indust.* **96,** 1072–1075.

Chen, Y. N. 1977 The sensitive tube spacing region of tube bank heat exchangers for fluid–elastic coupling in cross flow. Fluid structure interaction phenomena in pressure vessel and piping systems. ASME PVP-PB-026, pp. 1–18.

Chick, E. E. *et al.* 1988 NDE and mechanical removal of sludge in PWR steam generators—overview and utility experience. EPRI Report NP-5563.

Chilukuri, R., Stuhmiller, J. H. & Steininger, D. A. 1987 Large eddy simulation of turbulent buffeting forces in steam generator tube bank. *Int. Conf. on Flow Induced Vibration,* 12–14 May, England.

Chilukuri, R., Stuhmiller, J. H. & Steininger, D. A. 1987 Numerical simulation of turbulence deep within heat exchanger tube bundles. *ASME Symp. Flow Induced Vibrations,* San Diego, CA.

Cohen, P. 1977 Chemical thermohydraulics of steam generating surfaces, *AIChE/ASME 16th Natl. Heat Transfer Conf.,* August, Salt Lake City, UT.

Cohen, P. 1980 Chemical thermohydraulics of steam generating systems. *Conf. Water Chemistry and Corrosion in the Steam–Water Loops of Nuclear Power Stations,* March, Seillac, France.

Conners, H. J. 1970 Fluidelastic vibration of tube arrays excited by cross-flow. *Proc. Symp. on Flow-induced Vibration in Heat Exchangers, ASME Winter Annual Mtng,* pp. 42–56, New York.

Coponer, E. L., Egan, G. R. & Feiereisen, T. J. 1984 PWR steam generator chemical cleaning data base. EPRI Report NP-3477.

Corious, H. 1972 *Industries Atomique et Spatiales*, Vol. 2, p. 2.

Corious, H., Grall, L., LeGall, Y. & Vettier, S. 1959 Corrosion fissurante sous constrainte de l'Inconel dans l'eau a haute temperature. *3eme Colloque de Metallurgie Corrosion*, p. 161. North Holland, Amsterdam.

Council, W. G. 1982 Northeast Utilities letter to R. A. Clark, 12 January, USNRC.

Crum, J. R. 1986 Stress corrosion cracking testing of INCONEL alloys 600 and 690(R) under high-temperature caustic conditions. *Corrosion* **42,** 368–372.

Curlee, N. J. Jr & Baum, A. J. 1983 Tube support plate thermal and hydraulic testing. EPRI Report NP-3052.

De Penguern, L., David, J., Procaccia, H. & Wazzan, A. R. 1982 Thermal–hydraulic characteristics of pressurized water reactors during commercial operation: III. PWR steam generator response to a SCRAM at 50% load on an open grid transient (Bugey-4 nuclear power plant). *Nucl. Engng Des.* **70,** 173–186.

Destructive examination of Zion Unit I tube and antivibration bar samples. EPRI Report NP-4375-LD, June 1984.

Domian, H. A., Emanuelson, R. H., Sarver, L. W., Theus, G. J. & Katz, L. 1977 Effect of microstructure on stress corrosion cracking of alloy 600 in high-purity water. *Corrosion* **33,** 26–37.

Dynamic thermal–hydraulic behavior of PWR U-tube steam generators—simulator experiments and analyses. EPRI Report NP-1837-SR, May 1981.

Eaker, R. W., Rochester, D. P., Hansen, C. A., Jevec, J. M., Lamanna, L. S. & Dow, R. P. 1988 Steam generator chemical cleaning at Oconee nuclear station. *Nuclear Plant Jl* **Sept.–Oct.,** 76–80.

Fanselau, R. W., Thakkar, J. G., Hiestand, J. W. & Cassell, D. S. 1980 Thermal–hydraulic characteristics of a combustion-engineering series 80 steam generator. EPRI Report NP-1392.

Fanselau, R. W., Thakkar, J. G., Hiestand, J. W. & Cassell, D. S. 1980 CALIPSOS code report. EPRI Report NP-1391.

Fanselau, R. W., Thakkar, J. G., Hiestand, J. W. & Cassell, D. S. 1980 Thermal–hydraulic characteristics of a combustion-engineering series 80 steam generator. EPRI Report NP-1528.

Fanselau, R. W., Thakkar, J. G., Hiestand, J. W. & Cassell, D. S. 1981 Thermal–hydraulic characteristics of a Westinghouse Model 51 steam generator. EPRI Report NP-1721.

Fatigue performance of Ni–Cr–Fe alloy 600 under typical PWR steam generator conditions. EPRI Report NP-2957, March 1983.

Fink, G. C., Helyer, M. H. & Key, G. L. 1983 Steam generator chemical cleaning demonstration test No. 3 in pot boiler. EPRI Report NP-2983.

Fisher, N. J. & Ingham, B. 1989 Measurement of tube to support dynamic forces in fretting wear rings. *J. Pressure Vessel Technol.* **111,** 385–393.

Fisher, N. J., Olesen, M. J., Rogers, R. J. & Ko, P. L. 1989 Simulation of tube to support dynamic interaction in heat exchange equipment. *J. Pressure Vessel Technol.* **111,** 378–384.

Fletcher, W. D. & Malinowski, D. D. 1976 Operating experience with Westinghouse steam generators. *Nucl. Technol.* **28,** 356–373.

Flow induced vibration of steam generator. EPRI Report NP-4559, May 1986.

Frederick, G. & Hernalsteen, P. 1985 Comparative evaluation of preventive measures against PWSCC of MA I 600 steam generator tubes. *Post SMIRT Conf. Seminar No. 3,* 25–27 August, Ispra, Italy.

Fricker, A. J. 1988 Computer analysis of the fluidelastic vibration of a steam generator tube with loose supports. *ASME Int. Symp. on Flow Induced Vibration and Noise*, Chicago, IL.

Garud, Y. S. & Gerber, T. L. 1983 Intergranular stress corrosion cracking of Ni–Cr–Fe alloy 600 tubes in PWR primary water—review and assessment for model development. EPRI Report NP-3057.

Gay, N., Decembre, P. & Launay, J. 1988 Comparison of air–water to water–freon two-phase cross-flow effect on the vibratory behaviour of a tube bundle. *ASME Int. Symp. on Flow Induced Vibration and Noise*, Chicago, IL.

Gimond, C. 1986 *EPRI Workshop on Thermally Treated Alloy 690 Tubes for Nuclear Steam Generators*, Paper 14, 26–28 June, Pittsburgh, PA.

Gorman, D. J. 1976 Experimental development of design criteria to limit liquid cross-flow-induced vibration in nuclear reactor heat exchange equipment. *Nucl. Sci. Engng* **67,** 324–336.

Goyder, H. G. D. 1980 Unstable vibrations of a bundle of cylinders due to cross flow. *Proc. Int. Conf. on Recent Advances in Structural Dynamics, Institute of Sound and Vibration Research,* pp. 533–542, 7–11 July, University of Southampton, England.

Goyder, H. G. D. 1985 Vibrations of loosely supported steam generation tubes. ASME WAM, FL.

Goyder, H. G. D., Teh, C. E. & Stonehouse, F. 1986 Experimental determination of two-phase buffeting forces in tube bundles. *HTFS Research Symposium,* Paper RS639, September, Edinburgh, Scotland.

Goyder, H. G. D. 1987 The structural dynamics of the tube bundle vibration problem. *Int. Conf. on Flow Induced Vibrations,* Paper K4, Bowness-on-Windermere, England.

Goyder, H. G. D. 1987 Two phase buffeting of heat exchangers tubes. *Int. Conf. on Flow Induced Vibrations,* Paper E-2, Bowness-on-Windermere, England.

Goyder, H. G. D. 1988 Personal communication.

Granger, S. 1990 A global model for flow induced vibration of tube bundles in cross flow. *ASME PVP Conf.,* 17–21 June, Nashville, TN.

Grant, I. D. R. & Murray, I. 1972 Pressure drop on the shell-side of a segmentally baffled shell-and-tube heat exchanger with vertical two-phase flow. National Engineering Laboratory Report No. 500.

Green, S. J. & Steininger, D. A. 1980 Pressurized water steam generators—problems and progress. *Century 2 Nuclear Engineering Conf.,* 19–21 August, San Francisco, CA.

Green, S. J. & Paine, J. P. N. 1983 Steam generator materials—experience and prognosis. *Symp. on Environmental Degradation of Materials in Nuclear Power Systems—Water Reactors,* 22–24 August, Myrtle Beach, SC.

Green, S. J. 1986 Method for preventing steam generator failure or degradation. *SMIRT-8 Post Conference Seminar No. 3,* Ispra, Italy, 26–27 August 1985; *Int. J. Pressure Vessel Piping* **25,** 359–391.

Green, S. J. 1988 Thermal, hydraulic and corrosion aspects of PWR steam generator problems. *Heat Transfer Engng* **9,** 19–68.

Han, J. T. & Anderson, N. 1982 Prevention and mitigation of steam generator water hammer events in PWR plants. EPRI Report NUREG-0918.

Hara, F. 1982 Two-phase cross-flow-induced forces acting on a circular cylinder, flow-induced vibration of circular cylindrical structures. *ASME Pressure Vessel Piping* **63,** 9–17.

Haslinger, K. H. & Steininger, D. A. 1984 Steam generator tube/tube support plate interaction characteristics. *ASME Winter Annual Mtng,* New Orleans, 9–10 December 1984; *Symp. on Flow-induced Vibrations, 3, Vibration in Heat Exchangers,* pp. 45–61.

Haslinger, K. H., Martin, M. L. & Steininger, D. A. 1987 Pressurized water reactor steam generator tube wear predicted utilizing experimental techniques. *Flow Induced Vibration Conf.,* sponsored by BHRA, 12–14 May, Bowness-on-Windermere, England.

Hassan, Y. A. 1985 Thermal hydraulic predictions of a 19-tube once-through steam generator test using TRAC-PF1. *ASME HTD,* Vol. 51, pp. 93–100.

Hausler, R. H. 1983 Nonproprietary corrosion inhibitor for solvents to clean steam generators. EPRI Report NP-3030.

Heilker, W. J. & Vincent, R. Q. 1981 Vibration in nuclear heat exchangers due to liquid and two-phase flow. *ASME J. Engng Power* **103,** 358–366.

Hetsroni, G. 1982 *Handbook of Multiphase Systems.* Hemisphere, Washington, DC.

Hewitt, G. F. 1988 Personal communication.

Hibbitt, H. D., Karlsson, B. J. & Sorenson, E. P. 1985 ABAQUS-EPGEN: general purpose finite element code. *EPRI* Computer Code Manual NP-2709-CCM.

Hiestand, J. W. & Thakkar, J. G. 1984 ATHOS and FLOW3 simulation of the FRIGG heated rod bundle experiment. EPRI Report NP-3514.

Hildebrandt, P. C. *et al.* 1987 Weld region corrosion during chemical cleaning of PWR steam generators. EPRI Report NP-5267.

HITCH computer code: chemistry and pH estimates of concentrating aqueous solutions. EPRI Report NP-2388, May 1982.

Hofmann, P. J., Schettler, T. & Steininger, D. A. 1986 Pressurized water reactor steam generator tube fretting and fatigue wear characteristics. ASME 86-PVP-2.

Hoffman, P. J., Schettler, T., Wieling, N. & Steininger, V. A. 1990 Influence of contact conditions on vibration induced wear of metals. *Nucl. Engng Des.* **119,** 439–445.

Hren, J. J. 1983 *Introduction to Analytical Microscopy*. Plenum Press, New York.

Inch, W. W. R. 1981 Thermal–hydraulic analysis of the combustion-engineering engineering series 67. EPRI Report NP-1678.

Intergranular stress corrosion cracking of Ni–Cr–Fe alloy 600 tubes in PWR primary water—review and assessment for model development. EPRI Report NP-3057, May 1983.

Ishii, M. 1977 One dimensional drift-flux model and constitutive equations for relative motion between phases in various two-phase flow regimes. ANL-77-47, Argonne National Laboratory.

Jensen, M. K., Cooper, P. E. & Bergles, A. E. 1977 Boiling heat transfer and dryout in restricted annular geometries. *AIChE Symp. Ser.*, Vol. 73, No. 164.

Jevec, J. M. & Leedy, W. S. 1983 Chemical cleaning solvent and process testing. EPRI Report NP-1976.

Jevec, J. M., Miglin, B. P. & Leedy, W. S. 1987 Galvanic corrosion monitoring during chemical cleaning. *Corrosion/87*, Paper 384, 10 March.

Johnson, L. E. 1987 Fouling in nuclear once-through steam generators. Presented at *ASME Winter Annual Mtng*, ASME 87-WA/NE-12, 13–18 December, Boston, MA.

Johnston, B. S., Sharon, A., Kozawa, Y. & Bankoff, S. G. 1982 Boiling heat transfer in a narrow eccentric annulus, part I: dryout. ASME Paper 82-JPGC-NE-7.

Kalra, S. P. 1984 Modeling transients in PWR steam generator units. *Nucl. Saf.* **25,** 33–52.

Kawamura, K. 1981 Steam generator tube vibrations induced by turbulent jets from baffle plates. CRIEPI Report E281004.

Kawamura, K. 1983 Steam generator tube vibrations induced by two-phase jet flow from baffle plate. CRIEPI Report E282006.

Kawamura, K. & Yasuo, A. 1984 The effect of baffle plate design on steam generator tube vibrations induced by turbulent jets—vibrations of steam generator tube bundle support by several baffle plates. (CRIEPI) Report No. 283103.

Kawamura, K. & Yasuo, A. 1985 Estimation of the relationship between steam generator tube vibrations and tube to tube support interaction characteristics. CRIEPI Report 285056.

Keeton, L. W., Habchi, S. D., Singhal, A. K. & Srikantiah, G. 1986 Thermal hydraulic analysis/data comparisons using the ATHOS-3 code. ASME Paper 86-WA/NE-1.

Keeton, L. W., Singhal, A. K. & Srikantiah, G. S. 1986 ATHOS3: a computer program for thermal–hydraulic analysis of steam generator. EPRI Report NP-4604-CCM.

Keeton, L. W., Singhal, A. K. & Irani, A. 1986 ATHOS3 code analysis of tube plugging effects on the thermal–hydraulic characteristics of a once-through steam generator. ASME Paper 86-WA/NE-4.

Keeton, L. W. 1988 CFD Research. Personal communication.

Kidd, C. C. *et al.* 1988 NDE and mechanical removal of sludge on PWR steam generator—vendor practices. EPRI Report NP-5563.

Ko, P. L. 1979 Experimental studies to tube fretting in steam generators and heat exchangers. *ASME J. Press. Vessel Technol.* **101,** 125–133.

Ko, P. L. 1985 Heat exchanger tube fretting wear: review and application to design. *J. Tribol.* **107,** 149–156.

Kozawa, Y. & Aoki, S. 1982 Alternate drying and rewetting of heat transfer surface in tube-sheet crevice. ASME Paper 82-JPGC-NE-6.

Kwan, I. H. M. & Chung Pal, M. 1983 *AIChE Jl* **19,** 498.

Lasuo, A. & Kawamura, K. 1984 Steam generator tube vibration induced by turbulent jets from baffle plate with various flow holes water–air—a two phase flow experiment. CRIEPI Report 282567.

Layman, W. H. *et al.* 1979 Status of steam generators. *Am. Power Conf.*, 23–25 April, Chicago, IL.

Lee, A. Y., Masiello, P. J. & Steininger, D. A. 1986 Comparison of ATHOS predictions of tube bundle cross flow velocity with experimental data. ASME Paper 86-WA/NE-2.

Lee, J. Y. & No, H. C. 1986 Three-dimensional two-fluid code for U-tube steam generator thermal design analysis. *Proc. 2nd Int. Topical Mtng Nuclear Power Plant Thermal Hydraulics and Operations*, pp. 3-21–3-27, 15–17 April, Tokyo, Japan.

Lee, R. A. S. 1989 CECIL: a robot for secondary side maintenance of PWR steam generators. EPRI Report NP-5929.

Leibovitz, J. 1980 PWR chemistry. *Proc. 41st Int. Water Conf.*, pp. 335–342.

Lellouche, G. S. & Zolotar, B. A. 1982 A mechanistic model for predicting two-phase void fraction for water in vertical tubes, channels and rod bundles. EPRI Report NP-2246-SR.

Lever, J. H. & Weaver, D. S. 1982 A theoretical model for fluidelastic instability in heat exchanger tube bundles. *ASME J. Pressure Vessel Technol.* **104,** 147–158.

Liao, L. H., Parios, A. & Griffith, P. 1986 Heat transfer, carry-over and fallback in PWR steam generators during transients. EPRI Report NP-4298.

Loads on steam generator tubes during simulated loss-of-coolant accident conditions. EPRI Report NP-2682, November 1982.

Machnicki, J. 1987 Galvanically aggravated weld region corrosion assessment. *Corrosion/87*, Paper 391.

Margolis, S. G. & Redfield, J. A. 1966 FLASH: a program for digital simulation of loss-of-coolant accident. Westinghouse Atomic Power Division TM-534.

Martel, L. J. *et al.* 1977 EPRI steam generator programs. *Am. Power Conf.*, 18–20 April, Chicago, IL.

Martel, L. J. 1978 Steam generator owners group water chemistry program. *Am. Power Conf.*, 24–26 April, Chicago, IL.

Mauro, G., Sala, M. & Hetsroni, G. 1990 Improved Italian moisture separators. *Nucl. Engng Des.* **118,** 179–192.

Measurement and THEDA code prediction of thermal, velocity, and pressure fields in a once-through steam generator heated air model. EPRI Report NP-2765, December 1982.

Method of reducing carry-over and reducing pressure drop through steam separators. EPRI Report NP-1607, November 1980.

Model tests of a once-through steam generator for lane blocker assessment and THEDA code verification. EPRI Report NP-3042, June 1983.

Mundis, J. A. & Noble, D. M. 1981 Steam generator technology update. *Am. Power Conf.*, 27–29 April, Chicago, IL.

Mundis, J. A. 1983 Chemical engineering challenges in PWR steam generators. *American Institute of Chemical Engineers Annual Mtng*, 14–19 November 1982; *Chem. Engng Prog.*, pp. 39–46.

Nagano, H. *et al.* 1986 *EPRI Workshop on Thermally Treated Alloy 690 Tubes for Nuclear Steam Generators*, "Paper 10", 26–28 June, Pittsburgh, PA.

Nakamura, T. *et al.* 1978 Flow induced vibration data of 10MW model steam generator MB-3. MHI Report 25L004400.

Nakamura, T., Kanazawa, H. & Sakata, K. 1982 An experimental study on exciting force by two-phase cross-flow, flow-induced vibration of circular cylindrical structures. *ASME Pressure Vessel Piping* **63,** 19–29.

Nakamura, T. *et al.* 1986 A study on the flow induced vibrations of a tube array by a two-phase flow. Nihon Kikaigakkai Ronbunshu C. Hen 52(483).

Nordman, F., Dupin, M., Menet, O. & Fiquet, J.-M. 1989 Intergranular attack evaluation from hideout return. In *Water Chemistry of Nuclear Reactor Systems*, Vol. 5. BNES, London.

Numerical simulation of steam generators used in nuclear steam generators and reactor systems. EPRI Report NP-3063, June 1983.

Oberjohn, W. B., Fortino, R. T. & Steininger, D. A. 1982 A multi-dimensional thermal–hydraulic analysis of nuclear once-through steam generators. ASME Paper 82-FE-7.

Obry, P., Cheissoux, J. L., Grandotto, M., Gaillard, J. P., de Langre, E. & Bernard, M. 1990 An advanced steam generator design 3D code, thermalhydraulics of advanced heat exchangers. *ASME Winter Annual Mtng*, 25–30 November, Dallas, TX.

Olive, J. 1982 Simulation of the three dimensional two-phase flow in PWR. Steam generator. *10th IMACS World Congress on Systems Simulation and Scientific Computation*, Montreal, Canada.

Optimization of metallurgical variables to improve corrosion resistance of Inconel 600. EPRI Report NP-3051, July 1983.

Paidoussis, M. P. 1980 Flow-induced vibrations in nuclear reactors and heat exchanges—practical experiences and state of knowledge. In *Practical Experiences with Flow-induced Vibrations, Symposium*, 3–6 September 1979, Karlsruhe, Germany (Edited by Naudascher, E. & Rockwell, D.). Springer, New York.

Paidoussis, M. P. & Price, S. J. 1981 Fluidelastic instability of an infinite double row of circular cylinders subject to a uniform crossflow. ASME Report 81-DET-24.

Paidoussis, M. P., Price, S. J. & Mavriplis, D. 1984 A semi-potential flow theory for the dynamics of cylinder arrays in cross flow. *Proc. ASME Symposium on Flow Induced Vibrations*, Vol. 2, pp. 67–82. ASME Publications.

Paine, J. P. N. & Green, S. J. 1981 Materials performance in nuclear steam generators. *Nucl. Technol.* **55,** 10–29.

Paine, J. P. N. 1982 Operating experience and intergranular corrosion of Inconel Alloy 600 steam generator tubing. *Corrosion/82*, 22–26 March, Houston, TX.

Patel, B. M. & Hayes, J. K. 1984 Investigation of steam generator corrosion products under typical PWR operating conditions. EPRI Report NP-3068.

Pearce, D. L. 1982 Two-phase flow regimes in horizontal tubes. Presented at *European Two-phase Flow Group Meeting*, Paris.

Pearce, D. L. 1990 Flow regime calculations for U-bend region of PWR steam generator. Submitted.

Pearl, W. L. 1986 Chemical cleaning of Millstone Unit 1. EPRI Report NP-4597.

Pettigrew, M. J. & Gorman, D. J. 1973 Experimental studies on flow induced vibration to support steam generator design, part II—vibration of a small tube bundle in liquid and two-phase cross flow. *Proc. Int. Symposium on Vibration Problems in Industry*, Paper No. 4-24, Keswick, England.

Pettigrew, M. J. & Gorman, D. J. 1977 Experimental studies on flow induced vibration to support steam generator design—part III: vibration of small tube bundles in liquid and two-phase cross flow. Report AECL-5804.

Pettigrew, M, J. & Gorman, D. J. 1978 Vibration of heat exchange components in liquid and two-phase cross-flow. *Int. Conf. on Vibration in Nuclear Plants*, Paper 2.3, Keswick, England.

Pettigrew, M. J. & Campagna, A. O. 1980 Heat exchanger tube vibration: comparison between operating experiences and vibration analyses. In *Practical Experiences with Flow-induced Vibrations, Symposium*, 3–6 September 1979, Karlsruhe, Germany (Edited by Naudascher, E. & Rockwell, D.). Springer, New York.

Pettigrew, M. J. & Ko, P. L. 1980 A comprehensive approach to avoid vibration and fretting in shell-and-tube heat exchangers. ASME Publication PVP-41.

Pettigrew, M. J. 1981 Flow-induced vibration phenomena in nuclear power station components. *Power Ind. Res.* **1,** 97–133.

Pettigrew, M. J., Tromp, J. H. & Mastorakos, J. 1984 Flow-induced vibration of tube bundles subjected to two-phase cross-flow: current results. *HTFS Research Symp.*, Paper RS536, September, Warwick, England.

Pettigrew, M. J., Tromp, J. H. & Mastorakos, J. 1985 Vibration of tube bundles subjected to two-phase cross-flow. *J. Pressure Vessel Technol.* **107,** 335–343.

Pettigrew, M. J., Taylor, C. E. & Kim, B. S. 1989 Vibration of tube bundles in two-phase cross-flow: part 1—hydrodynamic mass and damping. *J. Pressure Vessel Technol.* **111,** 466–477.

Pettigrew, M. J., Tromp, J. H., Taylor, C. E. & Kim, B. S. 1989 Vibration of tube bundles in two-phase cross-flow: part 2—fluid-elastic instability. *J. Pressure Vessel Technol.* **111,** 478–487.

Prins, C. A. 1974 Aspects of two-phase, gas–liquid, separation related to nuclear steam supply systems. Ph.D. thesis, Department of Mechanical Engineering, Delft University of Technology, The Netherlands.

Procaccia, H., David, J., de Penguern, L. & Wazzan, A. R. 1982 Thermal–hydraulic characteristics of pressurized water reactors during commercial operation: II. Steady-state thermal measurements on the secondary side of a PWR steam generator (Bugey-4 nuclear power plant). *Nucl. Engng Des.* **70,** 159–171.

Procaccia, H., David, J. & Wazzan, A. R. 1984 Thermal–hydraulic characteristics of pressurized water reactors during commercial operation: V. Steady-state thermal measurements on the secondary side of a PWR steam generator (Tricastin 1 nuclear power plant). *Nucl. Engng Des.* **80,** 87–97.

Procaccia, H., David, J., de Penguern, L., Hamon, P. & Wazzan, A. R. Tests of types 51A and 51M steam generators at Bugey 4 and Tricastin 1 nuclear power plants. EPRI Report NP-2689.

PWR secondary water chemistry study. EPRI Report NP-516, February 1977.

PWR secondary water chemistry guidelines. EPRI Report NP-2704-SR, October 1982.

Rabinowicz, E. 1965 *Friction and Wear of Materials.* Wiley, New York.

Rao, M. S. M., Gupta, G. D., Eisinger, F. L., Hibbitt, H. D. & Steininger, D. A. 1987 Computer modeling of vibration and wear multispan tubes with clearances at tube support. *Int. Conf. on Flow Induced Vibration*, England.

Rao, M. S. M., Steininger, D. A. & Eisinger, F. L. 1988 Numerical simulation of fluidelastic vibration and wear of multispan tubes with clearances at supports. *Proc. Int. Symp. on FIV*, ASME.

Redfield, J. A., Murphy, J. H. & Davis, V. C. 1967 FLASH-2: a Fortran IV program for the digital simulation of multinode reactor plant during loss-of-coolant. Westinghouse Atomic Power Division TM-666.

Redfield, J. A. *et al.* 1969 FLASH-4; a fully implicit Fortran IV program for the digital simulation of transients in a reactor plant. Westinghouse Atomic Power Division—TM-840.

Remy, F. N. 1982 Flow induced vibration of tube bundles in two-phase cross flow. In *Proc. BNES Int. Conf. on Vibration in Nuclear Plants*, Paper 68-1, May, Keswick, England.

Remy, F. N. & Bai, D. 1982 Comparative analysis of cross flow induced vibrations of tube bundles. *Int. Conf. on Flow Induced Vibration in Fluid Engineering*, Reading, England.

Saha, P. *et al.* 1982 Independent assessment of TRAC-PD2 and RELAP5/MOD1 codes at BNL in FY1981. NUREG/CR-3148, BNL-NUREG-51645, Brookhaven National Laboratories.

Sandifer, J. B. 1984 The effect of support clearance on steam generator tube damping. In *Impact, Fragmentation and Blast (Vessels, Pipes, Tubes, Equipment), Pressure Vessels and Pipes*, Vol. 82, ASME.

Sarver, J. *et al.* 1987 Effect of carbide precipitation on the corrosion behavior of INCONEL alloy 690 (R). CORROSION/87, Paper No. 95, 9–13 March, San Francisco, CA.

Sawochka, S. G. *et al.* 1981 Corrosion-product transport in PWR secondary systems. EPRI Report NP-2149.

Scarberry, R. C. *et al.* 1976 Precipitation reactions in INCONEL alloy 600(R) and their effect on corrosion behavior. *Corrosion* **32,** 401–406.

Scarberry, R. C., Mankins, W. L. & Pohovey, M. J. 1986 Carbon solubility in alloy 690. *Proc. Workshop on Thermally Treated Alloy 690 Tubes for Nuclear Steam Generators*, EPRI Report NP-4665S-SR.

Schenk, H. J. 1976 Investigation of tube failures in Inconel 600 steam generator tubing at KWO Obrigheim. *Mater. Perform.*, p. 25.

Schneidmiller, D. & Stitteler, D. 1983 Steam generator chemical cleaning process development. EPRI Report NP-3009.

Schwartz, T. & Bouecke, R. 1985 Utilization of the ATHOS code for split flow economizer and flow distribution plate calculations of steam generators. *ASME HTD*, Vol. 51, pp. 57–69.

Sedriks, A. J. *et al.* 1979 Inconel alloy 690(R)—a new high nickel alloy for corrosive environments at elevated temperature. *Corrosion Engng* **28,** 82–95.

Serkiz, A. W. 1983 Evaluation of water hammer experience in nuclear power plants—technical findings relevant to unresolved safety issue A-1. NRC Report NUREG-0927.

Serra, E. 1981 Stress corrosion cracking of Alloy 600. EPRI Report NP-2114-SR.

Sexton, D. E., Kasaahara, M. & Uffer, R. A. 1982 Evaluation of water hammer potential in preheat steam generators. Report by Quadrex Corp. for the Nuclear Regulatory Commission, NUREG/CR-3090.

Shoemaker, C. E., Cordovi, M. & Stein, A. A. 1986 *Proc. Workshop on Thermally Treated Alloy 690 Tubes for Nuclear Steam Generators*, NP-4665S-SR.

Singhal, A. K., Keeton, L. W., Przekwas, A. J. & Weems, J. S. 1984 ATHOS—a computer program for thermal hydraulic analysis of steam generators. EPRI Report NP-2698-CCM.

Single-tube thermal and hydraulic tube support test. EPRI Report NP-2046, Vols 1 and 2, September 1981.

Smith, K., Klein, A., Saint-Paul, P. & Blanchet, J. 1985 Inconel 690: a material with improved corrosion resistance for P.W.R. steam generator tubes. *Meeting of the National Association of Corrosion Engineers*, September, Monterey, CA.

Smith, A. C. & Armstrong, R. C. 1984 Effect of geometry on thermal and hydraulic conditions in steam generator tube support crevices. ASME Paper 84-WA/NE-53.

Solomon, Y. 1977 An overview of water chemistry for pressurized water reactors. *Int. Conf. Water Chemistry of Nuclear Reactor Systems, British Nuclear Energy Society*, Bournemouth, England.

Soper, B. M. H. 1983 The effect of tube layout on the fluid–elastic instability of tube bundles in crossflow. *Trans. ASME, J. Heat Transfer*, pp. 744–750.

Srikantiah, G. S. & Kalra, S. P. 1983 Thermal hydraulic analysis of steam generators—the ATHOS Code. *11th Water Reactor Safety Research Information Meeting (NRC)*, 24–28 October, Gaithersburg, MD.

Steam generator sludge pile model boiler testing. EPRI Report NP-1941, July 1981.

Steam–water separation in a swirl-vane centrifugal separator. EPRI Report NP-2996. Vols 1 and 2, June 1983.

Stress corrosion cracking of Alloy 600 and Alloy 690 in all-volatile treated water at elevated temperatures. EPRI Report NP-3061, May 1983.

Stress corrosion cracking of Alloy 600. EPRI Report NP-2114-SR, November, 1981.

Styrikovich, M. A., Polansky, V. S. & Tsiklauri, G. V. 1987 *Two Phase Cooling and Corrosion in Nuclear Power Plant*. Hemisphere, Washington, DC.

Tanaka, H., Takahara, S. & Ohta, K. 1982 Flow-induced vibration of tube in arrays with various pitch-to-diameter ratios. *Flow Induced Vibration of Circular Cylindrical Ratios, Flow Induced Vibration of Circular Cylindrical Structures—Pressure Vessels and Pipes*, Vol. 63, ASME.

Taylor, C. E., Currie, I. G., Pettigrew, M. J. & Kim, B. S. 1989 Vibration of tube bundles in two-phase cross-flow: part 3—turbulence-induced excitation. *J. Pressure Vessel Technol.* **111,** 488–500.

Taylor, C. E., Pettigrew, J. J., Axisa, F. & Villard, B. 1986 Experimental determinations of single and two-phase cross flow-induced forces on tube rows. *ASME Symp. on Flow-induced Vibration—1986*, Vol. 104, pp. 31–40.

Tests of Types 51A and 51M steam generators at Bugey 4 and Tricastin nuclear power plants. EPRI Report NP-2689. October 1982.

Thakkar, J. G., Fanselau, R. W., Hiestand, J. W. & Cassell, D. S. 1981 Thermal–hydraulic characteristics of a Westinghouse Model F steam generator. EPRI Report NP-1719.

THEDA-2: a multi-dimensional steam generator thermal–hydraulic model. EPRI Report NP-3031-COM, Vols 1–3, December 1983.

Thermal and hydraulic code verification: ATHOS2 and model boiler No. 2 data. EPRI Report NP-2887, Vols 1–3, February 1983.

Thermal hydraulic code qualification: ATHOS2 and data from Bugey 4 and Tricastin 1. EPRI Report NP-2872, February 1983.

Thermal–hydraulic analysis of the combustion engineering series 67 steam generator. EPRI Report NP-1678, January 1981.

Thermal–hydraulic analysis of the Westinghouse Model 51 steam generator. EPRI Report NP-2683, October 1982.

Thermal–hydraulic analysis of once-through steam generators (OTSGs). EPRI Report NP-1431, June 1980.

Thermal–hydraulic analysis of the combustion engineering system 80 steam generator. EPRI Report NP-1546, September 1980.

Thermal–hydraulic characteristics of a combustion engineering series 67 steam generator. EPRI Report NP-1392, Vol. 2, June 1980.

Thermal–hydraulic characteristics of a combustion engineering system 80 steam generator. EPRI Report NP-1528, Vols 1 and 2, September 1980.

Thermal–hydraulic characteristics of a Westinghouse Model 51 steam generator. EPRI Report NP-1721, Vols 1 and 2, March 1981.

Thermal–hydraulic characteristics of a Westinghouse Model F steam generator. EPRI Report NP-1719, Vols 1 and 2, March 1981.

Thermal–hydraulic tests of steam generator tube support plate crevices. EPRI Report NP-2838, Vols 1–3, January 1983.

Theus, G. J. 1980 Summary of the Babcock & Wilcox Company's stress corrosion cracking tests of alloy 600. *EPRI Workshop on Cracking of Alloy 600 U-Bend Tubes in Steam Generators.*

Theus, G. J. & Emanuelson, R. H. 1983 Stress corrosion cracking of alloy 600 and alloy 690 in all volatile treated water at elevated temperatures. EPRI Report NP-3061.

Theus, G. J. & Nakayasu, F. 1986 Corrosion of steam generator tubing. *Proc. 2nd Int. Topical Mtng Nuclear Plant Thermal Hydraulics and Operation*, pp. 10-56–10-64, 15–17 April, Tokyo, Japan.

Thomas, D. & Grigul, V. 1984 Brennst. *Waerme-Kraft* **26,** 109.

Tincq, D., Boivin, J. Y. & Pierotti, G. 1988 PWR steam generator of French 1300 MWe plant interpretation of paluel field measurements with the three-dimensional computer code CAFCA. *3rd Int. Topical Mtng on Nuclear Power Plant Thermal Hydraulics and Operations.*

Transient modeling of steam generator units in nuclear power plants: computer code TRANSG-01. EPRI Report NP-1368, March 1980.

Transient simulation studies for PWR U-tube steam generators. EPRI Report NP-3412. March 1984.

Tube support plate thermal and hydraulic testing. EPRI Report NP-3052, May 1983.

Tube-to-tube sheet joint test. EPRI Report NP-3013, Vols 1 and 2, March 1983.

U.S. Nuclear Regulatory Commission 1979 Water hammer in nuclear power plants. NUREG-0582, July 1979.

Uffer, R. A. *et al.* 1982 Evaluation of water hammer events in light water reactor plants. Report by Quadrex Corp. for the Nuclear Regulatory Commission, NUREG/CR-2781.

Van der Vorst, M. J. & Steininger, D. A. 1982 Calculation of phase separation by centrifugal forces. ASME Reprint 82-FE-5.

Van der Vorst, M. J., Fortino, R. T. & Steininger, D. A. 1982 A multi-dimensional thermal–hydraulic analysis of nuclear once-through steam generators. ASME Reprint 82-FE-7.

Van der Welle, R. 1983 A contribution to the numerical description of rotating two-phase flow. Ph.D. thesis, Department of Mechanical Engineering, Delft University of Technology, The Netherlands.

Van Rooyen, D. 1975 Review of the stress corrosion cracking of Inconel 600. *Corrosion* **31,** 327.

Vroom, D. W., Babcock, D. A. & Cassell, D. S. 1982 Thermal–hydraulic tests of tube supports in a multi-tube steam generator model. ASME Paper 82-JPGC-NE-5.

Wallis, G. B. 1968 Vertical annular flow. *AIChE Annual Meeting*, Tampa, FL.

Wallis, G. B. 1969 *One Dimensional Two-phase Flow.* McGraw–Hill, New York.

Wang, S. F. & Chang, C. Y. 1986 Qualification of the steam generator thermal–hydraulic code HERMIT-UTSG using data from Bugey 4 and Tricastin 1. *ADF Proc. 2nd Int. Topical Mtng Nuclear Power Plant Thermal Hydraulics and Operations*, pp. 3-8–3-15, 15–17 April, Tokyo, Japan.

Wazzan, A. R., Procaccia, H., David, J. & de Penguern, L. 1982 Thermal–hydraulic characteristics of pressurized water reactors during commercial operation: I. Circulation ratio and carry-under in a PWR steam generator (Bugey-4 nuclear power plant). *Nucl. Engng Des.* **70,** 145–158.

Wazzan, A. R., Procaccia, H. & David, J. 1984 Thermal–hydraulic characteristics of pressurized water reactors during commercial operation: IV. Saturation pressure, circulation ratio and carry-under in a PWR steam generator (Tricastin 1 nuclear power plant). *Nucl. Engng Des.* **80,** 79–86.

Wazzan, A. R., Procaccia, H. & David, J. 1987 Thermal–hydraulic characteristics of pressurized water reactors during commercial operations: chemical analysis of secondary water in the steam generators of Bugey 4 and Tricastin 1. *Nucl. Engng Des.* **99,** 379–388.

Weaver, D. S. & Lever, J. H. 1982 A theoretical model for fluid–elastic instability in heat exchanger tube bundles. In *Flow-induced Vibration of Circular Cylindrical Structures, ASME, Pressure Vessels and Pipes*, Vol. 63.

Weaver, D. S. & Schneider, W. 1983 The effect of flat bar supports on the crossflow induced response of heat exchanger U-tubes. *ASME Engng Power* **105,** 775–781.

Weaver, D. S. & Fitzpatrick, J. A. 1987 A review of flow induced vibrations in heat exchangers. *Int. Conf. on Flow Induced Vibrations*, Bowness-on-Windermere, England.

Weeks, J. R. 1974 Corrosion of steam generator tubing in operating pressurized water reactors. In *Corrosion Problems in Energy Conversion and Generation* (Edited by Tedmon, C. S. Jr). The Electrochemical Society, Princeton, NJ.

Weeks, J. R. 1976 Materials performance in operating PWR steam generators. *Nucl. Technol.* **28,** 348–355.

Whalley, P. B. 1984 Flow pattern maps for the shell side of shell and tube heat exchangers. HTFS Report TM3.

Williams, C. L. & Green, S. J. 1980 Thermal and hydraulic aspects of PWR steam generators. *ANS/ASME Int. Topical Mtng on Nuclear Reactor Thermal–Hydraulics*, 5–8 October, Saratoga Springs, NY.

Williams, D. B. 1984 Practical analytical electron microscopy in material science. *Philips Electronics Instruments*, Mahwah, NJ.

Wilson, I. L. W. *et al.* 1976 The influence of specimen type and heat treatment on the caustic SCC of some stainless alloys. *Corrosion* **32,** 193–201.

Wilson, R. M. & Roarty, J. D. 1985 Westinghouse aims to improve reliability with its model F design. *Nuclear Engineering Int.*, October, p. 28.

Wisman, R. 1979 Fundamental investigation on interaction forces in bubble swarms and its application to the design of centrifugal separators. Ph.D. thesis, Department of Mechanical Engineering, Delft University of Technology, The Netherlands.

Withers, B. D. 1985 Steam generator owners groups—an industry effort. *Structural Mechanics in Reactor Technology Conf.*, Brussels, Belgium.

Wong, S. S. & Srikantiah, G. S. 1985 Numerical modeling of the phase separator process in BWR and PWR steam separators. *Heat Transfer Denver, AIChE Symp. Ser.*, Vol. 81, pp. 246–252.

Workshop proceedings: steam generator water hammer. EPRI Report WS78-132.

Yao, S. C., Hung, Y. H. & Tang, J. 1981 Analysis of dryout in steam generator crevices. ASME Paper 81-WA/NE-2.

Yao, S. C. & Hung, Y. H. 1982 Heat convection in annular type crevices. *J. Heat Transfer* **104,** 403.

Yeung, H. C. & Weaver, D. S. 1981 The effect of approach flow direction induced vibrations of a triangular tube array. ASME Reprint, 81-DET-26.